Report No. 69-25

STRUCTURES AND MATERIALS RESEARCH
DEPARTMENT OF CIVIL ENGINEERING

MODEL ANALYSIS OF THE A. D. EDMONSTON PUMPING PLANT DISCHARGE LINE MANIFOLDS

by
W. G. GODDEN
and
A. R. GRIFFITH

Report to
Department of Water Resources
State of California

September 1969

STRUCTURAL ENGINEERING LABORATORY
UNIVERSITY OF CALIFORNIA
BERKELEY CALIFORNIA

Structures and Materials Research
Department of Civil Engineering
Division of Structural Engineering
and Structural Mechanics

MODEL ANALYSIS OF THE A. D. EDMONSTON PUMPING PLANT DISCHARGE LINE MANIFOLDS

A Report of an Investigation

by

W. G. Godden
Professor of Civil Engineering

and

A. R. Griffith
Associate Engineer, Department of Water Resources

to

The Department of Water Resources
State of California
Under Contract No. 355974

College of Engineering
Office of Research Services
University of California
Berkeley, California

September 1969

TABLE OF CONTENTS

Page

Page

LIST OF TABLES

LIST OF FIGURES

LIST OF PLATES

ABSTRACT

This report presents experimental and theoretical stress data from a study on two pipe bifurcations subjected to internal pressure, the major part of the report being devoted to the model analysis. The prototype structures, as discussed in Chapter 1, were the E-1 and W-2 wye-junctions of the Tehachapi Pumping Plant Discharge Line Manifolds, the hydrostatic pressure being approximately 1000 psi. Two designs were studied, a 45° angle preliminary design and a 60° angle final design. The maximum diameter of the junction was 12 ft. 6 in. I. D., and the maximum pipe wall thicknesses in the two designs were 3.75 in. and 4.00 in. respectively.

In Chapter 2 the problems of modeling these structures in acrylic resin are discussed. The models were 1/15 true scale models, all components being machined to maintain adequate dimensional stability. The loading was applied by internal air pressure. Strains were measured both inside and outside the structures with 1/8 in. gage length SR-4 foil gages.

Material and instrumentation studies are discussed in Chapter 3. The results of a control study on a tube coupon are given first. Problems associated with material properties were studied by this means, together with construction techniques, instrumentation, and pressurizing. Beam coupons were used as a means of checking the consistency of elastic modulus.

One structural quantity was varied on both models - the geometry of the splitter-plate. Stress data is given in Chapters 6 and 7

for both models with full splitter-plates and with partial splitter-plates. Data is also given in Chapter 6 for the 45° model with its splitter-plate removed.

In Chapter 8 various analytical procedures are briefly discussed and results of finite-element solutions are presented. These are compared with experimental data from the model study, and also with data from a field test on a prototype steel junction of similar design.

I. INTRODUCTION

1.1 Objective

The primary objective of this investigation was to determine experimentally the state of stress at selected points in a complex wye-junction of the type shown in Fig. 1.1, subjected to an internal hydrostatic pressure. In doing this the following two purposes were achieved:

(a) To provide a model study of a prototype structure as a check on design suitability.

(b) To provide precise experimental data to be used as reference points in determining the accuracy and suitability for design purposes of certain computer analyses at present being developed for structures of this general type.

It was not the initial objective of this study to use model analysis as a design tool. This requires more time than was available, and depends on studying certain design changes experimentally. However, the study was planned with a view to being able to study one design problem experimentally - the effect of splitter-plate geometry on the total response of the system. A 'cut-back' procedure was applied to the splitter-plate for this purpose.

1.2 General Remarks

The problem of stresses in pipe junctions subjected to an internal pressure is a common one in many branches of industry and in power plants where pipe systems carry and distribute gasses or liquids under pressure. It occurs on a large scale in the design of manifolds in water schemes.

The particular investigation covered in this report was initiated by the State of California, Department of Water Resources, Division of Design and Construction, and the immediate problem was the design of the discharge line manifolds for the Tehachapi Pumping Plant (Plate 1.1 and Fig. 1.1). The largest pipe junction for the scheme is that designated E-1 and W-2, the largest pipe having an internal diameter of 12 ft. 6 in.

Two designs were studied for this joint. The structural aspects of both designs were analyzed both theoretically and experimentally. The hydraulic aspects of these designs are covered in another report.[2]

(a) Design I: This was a preliminary design using a 45° pipe intersection angle (Fig. 4.4 and Plate 4.7).

The design pressure was 1050 psi internal, and the plate thicknesses of the joint were 3.75 in. throughout. The maximum pipe diameter was 12 ft. 6 in. I. D., and this main pipe tapered down to 11 ft. 6 in. I. D., with a linear taper of length 15 ft. 0 in. The branch pipe joined the main pipe at an angle of 45° at the taper. The branch pipe remote from the joint was 4 ft. 6 in. I. D. with a wall thickness of 1.25 in., and joined the main pipe via a steep linear taper. The junction was reinforced by two normal circumferential stiffeners joined by a short plate, and by two oblique stiffeners. The main oblique stiffener reinforced the acute intersection between the tapers. Welded in line with this stiffener and acting with it was the splitter-plate inside the tube that controlled the hydraulic characteristics of the junction. At the time the study was started, the stresses in the splitter-plate were in doubt, and it seemed likely that the maximum stresses of the complete system would occur

in this plate. This part of the structure was, therefore, singled out for detailed investigation. The connection between the two tapers was made by welding both shells to a 20 in. diameter solid rod.

(b) Design II: This is the final design as adopted for construction. It uses a 60° pipe intersection angle (Fig. 4.1 and Plate 4.5). The design pressure is 1150 psi internal, the maximum pipe diameter is 12 ft. 6 in. I. D., and the wall thickness 4 in. The main pipe tapers down to 11 ft. 6 in. I. D. with a linear taper of length 14 ft. 0 in. The branch pipe is 4 ft. 6 in. I. D., and joins the main pipe via a steep linear taper. The diameter of the connection rod in this design is 13 in. In this design also it was expected that the maximum stresses would occur in the splitter-plate, and this was studied in detail, both by the number of gage locations and also by the cut-back procedure used in Design I.

1.3 Scope of Present Investigation

This study deals with the elastic response of two particular pipe junctions subjected to an internal hydrostatic pressure. Structural nonlinearity, if present, would be detected and measured. Inelastic material action associated with yielding of steel was not considered and was not simulated. The scope of the investigation was restricted to studying the state of stress at certain predetermined points in the structure. Within this restriction, the following aspects of the design were investigated:

(a) The effect of splitter-plate geometry on the stresses throughout the complete system. This was effected by starting each model with a full splitter-plate, then cutting back the free edge and observing the resulting changes in stress throughout the system. As in certain cases the maximum stresses occur in this plate, this was an important aspect of the study.

(b) The structural linearity of the system. This was studied by plotting the strain/pressure curves at selected gage points, including points on the shell subjected to bending and membrane stresses.

(c) The effect of the junction discontinuity on the hoop stresses in the pipe. This was studied by gaging the main pipe on the axis of symmetry.

These effects were studied experimentally to act as reference stress data for comparison with the computer analysis. The linearity check is an important check on any linear theory and on constructional accuracy. The splitter-plate study is important as there is a danger of overstressing either the free edge or the inside edge of this plate. The hoop-stress study is important if structural idealization is used to produce a simplified method of design.

The initial experimental work consisted of control studies related to properties of the model material and to instrumentation. Test Series I covered the study of Design I, the 45° junction; Test Series II covered the study of Design II, the 60° junction.

The report also includes the results of computer studies based on various finite-element analyses undertaken by the Aqueduct Section, Department of Water Resources, State of California. Details of these studies are included in Chapter 8 in order to compare available theoretical analyses with experimental data.

References

1.1 Stephens, N. M., Griffith, A. R., and Ferguson, B. C., "The Design of the Tehachapi Pumping Plant Manifolds", Conference paper presented at Western Water and Power Symposium, Los Angeles, California, April 8 - 9, 1968.

1.2 Amorocho, J., DeVries, J. J., and Curry, W., "Hydraulic Studies of the Tehachapi Pumping Plant Intake Channel and Manifold", Conference paper presented at Western Water and Power Symposium, Los Angeles, California, April 8 - 9, 1968.

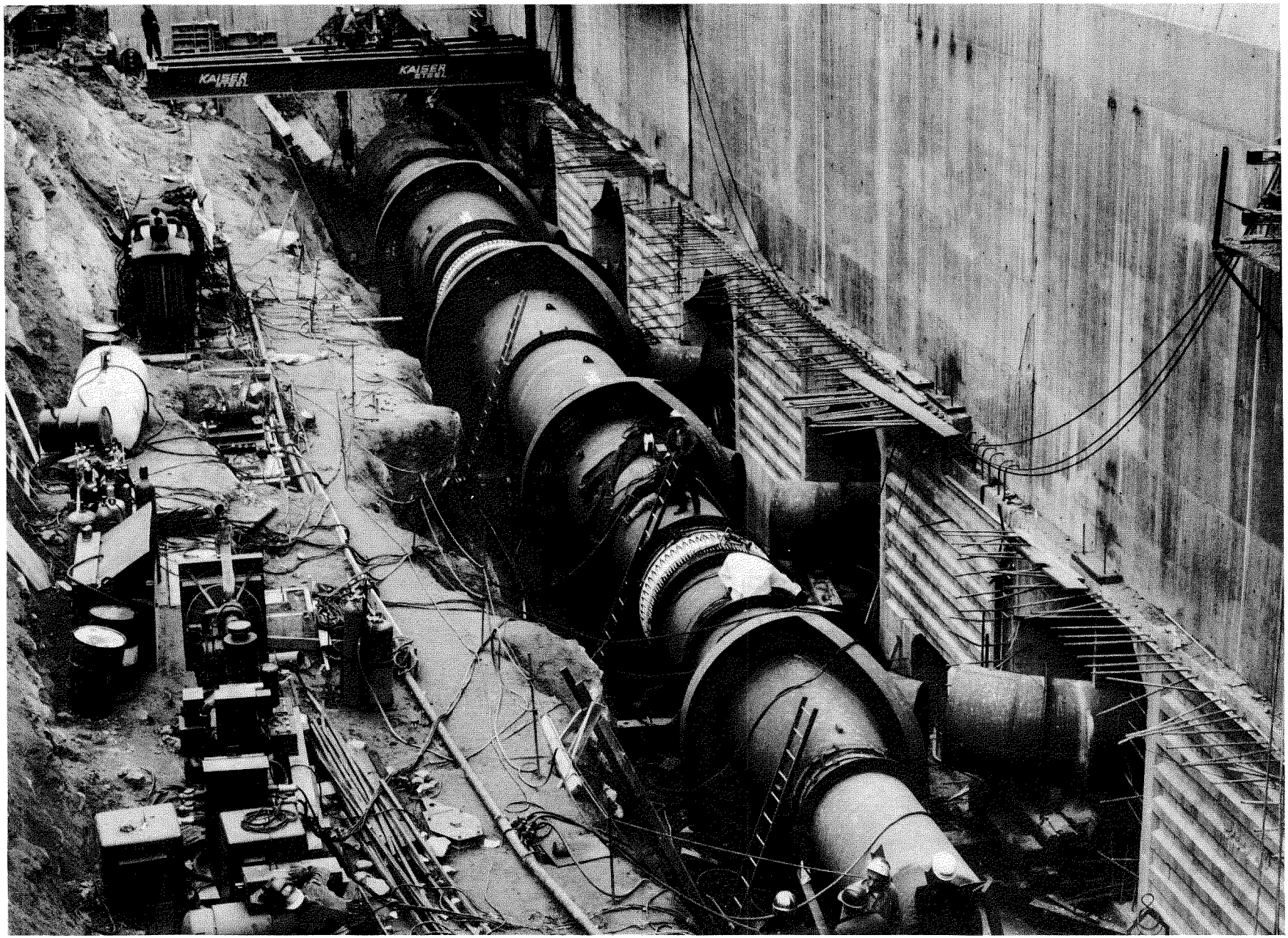

PLATE I.I CONSTRUCTION OF THE EAST DISCHARGE LINE MANIFOLD AT THE A. D. EDMONSTON PUMPING PLANT

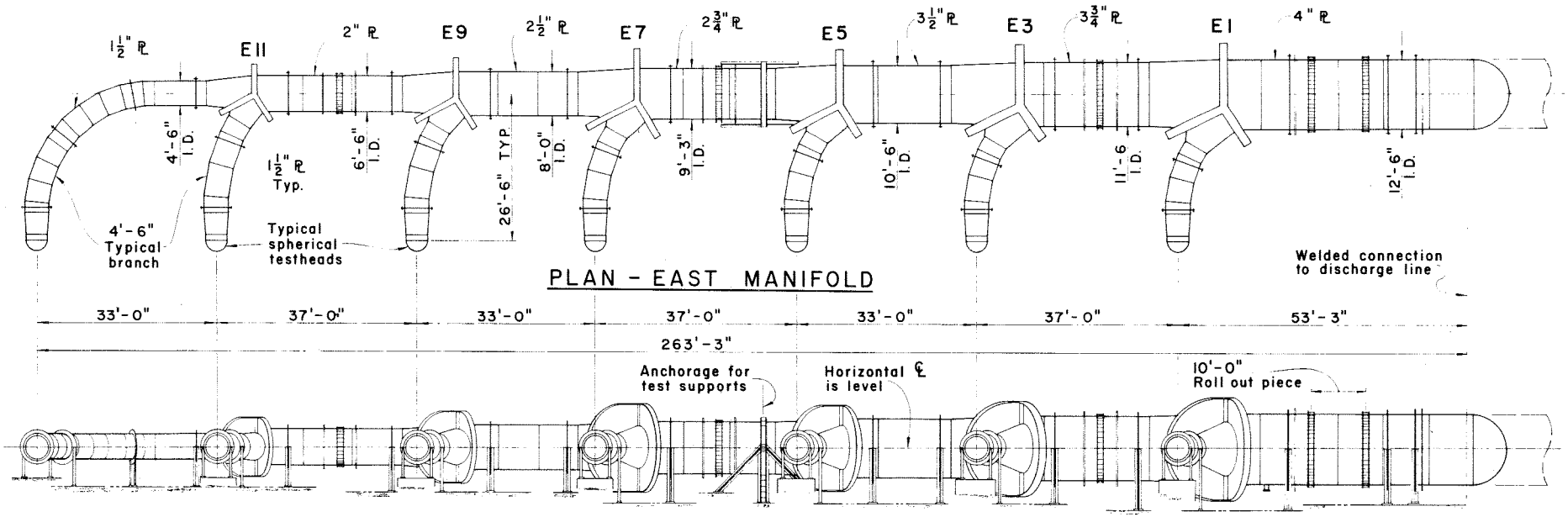

PLAN - EAST MANIFOLD

ELEVATION

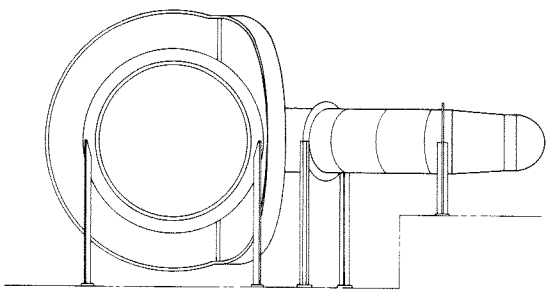

TYPICAL SECTION

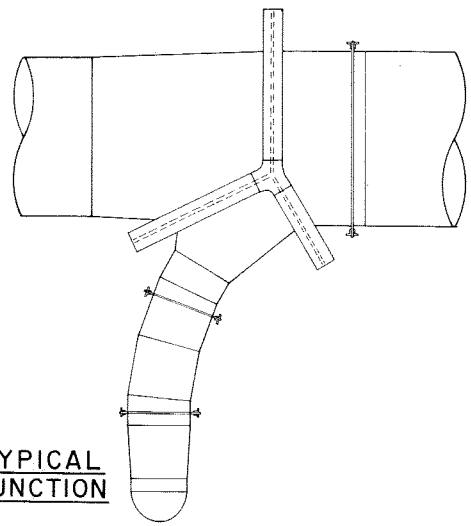

TYPICAL JUNCTION

FIG. I.I LAYOUT OF EAST DISCHARGE LINE MANIFOLD

II. MODEL ANALYSIS AND SIMILITUDE

2.1 Similitude Requirements

In a complex shell-type structure of this kind, subjected to both membrane and bending effects, a model study has to be 'true scale'. That is, all linear dimensions must be to the same linear scale L_r.

The structural behavior under consideration is that associated with linearly elastic material properties. Then provided the value of Poisson's ratio ν is the same in model and prototype, the relationship between stress, strain, and modulus of elasticity E in the model and the prototype is governed by:

$$\sigma_r = E_r \varepsilon_r$$

where the subscript r denotes the dimensionless ratio between similar quantities at homologous points (for example, $\sigma_r = \sigma_m/\sigma_p$ where σ_m = stress in model and σ_p = stress in prototype).

The true-scale requirement enables the model to meet the condition that the model will respond to loading in a manner similar to the prototype, and thus it is possible to predict the elastic behavior of the prototype from the model.

The true-scale requirement strictly includes elastic displacement effects Δ, that is

$$\Delta_r = L_r$$

$$\varepsilon_r L_r = L_r$$

hence

$$\varepsilon_r = 1$$

This means that if the elastic deformations are included in the true-scale demands of the model, the strains at homologous points in the model and the prototype will be identical.

Whether or not it is essential to retain this requirement depends on the behavior of the system. In cases where structural non-linearity is present, the requirements must be retained or the results will not be valid. If the system is linear in its response to loading, then clearly the strains are proportional to load and the requirement that $\Delta_r = L_r$ can be waived. This matter was studied on the model, and within the range of pressure applied no structural nonlinearity could be detected.

From the above it is obvious that for $\varepsilon_r = 1$, the ratio of stresses and pressures are governed by

$$\sigma_r = p_r = E_r$$

where the stresses are solely due to the applied pressure.

Stresses due to self-weight are a different matter. If w is the specific weight of the material where this weight produces stress, then the ratio of the resulting stress, specific weight and geometric scale is given by

$$\sigma_r = w_r L_r$$

The strain ratio is given by

$$\varepsilon_r = w_r L_r / E_r$$

It is thus only possible to retain $\varepsilon_r = 1$ when $w_r L_r / E_r = 1$. Usually this is not practicable, and in most cases where this effect can be neglected in model design ε_r (due to dead loads) < 1. A true-scale model in Plexiglas thus meets all similitude requirements except two:

(a) Poisson's ratio is a dimensionless quantity and hence should strictly have the same value in model and prototype. However, from previous experience and from computer studies where the value of ν can be changed at will, it is known that in most cases, shell type structures are not particularly sensitive to the precise value of ν. It was decided in this case to neglect the errors in measured stress caused by the difference between the values of ν in model and prototype. If there should be any question about the validity of this decision, the effect of ν variation can be studied in the finite-element solution. Also, as the model is being used primarily to vindicate the accuracy of the theoretical solution, the model could be considered as a small prototype and the value of ν associated with the model material used in the theoretical solution. In this way the experimental data presents valid information on which to judge the accuracy of the computer solution.

(b) The weight of water is neglected in the model. The model uses air pressure which applies a constant pressure to the inside surfaces of the structure. It could be argued that this method of loading is not valid since the prototype is loaded by hydrostatic pressure and water is not weightless. However, the hydrostatic pressure on the prototype represents a head of approximately 2000 ft., and the weight of water in the structure represents a differential head of approximately 12 ft. in 2000 ft. As the spacing of the supports for the manifold structure (see Fig. 1.1) is such that large beam bending moments are not produced in the pipe wall, this effect is clearly negligible. Hence it was decided to study the structure under the action of a constant pressure.

2.2 Considerations in the Design of the Model

The chief factors to be decided in designing a model for a study of this kind are scale, material, and the method of loading. These are not independent but will be discussed separately.

(a) Choice of Scale

The considerations for the choice of linear scale are as follows:

The scale should be kept at a minimum, consistent with other factors, to keep the cost-time factor to a minimum.

The scale should be large enough to allow access to the inside of the model after construction. Access is required for internal instrumentation, and for cutting back the splitter-plate during the test series.

The shell wall of the model should be thick enough for measuring bending strains as well as membrane strains.

The shell wall should be thick enough to make errors due to surface stiffening of the strain gages negligible. This factor is related to the material being used for the model.

All dimensional tolerances, including plate thicknesses, should be within 1%.

In practice, the last of these factors, namely the constructional errors, controls the choice of scale. At a linear scale of 1/15 as finally selected, the prototype shell thickness in Design I of 3.75 in. becomes 0.250 in. in the model. This has to be machined to $\pm$ 0.002 in. to maintain the required dimensional stability. This scale is also minimum for adequate access to the inside of the model after it is constructed.

(b) Choice of Material

This is closely related to the method of pressurizing. From similitude considerations, if $E_r = 1$, as when the prototype material is used in the model, $p_r = 1$, the pressure in the model and the prototype being equal. A model pressure of 1000 psi would require hydraulic pressurizing, and the internal strain gages would be under water. It was decided to reduce the required pressure by reducing E_r, and to use air pressure.

The simplest material to use was found to be acrylic resin. This has an E of approximately 4×10^5 psi, giving $E_r \approx 4/300 = 1/75$. Hence the required model pressure would be $p_m = 1050/75 \approx 14$ psi. This can be easily applied by a hand pump and measured by mercury manometer.

The precise material selected was methyl methacrylate under the trade name Plexiglas. In a model of this kind made out of separate components and cemented together, it is important that E is constant over the various components, and that the cementing operations do not introduce unwanted characteristics at the joints. For purposes of material control, all the components were made out of plexiglas sheet, heat formed where necessary, and subsequently machined to exact dimensions. All sheets were subjected to coupon tests to ensure that the value of E did not vary appreciably. Even where cast acrylic resin tubes were available, these were not used on account of the difference in E between commercially available tube and sheet stock. In all cases sheet stock was used, and tubes were fabricated by heat forming, cementing, and machining.

There are two problems associated with the use of acrylic resin. The first is that the value of Poisson's ratio is approximately 0.4 compared with the value for steel of approximately 0.25. It was considered that the errors in measured stresses resulting for this mismatch would be small as discussed in Sec. 2.1.

The second problem connected with the use of acrylic resin is that it is strictly a visco-elastic material and not elastic. This results in creep under sustained loading, a factor that must be considered when deciding on the test procedure.

(c) Method of Pressurizing

For the reasons stated above it was decided to use air pressure and not water pressure in the model. The difference between these two methods of loading is that air pressure approximates to constant loading on account of the compressibility of air, and water pressure approximates to constant strain. Constant strain is ideal for a linearly viscoelastic material, as the measured strains remain constant with time, even when stress relaxation takes place; constant load results in creep causing a strain change in the gages with time.

The other problem associated with using air pressure is that of possible temperature change due to pressurizing. Temperature changes are undesirable for two reasons. First, they affect the strain gage readings; this can be minimized, however, by careful choice of gage and by temperature compensation techniques. Second, acrylic resin is temperature sensitive, and the value of E changes with temperature. The problem of temperature rise due to pressurizing was studied carefully as it affected the method of pressurizing, and was not found to be significant.

III. MATERIAL AND INSTRUMENTATION STUDIES

3.1 General

The study of Plexiglas as a suitable material for these model tests required an investigation of certain factors affecting mechanical properties, and the design of tests to determine these properties and to study instrumentation problems.

(a) State of stress

The structure is subjected to both membrane stress (primarily biaxial tension) and bending. Hence the dependence of E on the state of stress is important and must be determined. Available data[3] suggests that the value of E as measured in tension is slightly higher than that measured in bending. This was checked by two coupons made from the same piece of material, one being a tube coupon (see Sec. 3.2) subjected to internal pressure, and one being a beam coupon (see Sec. 3.4) subjected to bending.

(b) Temperature

The dependence of E on temperature in acrylic plastics is well documented[10], the value of E measured in flexure decreasing from 360 ksi to 230 ksi due to a temperature rise from 50°F to 100°F. This sensitivity of mechanical properties to temperature demands a careful temperature control in the models study. The control affects both the testing environment and the self heating effects associated with the strain gages.

(c) Age Effects

Long term studies on the ageing of cellulose acetate and cellulose nitrate sheets[8] indicate that the modulus of elasticity may increase as much as 30% in 12 months, depending on the exposure conditions. No such information was found in the literature for Plexiglas, and in some previous studies the effect has been neglected[2,7]. But the coupon studies discussed in Sec. 3.2 and Sec. 3.3 do indicate the possibility of an increase in the elastic modulus of some Plexiglas material with time.

(d) Creep

The study of elastic response ideally demands that there be no creep in the model material. Plexiglas creeps under sustained load, and for precise work this must be allowed for even in cases where the stresses are small.

Coupon tests were required to determine E, ν, the mechanical properties of cemented joints, and for studying strain measurement procedures. A thick-walled cylinder coupon was selected for determining E and ν under biaxial tension, for studying butt-joints and tube-to-bulkhead joints, and for studying gaging problems. A simpler general test had to be used for determining E, however, as the elastic modulus had to be determined for material coming from each different source. For this purpose a simple bending test was used. The results of the bending tests were related to the tube coupon results by conducting both tube and bending tests in one case on coupons made from the same piece of material.

3.2 Tube Coupon Tests

Details of the tube coupon are shown in Fig. 3.1 and Plate 3.1. The coupon consisted of stock cast-tube machined inside and outside to the dimensions shown. Two 5 in. lengths were machined and then connected by a 45° circumferential cemented butt joint. PS-18 cement was used for this joint in accordance with the manufacturer's specifications[10] in order to study cementing procedures and joint characteristics for the model.

The bulkheads consisted of circular blanks and annular rings made of aluminum. A silicone rubber O-ring was used to provide an air seal between the blank and annular ring. One side of the ring had a machined groove to take the tube ends, and PS-18 cement was used for this joint also. Initial pressurizing indicated that all joints were sufficiently strong and that O-rings provided a perfect seal.

Two-element SR-4 foil rosettes (Reference C40-121-R2T by Budd) were used for strain measurement. These gages are temperature compensated for Plexiglas. Five such rosettes were used for measuring the axial and circumferential strains at the locations shown in Fig. 3.1. Even numbered elements measured circumferential strains, and odd numbered axial strains. Two rosettes, cemented on 1/2 in. Plexiglas cubes were used as inside and outside dummy gages. The strain observations due to internal pressure were used to provide the following data:

(a) Elastic modulus and Poisson's Ratio. The biaxial state of stress in the tube wall being known by thick wall tube theory, the measured strains at the five points gave the effective value of E and ν at each point.

(b) Mechanical properties of cemented joints. The influence of PS-18 on the mechanical properties of the parent material was studied by comparing the strain readings of rosettes 1-2 and 3-4.

(c) Surface reinforcing effects of the gages. Gages 7-8 are on the inside surface opposite 5-6, and at this point there is stiffening on both surfaces. The stiffening effect can be studied by comparing the data from gages 1-2 and 5-6. It should be noted that the 0.200 in. wall thickness of the tube coupon is less than the 0.250 in. wall thickness of the 45° tube model and the 0.267 in. wall thickness of the 60° model; hence the stiffening effects should be more pronounced in the coupon.

(d) Gage stability. This was studied by observing the zero stability of the gages under zero pressure and constant environmental conditions.

(e) Creep characteristics of the material. This was studied by taking strain readings against time at constant pressure.

(f) Age effects. Age hardening of the material was studied by taking strain data from the same coupon over a period of 16 months.

3.3 Results of Tube Coupon Tests

The tube was pressurized by a hand operated air pump to an internal pressure of approximately 25 psi in ten equal increments. Maximum strains were thus within 600 μin./in. All readings were taken after creep had essentially stabilized. Temperature was recorded both inside and outside the tube to check against the possibility of an internal temperature rise due to an increase in air pressure. The strain/pressure plots for all gages were essentially linear, and the

results of E and ν deduced from thick-wall tube theory and the slope of the graphs are given in Table 3.1. Results are given for two different tests on the same coupon. Both tests were conducted at the same temperature but were separated in time by a 16 month interval. The following deductions can be made:

(a) A comparison of data from elements 1 and 9, and 2 and 10, indicates the level of consistency between the gages.

(b) A comparison of data from elements 1 and 5 indicates that the surface reinforcing effect of these gages is negligible for a 0.200 in. wall thickness.

(c) A comparison of data from gages 1-2 and 3-4 shows that the cementing procedure used for this butt joint produces an effectively homogeneous connection. The use of PS-18 does not appreciably alter the local value of E from the parent material.

(d) Values of E and ν are computed using the known stresses in a pressurized thick-wall cylinder.

Circumferential stress, outside surface:

$$\sigma_{to} = \frac{2pr_1}{(r_o^2 - r_i^2)} = 8.53\ p$$

Circumferential stress, inside surface:

$$\sigma_{ti} = p\left(\frac{r_o^2 + r_i^2}{r_o^2 - r_i^2}\right) = 9.53\ p.$$

Axial stress;

$$\delta = p\left(\frac{r_i^2}{r^2 - r_i^2}\right) = 4.27\ p$$

Radial stresses: outside surface $\sigma_{ro} = o$

inside surface $\sigma_{ri} = p.$

The values of E and ν resulting from this data are shown in Table 3.1.

(e) Zero stability depends on heat dissipation, the heat generated by the gages being proportional to the square of the voltage. At the start of the program, a BLH Portable Strain Indicator with a 5 volt bridge input was used. A minimum time of 20 seconds was required for the gage reading to stabilize, and some gages took longer. Later a Budd Portable Strain Indicator with a 1.5 volt bridge input was used. At this voltage, drift was negligible and observations could be taken almost instantaneously. Repeatability was also greatly improved.

(f) A comparison of strain data for the tube coupon over a 16 month period shows that the slopes of the strain-pressure graphs have significantly reduced indicating that the age effect in the tube coupon material cannot be neglected. The average value of E increased from 3.55×10^5 psi in April 1967 to 4.09×10^5 psi in August 1968, a 14% increase over a 16 month interval. This should be compared with the data from the beam coupon tests of the same material discussed in Sec. 3.5. During the same period, the average value of Poisson's ratio decreased from 0.42 to 0.373.

3.4 Beam Coupon Tests

Tube coupon tests were conducted for the reasons mentioned above. However, they are too time consuming for checking the consistency of material properties from sample to sample. For this purpose a simple bending test was adopted.

Beam coupons were machined from every different source of material used in the models. In the case of sheet stock, a coupon was made from each individual sheet as a consistency check.

In order to relate the results of the bending tests to the tube coupon tests, a beam specimen (beam coupon 1) was machined from the tube wall of the material used in the tube coupon. E in bending was measured by a 3-point loading deflection test (Table 3.2).

In addition to checking consistency of material properties, beam tests were used to study the effect of cemented joints on the material properties. Coupons 9 and 10 were beam coupons with a transverse butt joint and a longitudinal shear joint respectively. These results were compared with coupon 8, an uncemented coupon made from the same sheet of material.

In the beam coupon tests, measurements were made either of deflection by micrometers, or of strains by SR-4 gages.

3.5 Results of Beam Coupon Tests

The results of the beam coupon tests, are tabulated in Table 3.2.

(a) Consistency of material properties:

Coupons 3 through 8 were all from different sources. The range of measured values for E was 4.24 to 4.31 x 10^5psi. The average value was 4.28 x 10^5psi, and the maximum deviation 1.4%. This consistency was considered acceptible for the construction of the model.

The effective E for the cemented coupons 9 and 10 indicated no measurable departure from coupon 8, a coupon made of the same material but without any joint. Although tests 9 and 10 are not very sensitive to local reduction in stiffness due to cementing, they do represent the way the cemented joints act in the model in areas under bending.

(b) Value of E in biaxial tension versus bending.

The tube coupon and beam coupon 1 were from the same source. On the tube coupon the average value of E was 3.55×10^5 psi; on the beam coupon the value was 3.38×10^5 psi, approximately 5% lower than the biaxial tension value. This variation was not considered important, though it could possible be allowed for in the model by uncoupling the membrane and bending stresses and adjusting the bending stresses accordingly.

(c) Ageing effect.

The modulus of elasticity of beam coupon 1 increased from 3.38×10^5 psi in April 1967 to 3.90×10^5 psi in August 1968, indicating an increase of approximately 14% over a 16 month interval. Both tests were conducted at the same temperature. The percentage increase in the elastic modulus is the same as that indicated by the tube coupon tests on the same material, Sec. 3.3.

On the other hand, the average value of E for beam coupon 8, which was machined out of the sheet Plexiglas material used for the fabrication of the 60° wye-junction model, remained constant during a 10 month period. The value was 4.24×10^5 psi at 73°F in Nov. 1967 and 4.17×10^5 psi at 83°F in September 1968. As shown in Fig. 5.2

of Chapter V, the reduction in the value of E can be attributed to the increase in test temperature. The value of E at 83°F was interpolated to that at 73°F using Fig. 5.2 and was found to be 4.24×10^5 psi.

It can also be observed from the values of E for beam coupons with butt and shear joints (Coupons 9 and 10 respectively), that there is no apparent variation in the elastic modulus during the 10 month period. These coupons were also machined from the material used for the 60° wye-junction model.

3.6 Strength Tests of Cemented Joints

Two test series were carried out for determining the strength of cemented joints. Test Series I consisted of tensile strength tests for PS-18 butt and fillet Plexiglas-to-Plexiglas joints. Test Series II consisted of tensile tests for PS-18 fillet Plexiglas-to-aluminum joints.

Test Series I: The two tensile specimens are shown in Fig. 3.2 and were machined from sheet Plexiglas. The components were annealed at 195°F for 5-1/2 hours, then joined using PS-18 cement. All procedures and precautions laid down by the manufacturer for the use of PS-18 were observed. The joint was cured at room temperature for 24 hours, followed by 5-1/2 hours of annealing at 195°F. The results of the tests are tabulated in Fig. 3.2.

Test Series II: The strength tests for the Plexiglas-to-aluminum joints using PS-18 fillets were required to evaluate the suitability of the bulkhead-tube connections in the two models. The tests were carried out in a similar manner to those of Test Series I. The three specimens and the corresponding results are shown in Fig. 3.3.

As is evident from the results of the two test series, PS-18 cement can be effectively used for joining the various model components without appreciable loss in strength. It should also be noted that in all cases the failure started at one edge, due to eccentricity of loading, producing a lower ultimate load than might reasonably be expected in the models.

3.7 Material Properties

A study of the technical literature and the coupon tests carried out in this project indicates that factors such as temperature, ageing, and state of stress have a large enough influence on the elastic modulus of Plexiglas to require careful control of these effects in the model tests. Even if the models were to be tested under constant environmental conditions, eliminating the effect of temperature variation, ageing effects may still take place.

The effect of time on E for the stock cast tube material used for the tube coupon tests suggests that the material might have been obtained shortly after its manufacture. The negligible effect of time on E for the sheet material used in the 45° and 60° wye-junctions indicates that this material may have already age hardened, or that the production procedure is different.

The accuracy of the model results depends primarily on the accuracy to which the value of elastic modulus is known, allowing for creep. Considering the sensitivity of E to temperature, it is desirable to have the test procedure so that the measured strain data is self-calibrating. This is achieved by having strain gages at a point of

known strain as control for the entire test. In this structure, such a point can be on the shell far enough removed from the joint so that the state of stress is that for a cylinder under internal pressure.

For the purpose of designing the model, the properties of Plexiglas were taken as follows:

$$E \text{ in biaxial tension} = 4.28 \times 10^5 \text{psi}$$

$$E \text{ in bending} = 4.07 \times 10^5 \text{psi}$$

$$\nu = 0.375$$

Creep characteristics make it desirable to keep stresses in the model within 500 psi, and that strain measurements be made approximately 5 minutes after loading or unloading, so that strain equilibrium is reached.

References

3.1. Delmonte, J., "Elastic Properties of Plastic Materials," Trans., ASME, 1945, V. 67 pp. 477-491.

3.3. Staff, C. E., Guacknobos, H. M., Hill, J. M., "Longtime Tension and Creep Tests of Plastics," Trans. ASME, 1950, V. 72, pp. 697-704.

3.3. Marin, J., Pao, Y. H., Cuff, G., "Creep Properties of Lucite and Plexiglass for Tension, Bending, Compression and Torsion," Trans. ASME, 1951, V. 73, pp. 705-719.

3.4. Marin, J., Pao, Y. H., "On the Accuracy of Extrapolated Creep Test Relations for Plexiglass Subjected to Various Stresses," Trans. ASME, 1952, V. 74, pp. 1231-1240.

3.5. Knowles, J. K., and Dietz, A. G., "Viscoelasticity of Polymethylmetherylate--An Experimental and Analytical Study," Trans. ASME, V. 77, pp. 177-181.

3.6. Hall, H. W., and Russel, E. W., "Polymethylmethacrylate Plastics: Crazing, Thermal and Mechanical Properties," Aero. Res. Counc. Lond., Mem. 2764, 27 pages, 1953.

3.7. "Plastic Properties Chart," Modern Plastics, Oct. 1939, p. 186.

3.8. Lawton, T. S., and Nason, H. K., "Effect of Environment on Permanence of Cellulose Acetate and Cellulose Nitrate Sheets," Modern Plastics, Jan. 1945, V. 22.5, pp. 145-179.

3.9. Axilrod, B. M., and Sherman, M. A., "Effect of Stress Solvent Crazing on Tensile Strength of Methymethacrylate," AMR, V. 5, Ref. 136.

3.10. "Technical Data on Plastic Materials," Plastic Materials Manufacturers' Assn., Washington, D. C. (May 1943).

3.11. Rendor, M. A., and Van Horn, D. A., "A Structural Model Study of Load Distribution in Box-Beam Bridges," Fritz Engineering Laboratory, Report No. 322.1, Lehigh University, May 1968.

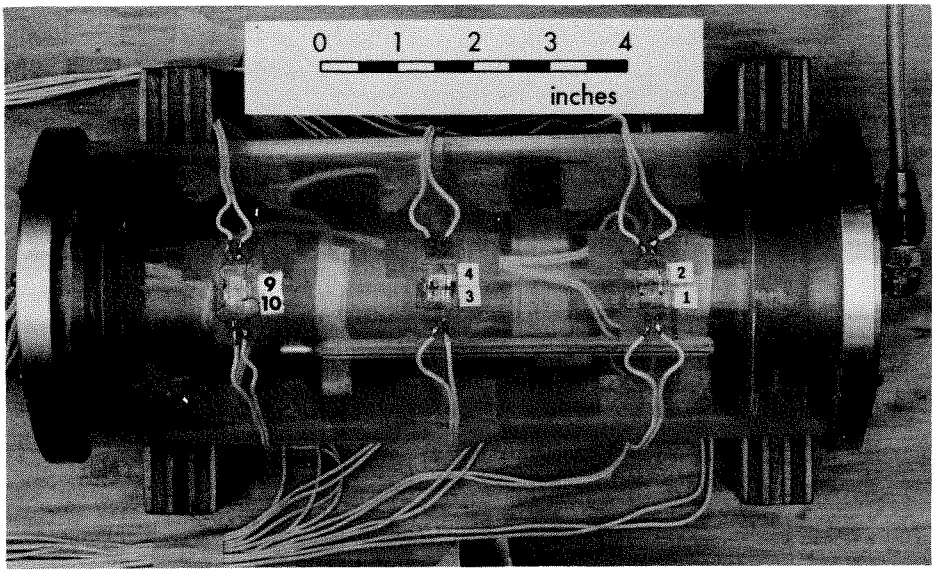

PLATE 3.1 PRESSURIZED TUBE COUPON FOR MATERIAL AND INSTRUMENTATION STUDIES

Gage No.	May 1967, 77°F			August 1968, 78°F		
	Strain (μin/in) at 25.0 psi	$Ex10^{-5}$ psi	ν	Strain (μin/in) at 25.0 psi	$Ex10^{-5}$ psi	ν
1	480	3.65	0.43	420	4.08	0.390
2	40			54		
3	495	3.60	0.41	420	4.12	0.375
4	65			64		
5	500	3.42	0.46	430	3.94	0.410
6	20			47		
7	600	3.58	0.34	507	4.25	0.306
8	85			98		
9	480	3.50	0.47	420	4.07	0.385
10	20			53		
	Average Value:	3.55	0.42	Average Value:	4.09	0.373

TABLE 3.1 RESULTS OF TWO TESTS ON THE SAME TUBE COUPON

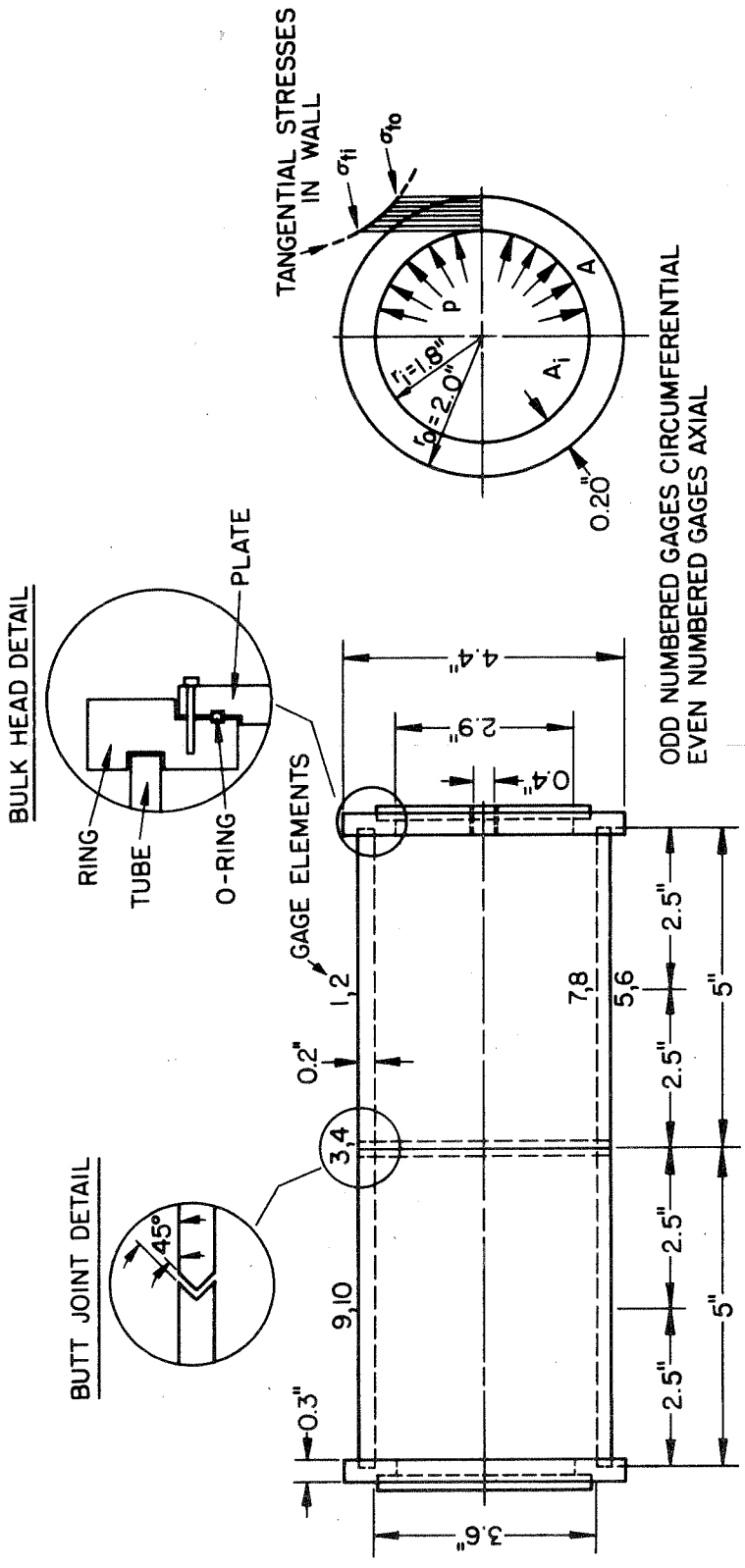

FIG. 3.1 TUBE COUPON

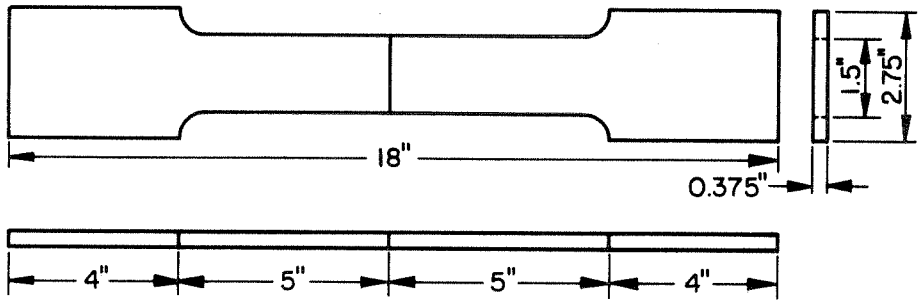

(a) PLEXIGLAS-PS-18-PLEXIGLAS BUTT JOINT

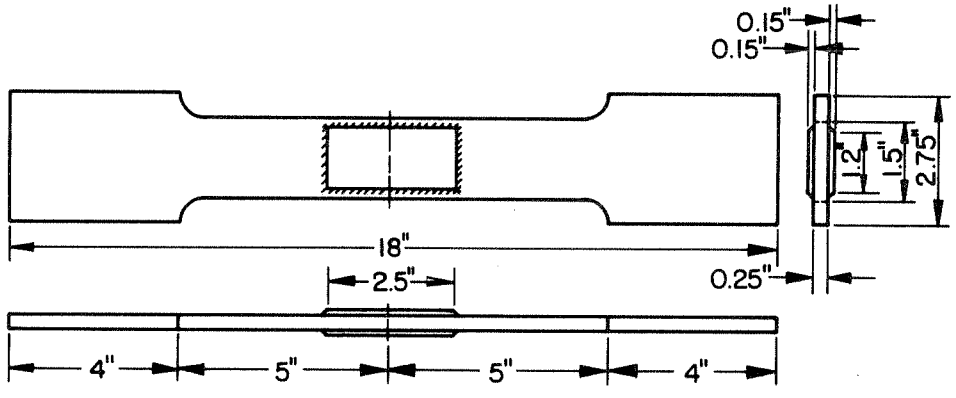

(b) PLEXIGLAS-PS-18-PLEXIGLAS FILLET JOINT

Specimen	Joint Type	Tensile Load at Failure (lb.)	Mode of Failure
a	Butt	1365	In both cases failure initiated at the joint and propogated through parent material
b	Fillet	920	

FIG. 3.2 TENSILE STRENGTH TESTS OF PLEXIGLAS TO PLEXIGLAS PS-18 JOINTS

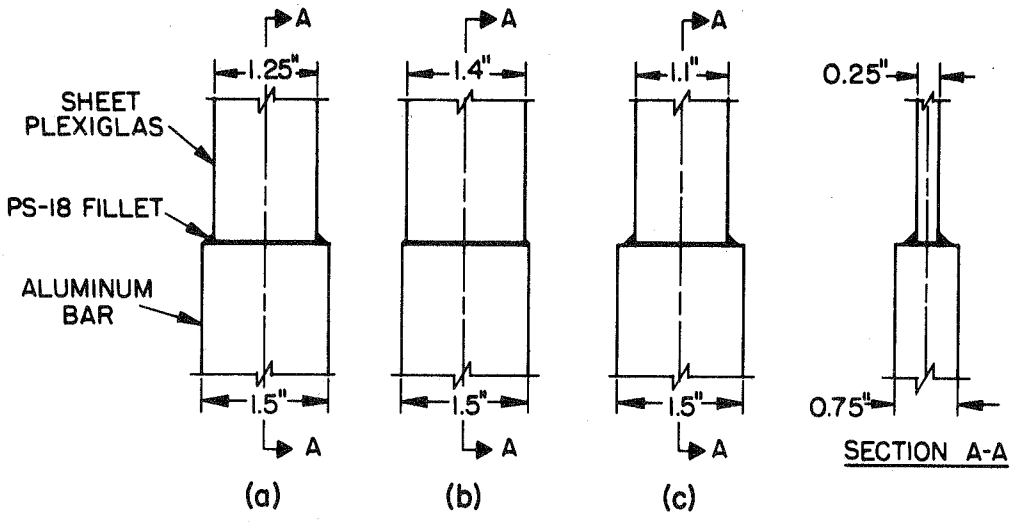

Specimen	Fillet Size (in.)	Tensile Load at Failure (lb.)	Mode of Failure
a	0.15	385	In all cases bond failure at one edge followed by crack propogating through parent material
b	0.15	325	
c	0.15	225	

FIG. 3.3 TENSILE STRENGTH TESTS OF PLEXIGLAS TO ALUMINUM PS-18 JOINTS

IV MODEL DESIGN AND CONSTRUCTION

4.1 General

In order to maintain consistent material properties between the various components of the model, all shell, web, and flange components were fabricated from sheet Plexiglas. Bar components were fabricated from extruded Plexiglas rods. Control coupon tests were carried out on every sheet and rod stock used in the model to check on the consistency of elastic modulus throughout the model.

The construction procedure described below was that used for the 60° model. The 45 degree model, the first to be made, was constructed in essentially the same manner. The 60° and 45° designs are detailed in Figs. 4.1 through 4.3, and Figs, 4.4 through 4.6 respectively.

The model was assembled from sub-assemblies consisting of tubular and tapered sections, stiffeners, and bulkheads.

4.2 Pipe Assemblies

All cylinder and taper components, parts 1 through 5 (see Fig. 4.1) were heat formed out of 3/8 in. sheet stock, then machined to the final wall thickness. The procedure was as follows:

(a) A wooden former was made for each component. These were made 1/16 in. undersize to allow for the machining of the inside surface of the component to its final size. Plate 4.1 shows the formers for parts 2 and 4.

(b) Each component was heat formed in two halves, joined by flat butt joints parallel to the tube axis and cemented with PS-18.

(c) The component was annealed at 160°F for 24 hours on its former. This increases the strength of the cemented joints and also stress relieves the component making possible the subsequent accurate machining operations.

(d) A 1 in. thick Plexiglas plate was cemented to one end of the component after removing the former. This enabled the component to be held in a lathe.

(e) The component was machined inside and outside to its final dimensions, polished, and 45° V-butts were machined along the planes joining Parts 1 and 2, Parts 2 and 3, and Parts 4 and 5.

(f) The sub-assembly consisting of Parts 1, 2, and 3, was cemented together (Plate 4.2) and held under a small axial pressure during the cement hardening period.

4.3 Stiffener Assemblies

The stiffener assemblies consisted of webs, flanges, solid rods, and a splitter-plate. Details are given in Figs 4.1 and 4.2, and Plate 4.3 shows some of these components during construction.

All web components, including the splitter-plate, were machined both sides as full circles, and subsequently cut to the correct geometry. All flange components were made flat, both sides being machined, and subsequently heat formed to shape. The solid rod, Part 7, was machined to the required diameter as a straight rod, then heat formed and held in a jig to the required profile.

The splitter-plate assembly, consisting of Parts 6 through 9 was constructed as a sub-assembly in a jig. The splitter-plate itself, Part 6, was made with a straight free edge, (Plates 4.3 and 4.6), and

after the model was tested with this profile the edge was cut back to its final design configuration. In the 45° model, the final test on the model was with the splitter-plate completely removed.

The other ring stiffeners, (Parts 14 and 16) were cemented to the tubes and then the flanges (Parts 15 and 17) were attached.

4.4 Bulkheads

The bulkheads were all of similar design, and similar to those used in the tube coupon (Fig. 3.1). The bulkheads for the 60° model are shown in Plate 4.4. Each consists of an annular ring machined to accept the pipe and fitted with an O-ring to form an airtight seal between ring and circular closure plate. The gage leads were passed through holes in the ring. All bulkhead components were machined from 1/2 in. thick aluminum sheet.

4.5 Assembly of Model

The assembly procedure for the complete model was as follows:

(a) The main pipe sub-assembly (Parts 1, 2, and 3) was held in a jig, fitted with the vertical pins (Parts 10 and 12) and then cut on a band saw along the lines of intersection with the branch taper (Part 4). This was slightly undercut as the final fitting was by hand.

(b) The branch taper (Part 4) was held in a jig (Plate 4.1) and cut along the lines of intersection with the main pipe taper (Part 2).

(c) The surfaces on Parts 2 and 4 where these components intersect along line CC (Fig. 4.1) were hand finished.

(d) The surfaces where Parts 2 and 4 intersect the splitter-plate assembly along line AA (Fig. 4.1) were hand finished to fit the splitter-plate assembly. This was the most difficult of all the operations. It was especially difficult on the 45° model on account of the complex form of the developed surface between the main pipe taper and the solid bar (Part 7).

(e) All the above components or sub-assemblies were cemented together.

(f) The remaining ring stiffeners and flanges were cemented in place.

(g) The bulkhead rings (Plate 4.4) were cemented to the three tubes as shown in Plate 4.5.

(In cementing all joints, the PS-18 cement was injected by hypodermic needle and a pressure applied between components to prevent the forming of air bubbles. In the case of fillet joints, the required amount of cement was built up in a series of runs.)

(h) The complete model was annealed for 24 hours at 160°F.

(i) SR-4 gages were attached and wired.

The assembled 60° model is shown in Plates 4.5 and 4.6; the 45° model in Plates 4.7 and 6.1.

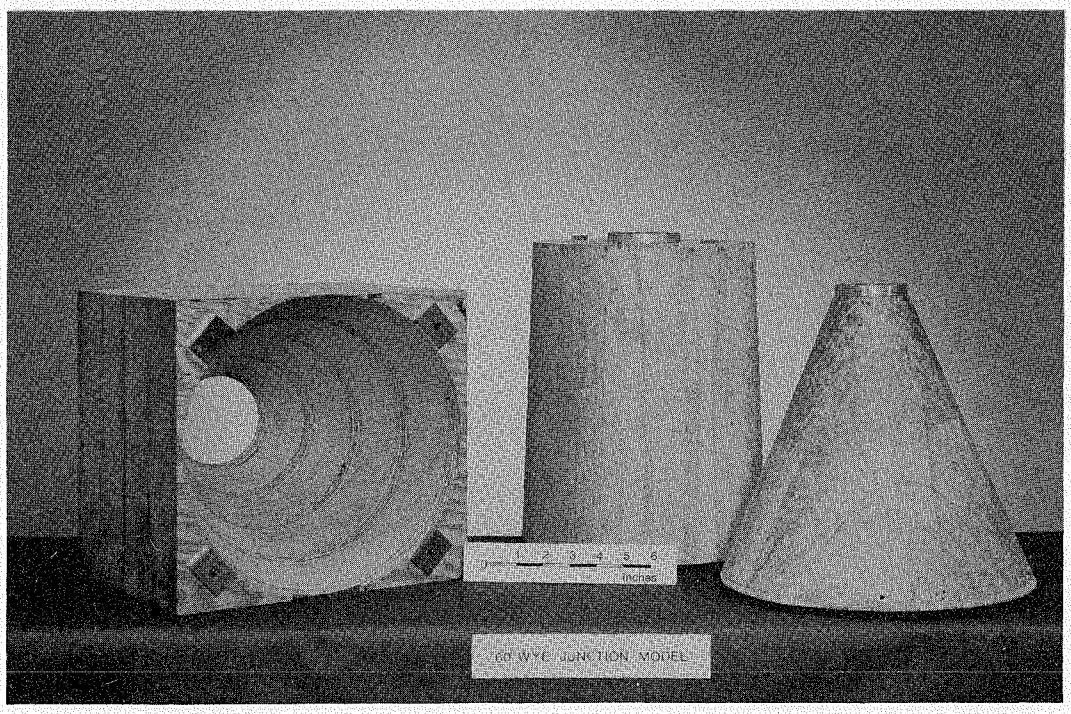

PLATE 4.1 WOODEN JIGS FORMING MAIN PIPE AND BRANCH PIPE

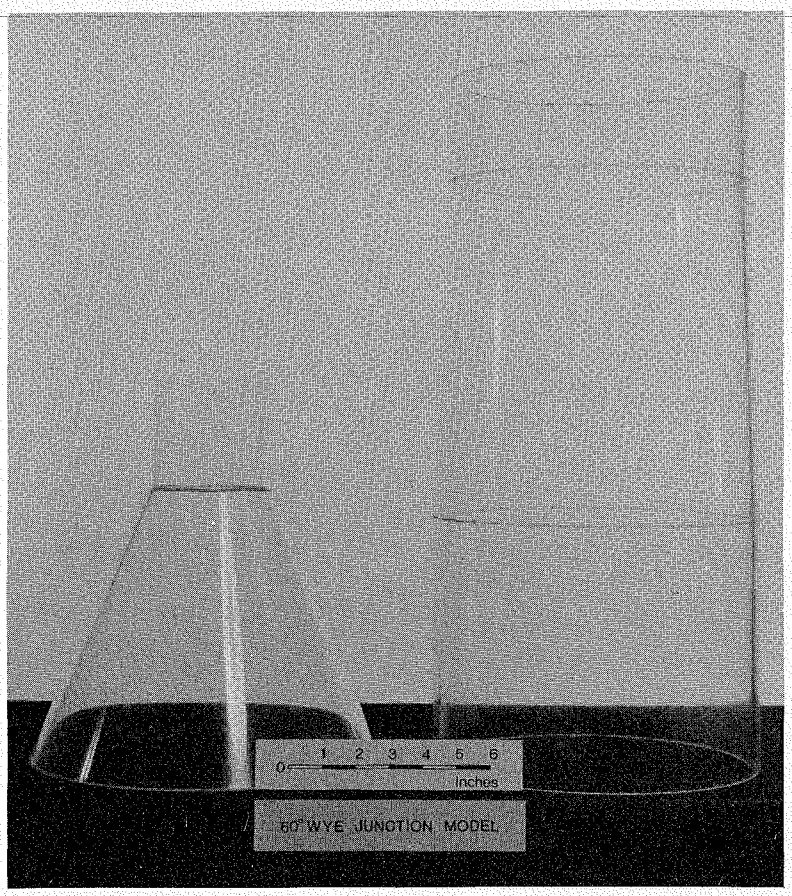

PLATE 4.2 MAIN PIPE AND BRANCH PIPE COMPONENTS

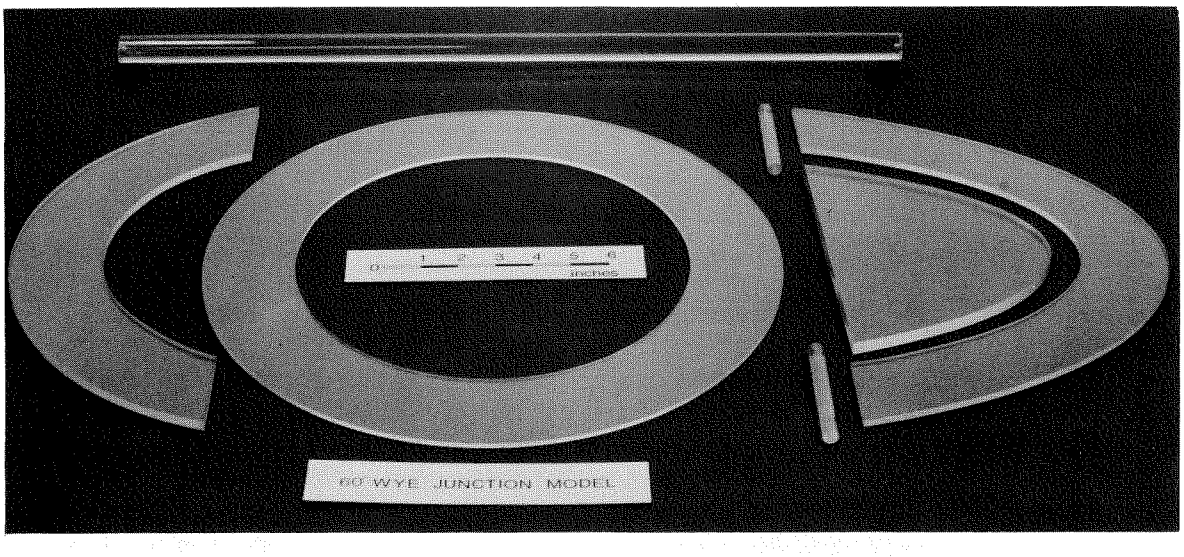

PLATE 4.3 STIFFENER COMPONENTS

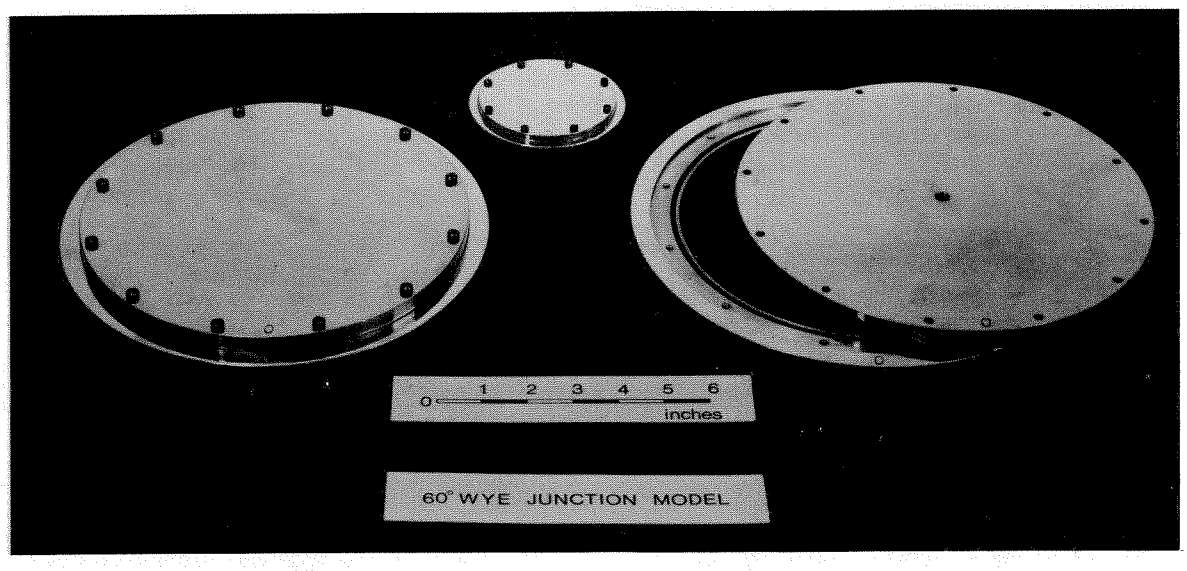

PLATE 4.4 BULKHEADS

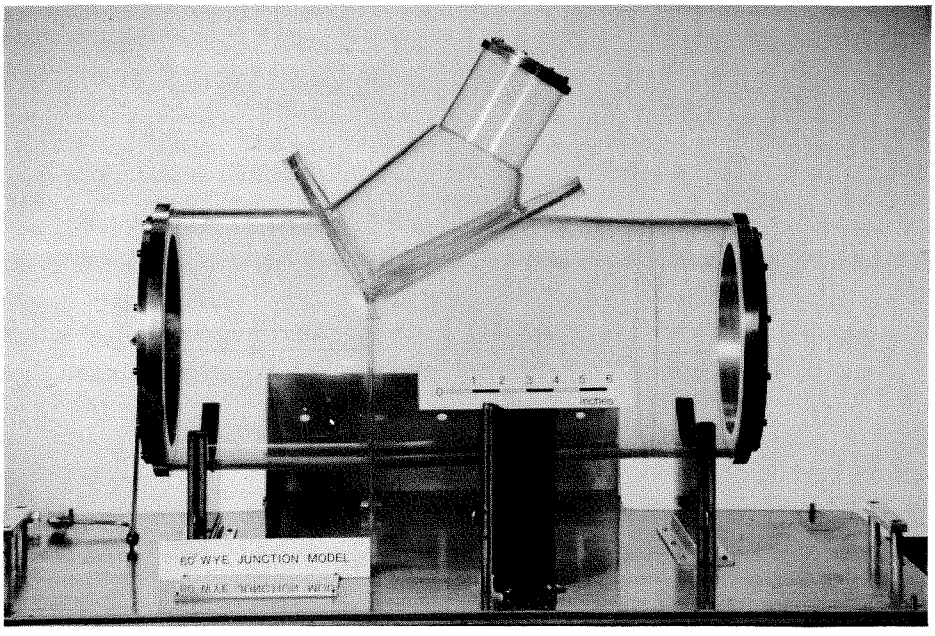

PLATE 4.5 ASSEMBLED 60° WYE-JUNCTION MODEL

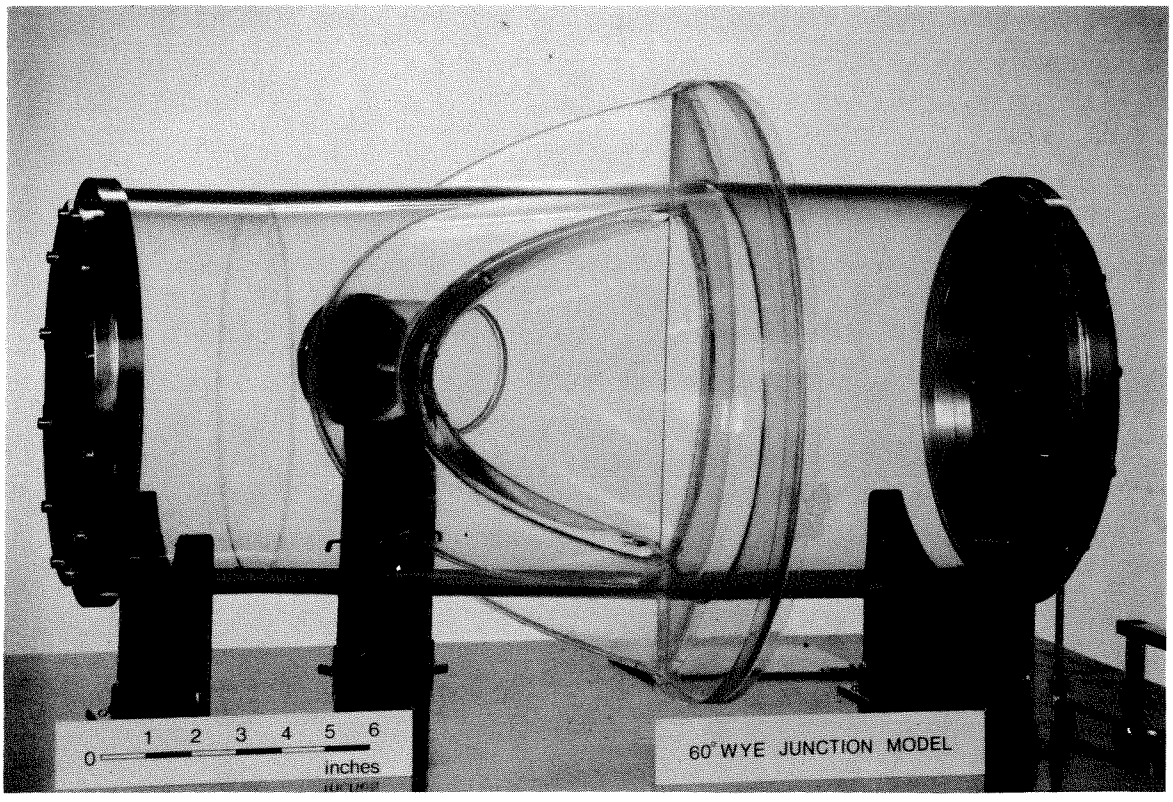

PLATE 4.6 60° WYE-JUNCTION MODEL SHOWING FULL SPLITTER-PLATE GEOMETRY

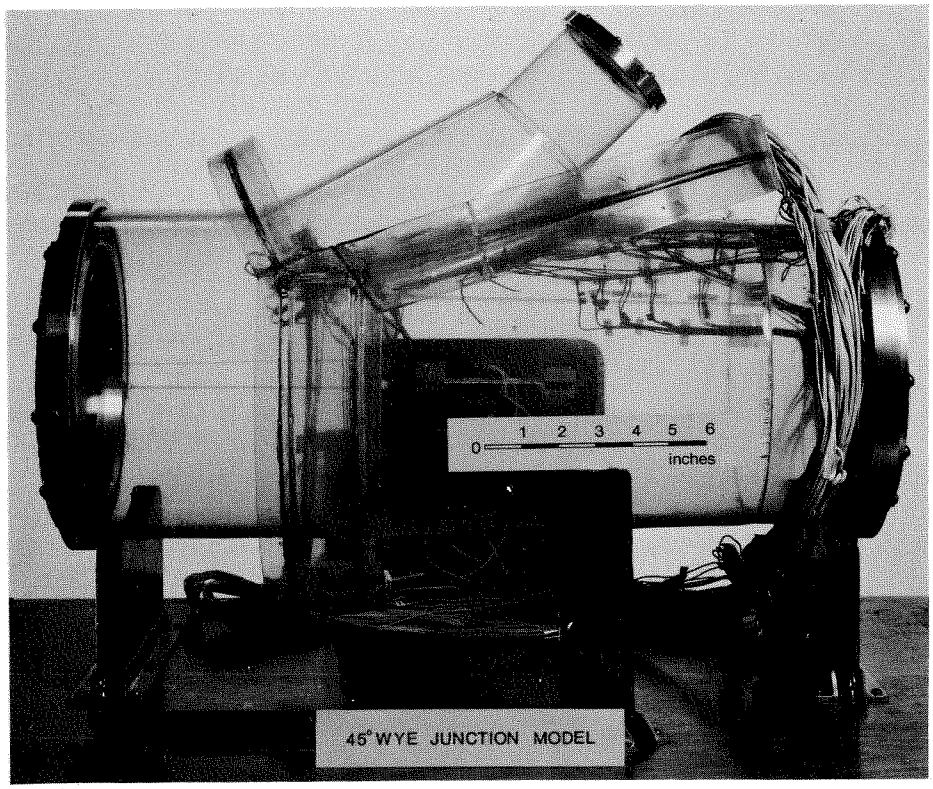

PLATE 4.7 ASSEMBLED 45° WYE-JUNCTION MODEL WITH INSTRUMENTATION

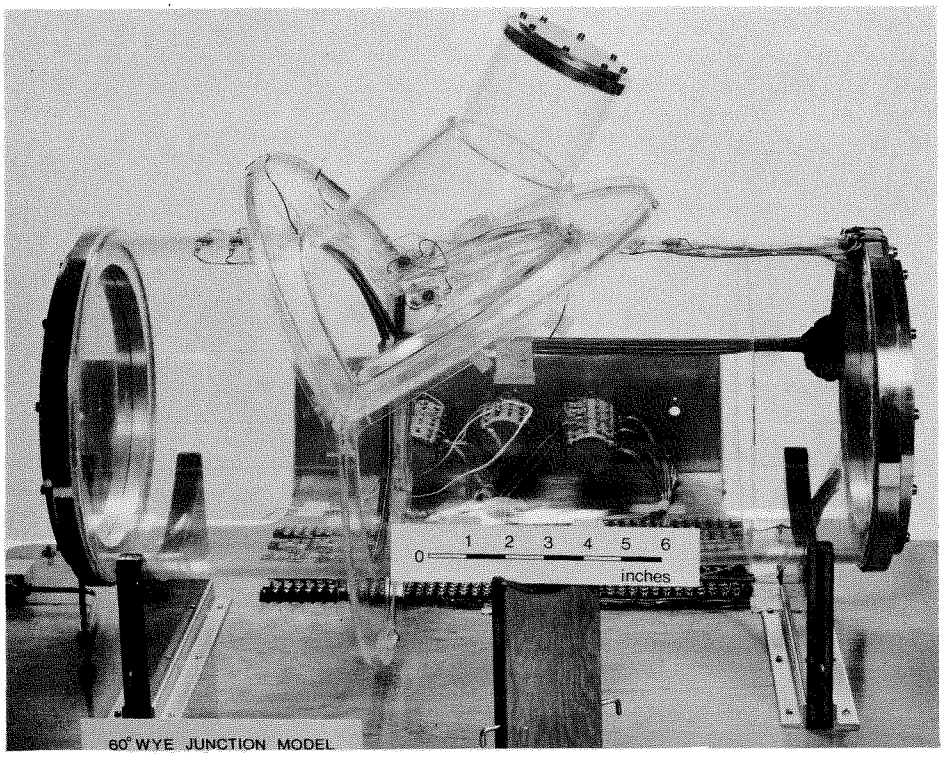

PLATE 4.8 ASSEMBLED 60° WYE-JUNCTION MODEL WITH INSTRUMENTATION

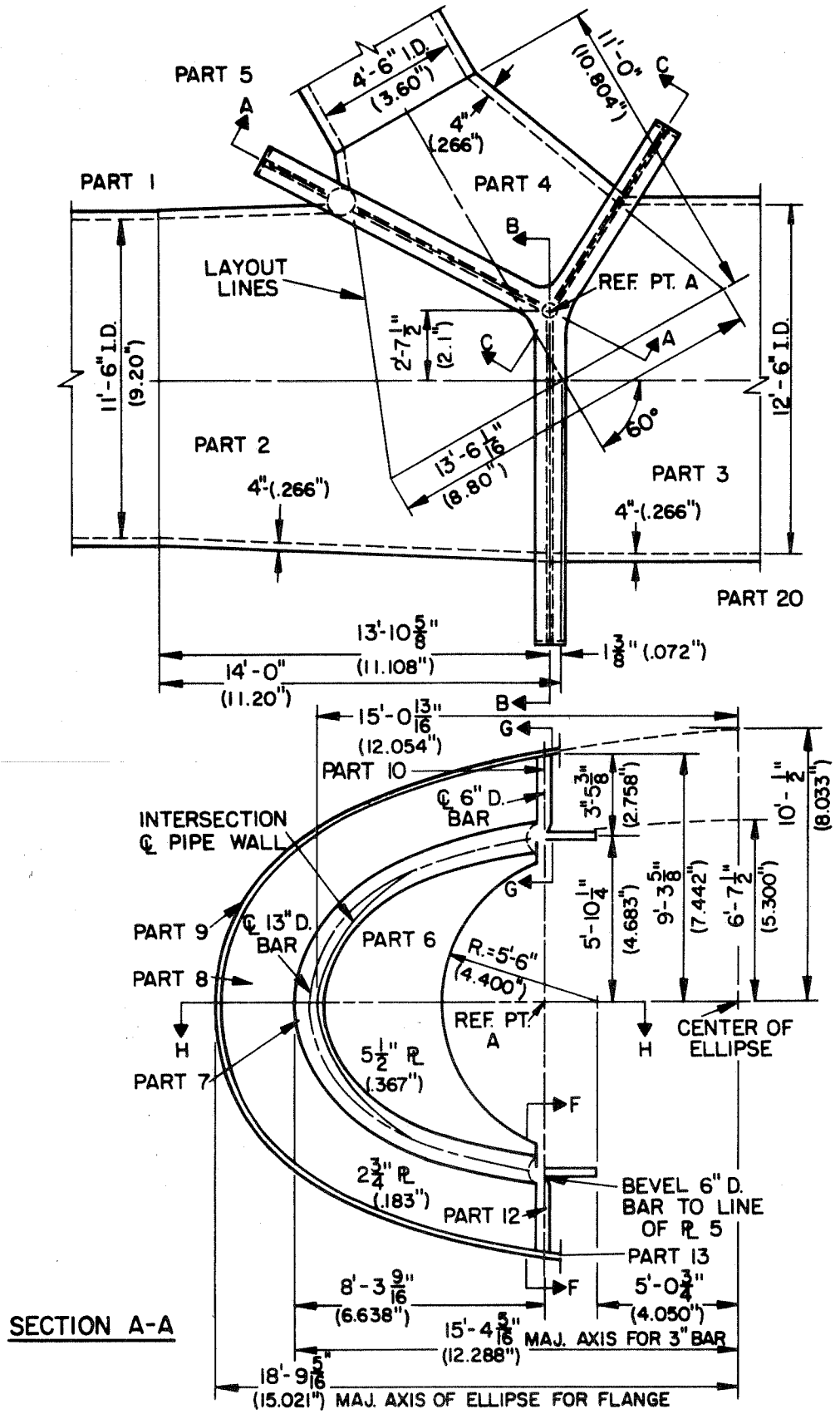

SECTION A-A

FIG. 4.1 60° WYE-JUNCTION, PROTOTYPE AND (MODEL) DIMENSIONS

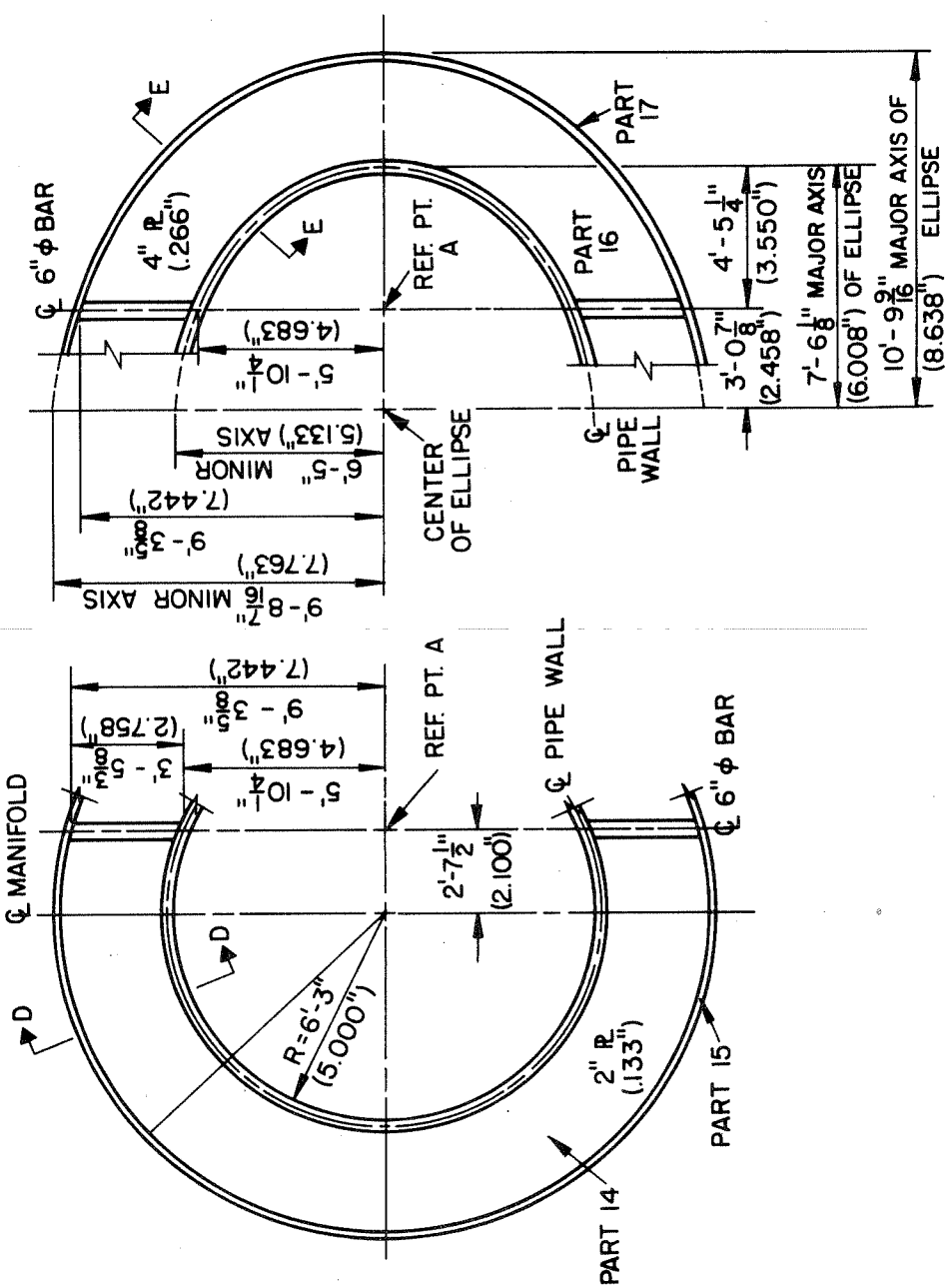

SECTION B-B
1" = 5'-0"

SECTION C-C
1" = 5'-0"

FIG. 4.2 60° WYE-JUNCTION, PROTOTYPE AND (MODEL) DIMENSIONS

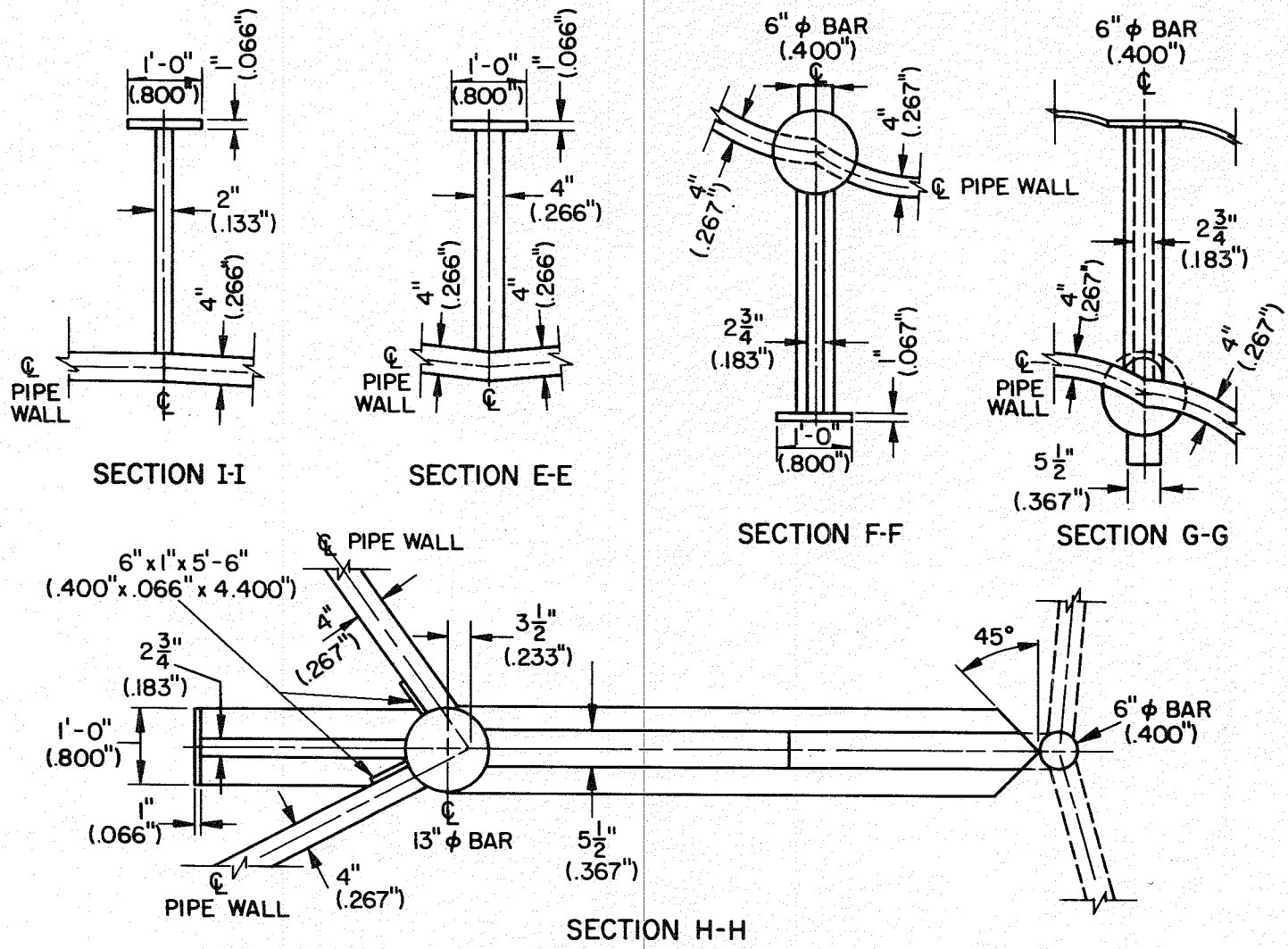

FIG. 4.3 60° WYE - JUNCTION, PROTOTYPE AND (MODEL) DIMENSIONS

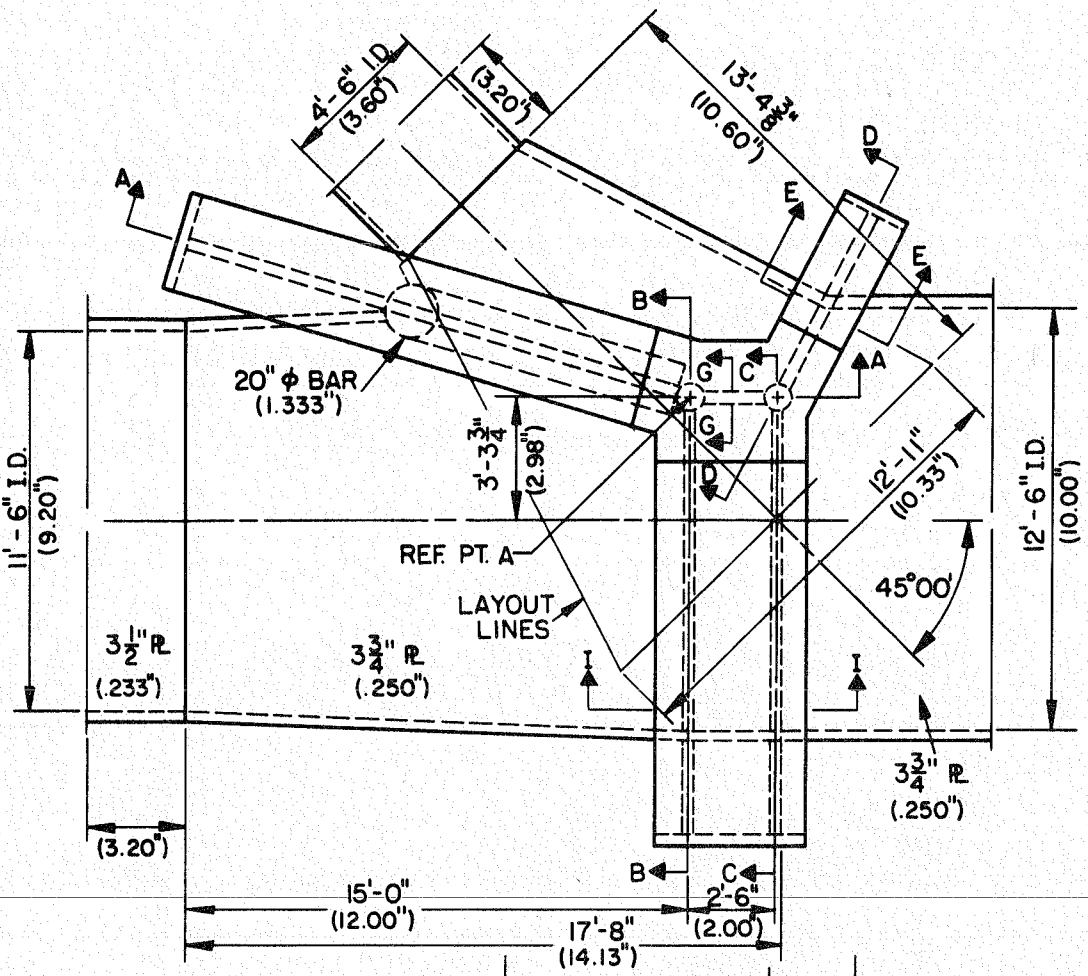

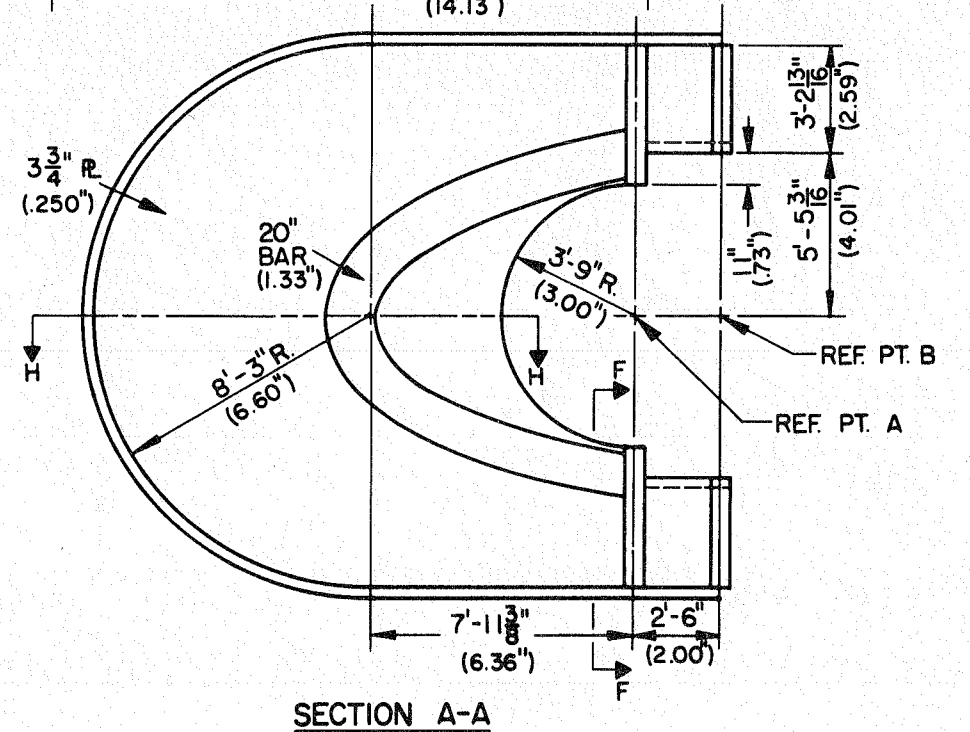

SECTION A-A

FIG. 4.4 45° WYE-JUNCTION, PROTOTYPE AND (MODEL) DIMENSIONS

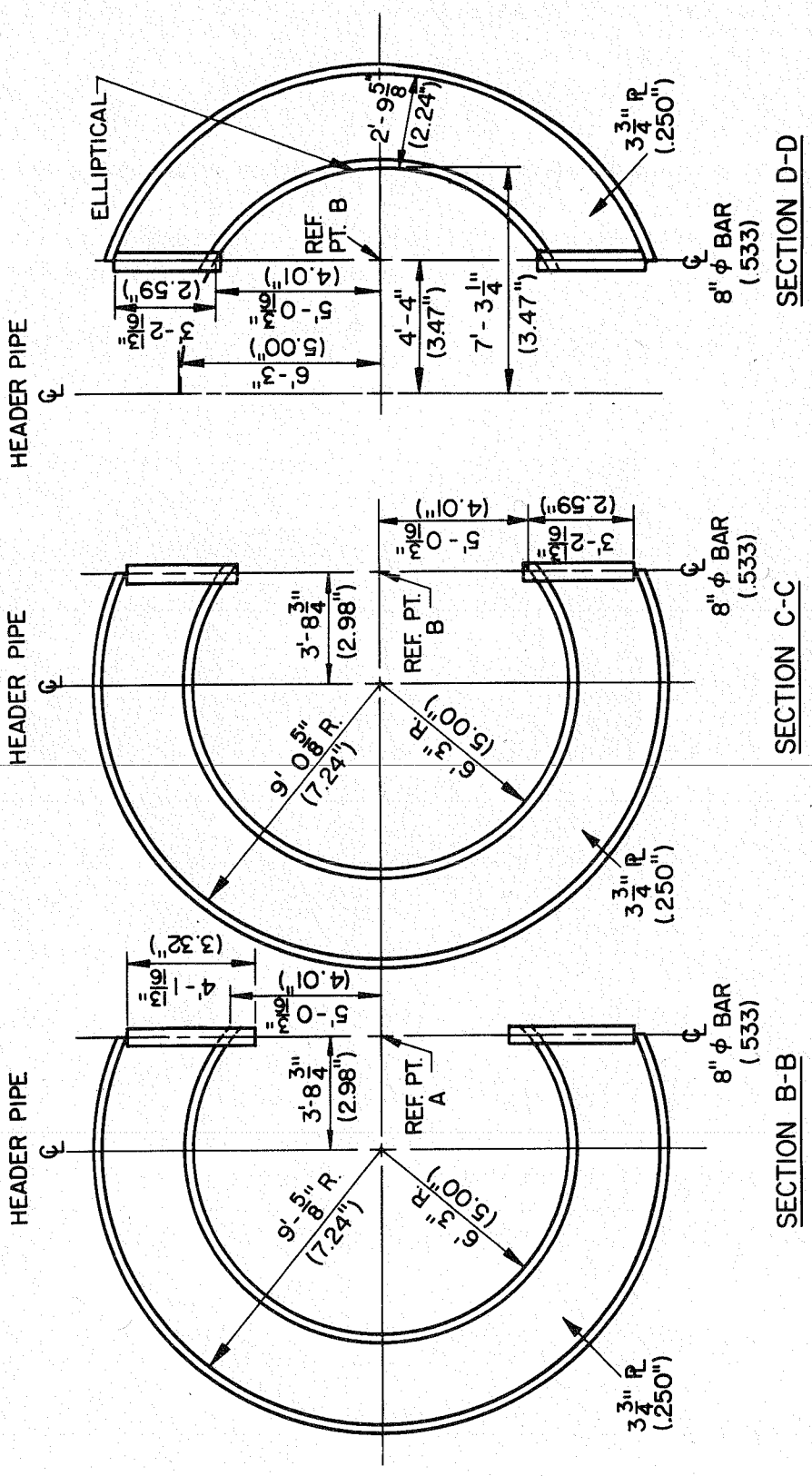

FIG. 4.5 45° WYE - JUNCTION, PROTOTYPE AND (MODEL) DIMENSIONS

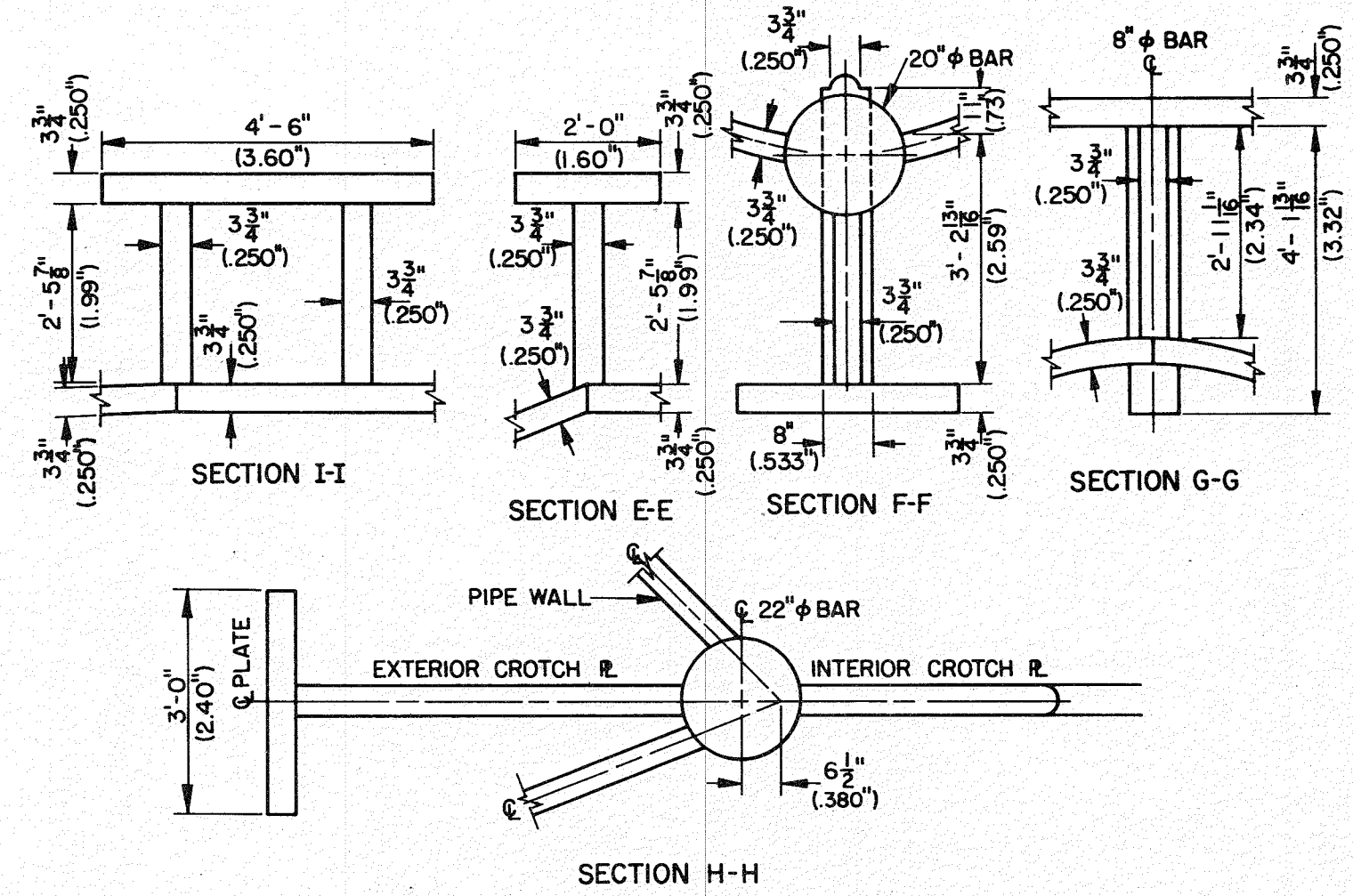

FIG. 4.6 45° WYE-JUNCTION, PROTOTYPE AND (MODEL) DIMENSIONS

V TESTING PROCEDURE

5.1 Instrumentation

One-element, two-element, and three-element foil gages were used for strain measurement. All strain gages were type 040-121-120 by Budd Instruments. These gages are temperature compensated for plastics with a coefficient of linear expansion of 40 μin/in/°F. GA-1 cement by Budd was used for fixing the gages and Freon was used for conditioning the surface. The choice of one-element, two-element or delta rosettes depended upon the state of stress at the gage locations.

Three inside dummy gages were used with the inside gages and three outside dummies with the outside gages. The dummies were arranged so that when strain readings were taken in numerical sequence no dummy was used more frequently than every fourth time. Silver contact switches were used in the bridge circuit.

5.2 Pressure Application and Measurement

As discussed in Chapter III, on account of the temperature sensitivity of material properties, it is desirable to keep plastic models under constant environmental conditions. This also minimizes the problem of zero drift in the strain gages which was found to be necessary in spite of the fact that temperature compensated gages were used, as well as both inside and outside dummy gages.

It was initially considered important to study and control the temperature rise inside the model due to pressurizing. To prevent the temperature rise as much as possible, air pressure was applied via an intermediate air tank under controlled temperature and pressure conditions.

With this procedure it can be arranged that the mixture of air inside the model has the same temperature before and after pressurizing. It was intended that this device, which was earlier employed in tube coupon tests, be used for the model tests. However, initial tests on the 45° wye-junction model showed that the temperature rise due to pressurizing was small considering the procedure used and the resulting zero drift in the gages was negligible. It was therefore considered unnecessary to resort to this procedure and the final procedure adopted is shown in Fig. 5.1.

A hand pump was used for pressure application; this gave the necessary control of the rate of pressure application. Pressure was measured by a mercury manometer. To maintain constant environmental conditions during the test, the model was enclosed in a plexiglas chamber (Plate 7.1). To measure the temperature variations, thermometers were located both inside and outside the model.

5.3 Strain Measurement

For the 45° wye-junction model, strains were recorded on a portable strain indicator using a 5 volt rms input. For the 60° wye-junction, a Budd (model P-350, 1.5 volt rms input) strain indicator was used. The change in the instrument was prompted by the fact that the input voltage of the latter is lower, giving a better thermal stability and a shorter waiting period for the readings to stabilize. Also, strain readings could be taken to a greater accuracy, 2 μin/in. as against 10 μin/in.

5.4 Test Procedure

For both models, the initial phase of testing consisted in checking the stability characteristics of each gage element. It was found necessary to subject the models to approximately 10 load cycles to half design pressure to stabilize the gage elements. An element was considered to be stabilized if the zero reading of the gage before and after loading was within 10 μin/in.

The pressure applied to the model was restricted in order to keep the observed strains within 1000 μin/in. The rate of application and release of pressure was kept low. The temperature variation due to pressure change could thus be limited to within ± 1°F.

The standard temperature for the coupon test was 75°F and as far as possible, the models were tested at this temperature. When this was not possible, a correction was made to the results according to Fig. 5.2. The figure shows the values of E_t/E_{75} plotted against temperature at two high strain reference points in the model.

At all gage locations, strains were taken for incremental pressure values. Zero readings were taken immediately before and after each pressure increment to minimize drift.

All high strain points were studied for structural linearity by plotting strain-pressure graphs for 1.0 psi pressure increments.

The above procedure gave a variation in strain readings, as taken from the slope of the strain-pressure graph, within ± 1% referred to the maximum strain value measured in the model.

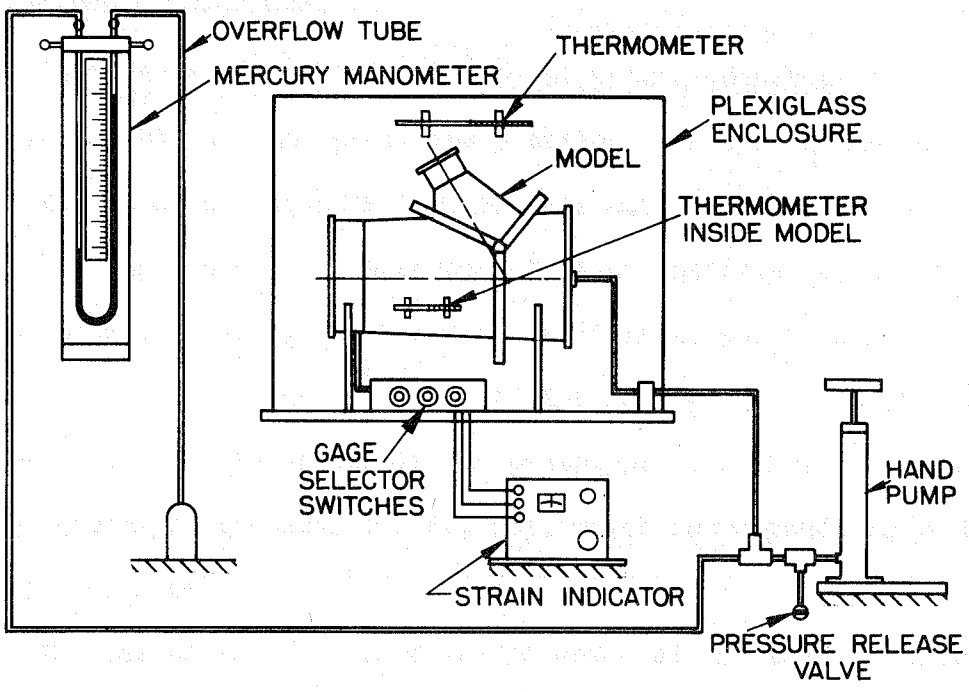

FIG. 5.1 EXPERIMENTAL SET-UP

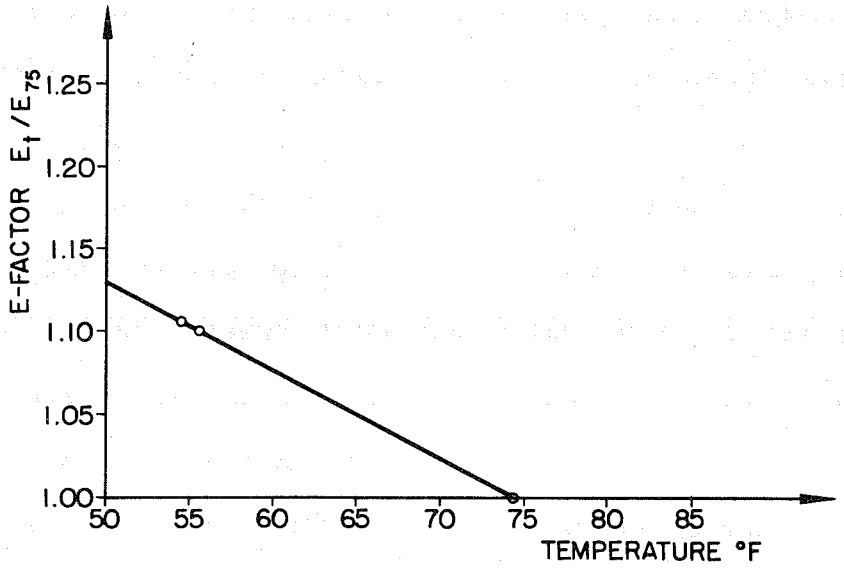

FIG. 5.2 VARIATION OF ELASTIC MODULUS OF PLEXIGLAS WITH TEMPERATURE

VI TEST SERIES I - 45° WYE-JUNCTION

6.1 Design of the Structure

Test Series I consisted of the structural behavior of the 45° wye-junction. This was the preliminary design, the development of the final 60° design being based in part on this data.

The basic design is according to that specified by the Department of Water Resources, State of California, and is shown in Figs. 4.4 through 4.6. The thickness of the tube walls, stiffener webs and flanges, and splitter-plate in the prototype is 3.75 in. throughout. The design prototype pressure is 1050 psi, which corresponds to 15.00 psi pressure in the model.

The design is a standard one in which all of the stiffeners, except the splitter-plate, are external to the tube. In Test Series I, three designs were studied, the differences in the designs being in the configurations of the splitter-plate; these were respectively full splitter-plate design, partial splitter-plate design, and design without splitter-plate.

The full splitter-plate design is shown in Fig. 6.1. In this design the free edge of the splitter-plate is vertical, and the splitter-plate provides maximum stiffening at the joint. In the partial splitter-plate design the free edge of the splitter-plate has a semi-circular cut-out with a prototype radius of 3 ft. 9 in., as shown in Fig. 6.3 and Plate 4.8. The stiffening effects of the splitter-plate are therefore reduced and the effectiveness of the external stiffeners increased. The design without splitter-plate is shown in Fig. 6.4. In this case all the stiffening is provided by the solid bar and the external stiffeners.

From these three variations in splitter-plate design, the effect of the geometry of the splitter-plate on the structural behavior of the whole system was studied by model.

6.2 Test Procedure

Strains were measured at 44 locations using 83 gage elements as shown in Figs. 6.5 and 6.6.

(a) Full splitter-plate design.

The full splitter-plate design was studied first. Strain data was taken at pressures of 3.75, 7.50, and 11.25 psi. This corresponds to 1/4, 1/2, and 3/4 of the design pressure respectively. Three sets of observations were taken for each of these pressures to study the consistency of observations. In addition to these observations, strain readings were taken at pressure increments of 1.0 psi at 17 gage points. This was to study the linearity of the structure at locations of high strain and at gage elements which even after repeated load applications indicated zero drift of more than 10 μin/in.

(b) Partial splitter-plate design.

For testing the partial splitter-plate design, a 3 in. radius cut-out was made in the full splitter-plate. This was done by attaching a semicircular template to the splitter-plate, machining, and hand-finishing to the desired dimensions.

For the partial splitter-plate model, strain data was taken at pressures of 5.00 and 7.50 psi. Because of high stresses along the free edge of the splitter-plate, it was not considered advisable to test the model at higher pressures. In this case detailed linearity

tests using pressure increments of 1.00 psi. were carried out for 13 gage points.

(c) Design without splitter-plate

To study this design, the splitter-plate was removed by machining the surface along the solid rod and hand finishing. Due to very high stresses at gage location 13, the maximum pressure was limited to 5.00 psi. Detailed linearity tests were made at 11 gage points.

Strain-pressure graphs at representative gage points are given in Figs 6.23 through 6.25. The gage locations are given in Figs 6.5 and 6.6. Reduced stress data at all gage locations is given in graphical form in Figs 6.7 through 6.22. The results are also given in Tables 6.1 through 6.3.

6.3 Linearity

A study of the strain-pressure graphs of Fig. 6.23 for the various gage locations indicates that the full splitter-plate structure behaves essentially in a linear manner. At almost all gage locations, except those on the splitter-plate, the strain-pressure line goes through zero. The fact that some gages on the splitter-plate show linear behavior which does not pass through zero (gages 1, 2, and 3, Fig. 6.23) is possibly due to a slight initial curvature in the nominally straight splitter-plate. During the initial pressure increments, the curvature straightens and thereafter the plate behaves linearly. This effect is local and does not apparently affect the gages remote from the splitter-plate.

A study of the partial splitter-plate model (Figs. 6.24) and of the structure without splitter-plate (Figs. 6.25) indicates that the structure behaves essentially linearly at all gage points where this was

studied. The linearity at gage point 6 (Fig. 6.24) which is at the mid-height of the partial splitter-plate design and is close to the free edge, indicates that the eccentricities of the plate in this area are negligible.

6.4 Reduction of Strain Data

For determining the strain values at design pressure, the slope of the strain-pressure graph was used in all cases. This means that the initial eccentricity effects discussed in Sec. 6.3 were eliminated. Strain data was reduced by computer to give principal prototype stresses at the full design pressure.

The reduced stress data corresponding to the gage locations shown in Figs. 6.5 and 6.6 is given in Tables 6.1 through 6.3. Stress distributions for the prototype structures along various cross-sections together with principal stresses at selected locations are plotted in Figs. 6.7 and 6.22.

6.5 Discussion

The stress distributions plotted in Figs. 6.7 through 6.11 indicate that the maximum stress in the full splitter-plate design is developed in the splitter plate. As shown in Fig. 6.7, the maximum stress occurs on the axis of symmetry, at the junction between the solid bar and the splitter-plate. It is interesting to note that the splitting stress along the axis of symmetry shows a drop from 19.3 ksi to 11.9 ksi between the solid bar and the free edge. This means that from the structural standpoint, the splitter-plate can be cut-back without appreciably increasing the maximum stress level in the structure.

The partial splitter-plate design (Fig. 6.12), indicates a steep rise in stress, from 20.2 ksi to 35.7 ksi, from the solid bar to the free edge of the splitter-plate. Clearly, from a purely structural standpoint, this is an excessive cut-back of the splitter-plate and there is a configuration between these two designs where the stress along the axis of symmetry of the plate is essentially constant.

It can also be noted from Figs. 6.7 and 6.12 that the stiffener in the plane of the splitter-plate external to the tube has a very small stress level and contributes little to the structural action of the system, irrespective of the geometry of the splitter-plate. This is also true in the case of the structure without the splitter-plate as shown in Fig. 6.18. It can therefore be concluded that this stiffener as designed has little structural action and that the splitting force is being taken primarily by the tension in the bar, the internal portion of the splitter-plate, and the shell action of the main pipe and the branch pipe. It will be noted that in the 60° design, the size of this external stiffener is greatly reduced.

A study of the stresses along sections BB and CC for the three model designs (Figs. 6.9, 6.10, 6.14, 6.15, 6.20 and 6.21) shows that the distributions along these sections are not significantly influenced by the splitter-plate geometry. The stresses along these sections are relatively small. The stresses at section DD, however, are higher and more sensitive to the change in splitter-plate geometry. In view of these observations, the number of external stiffeners in the 60° junction was reduced from 4 to 3, the prototype thickness of the web stiffener corresponding to sections AA and BB was reduced to 2.75 in.

and 2.00 in. respectively, and that of the stiffener web corresponding to section DD was increased to 4.00 in. The thickness of the stiffener flanges was reduced from 3.75 in. to 1.00 in. throughout.

Figs. 6.11 and 6.17 show the tube wall stresses on the axis of symmetry in the vicinity of the solid bar. The theoretical thick-wall stresses neglecting the effect of discontinuity are also given. These stress distributions indicate that the effect of the junction on the tube wall stress is local and dies out in the prototype between 2ft. and 2 ft. 6 in. from the solid bar. This is valid for the full and partial splitter-plate designs. Also the hoop stresses in the tube wall are essentially the standard thick-wall stresses. However, in the case of the design without splitter-plate (Fig. 6.22), the effect of the discontinuity does not die out even within the taper and significant bending moments are introduced in the tube wall.

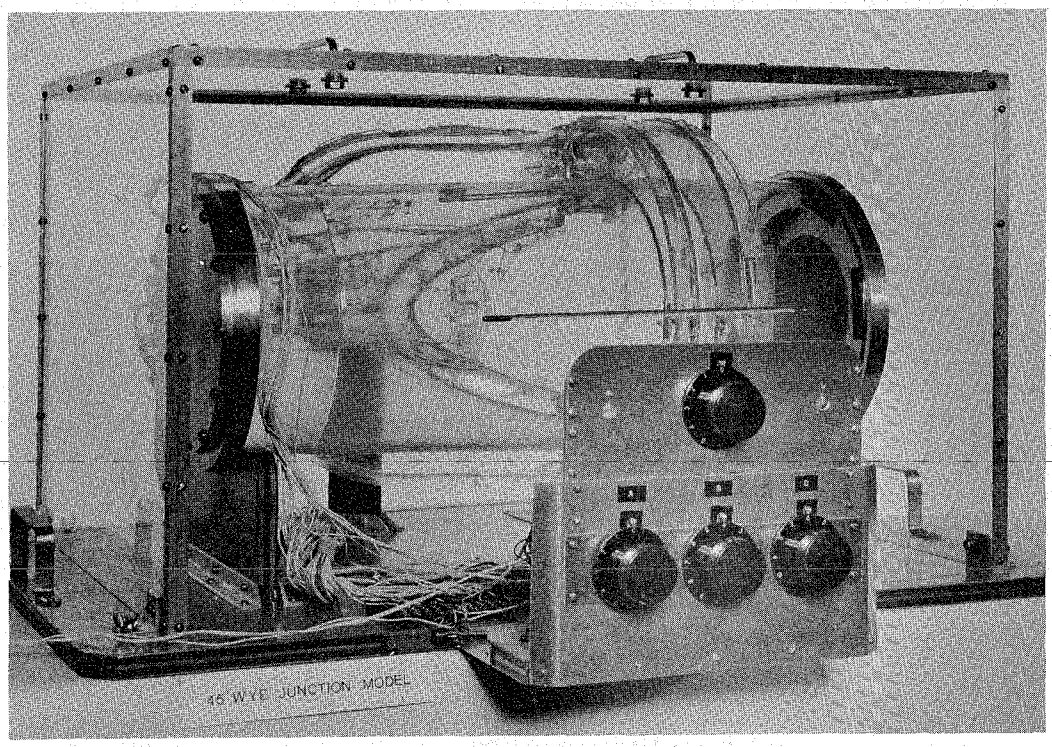

PLATE 6.1 45° WYE-JUNCTION WITH PARTIAL SPLITTER-PLATE UNDER TEST

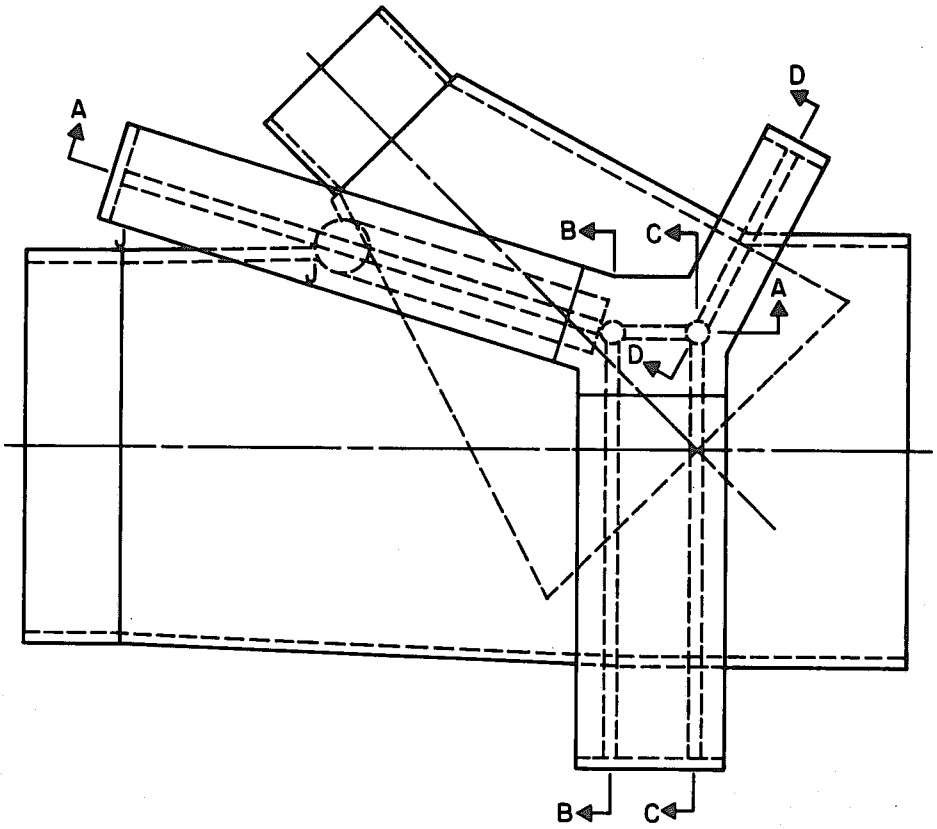

FIG. 6.1 SECTION REFERENCES FOR 45° WYE-JUNCTION MODEL.

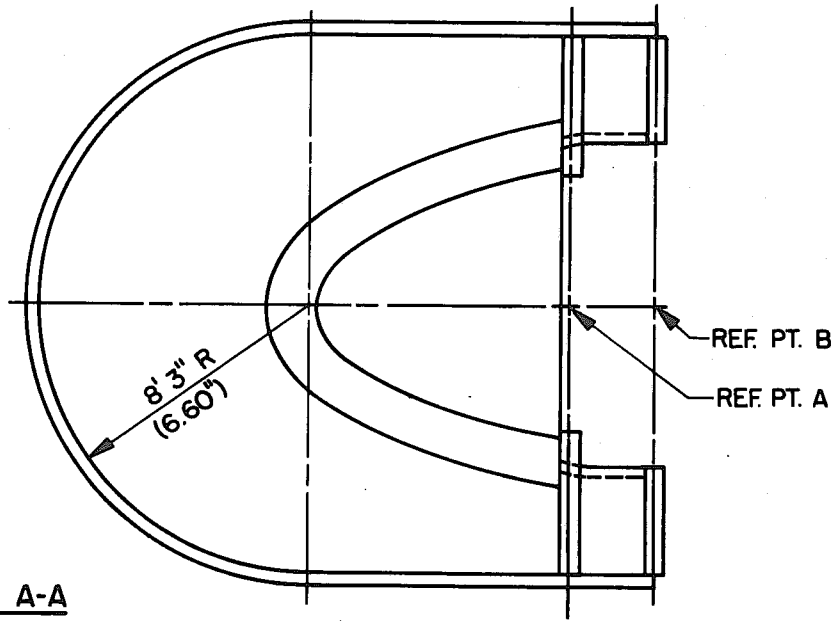

SECTION A-A

FIG. 6.2 45° WYE-JUNCTION WITH FULL SPLITTER PLATE

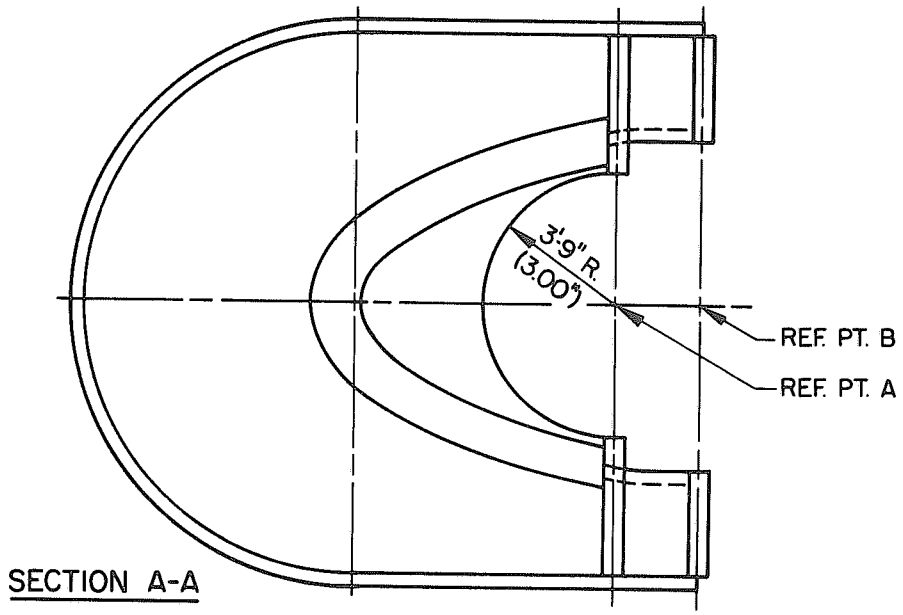

FIG. 6.3 45° WYE-JUNCTION WITH PARTIAL SPLITTER PLATE

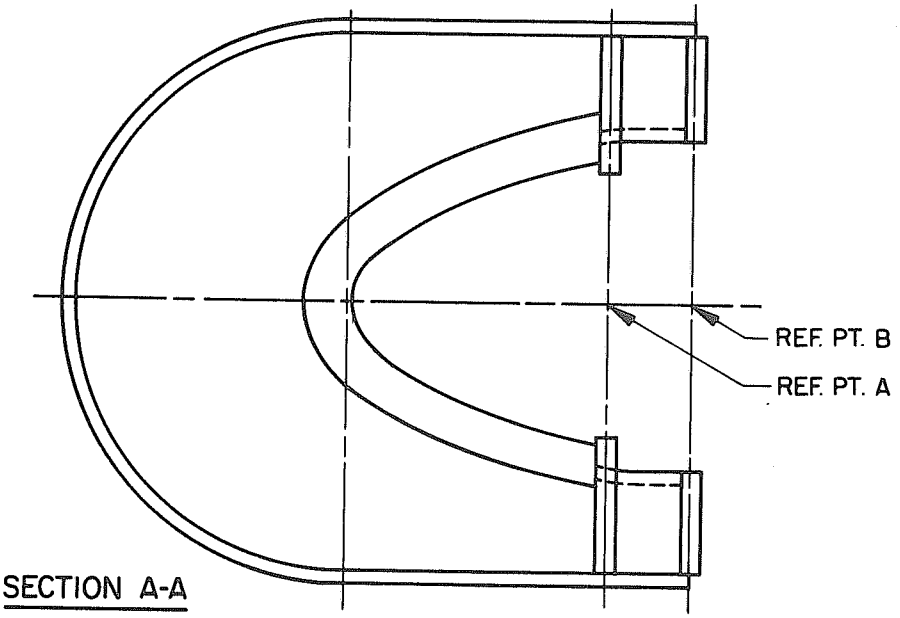

FIG. 6.4 45° WYE-JUNCTION WITHOUT SPLITTER PLATE

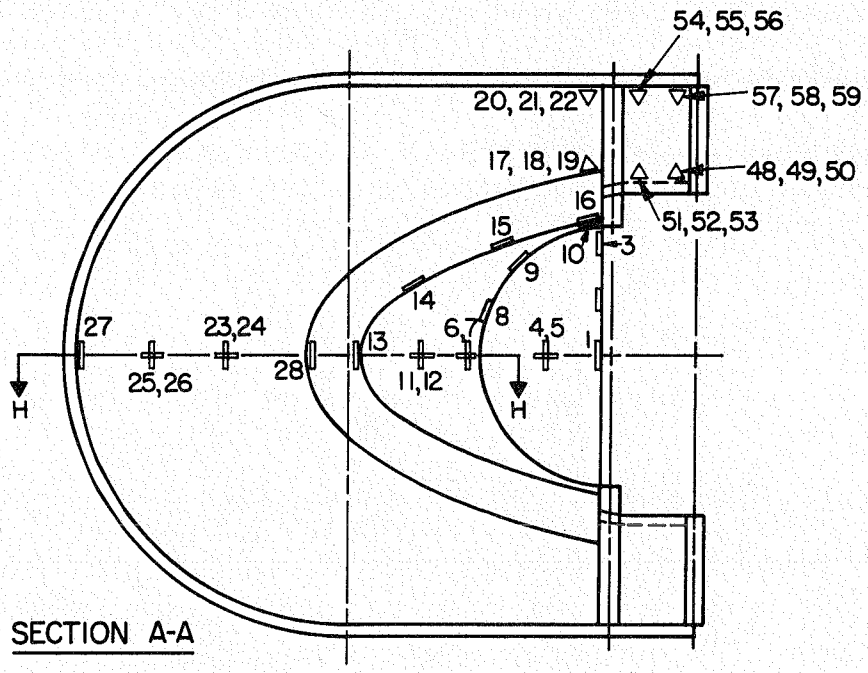

GAGE NUMBERING:

2-ELEMENT GAGES:

FIRST NUMBER FOR ELEMENT PARALLEL TO TUBE AXIS.

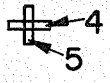

3-ELEMENT (DELTA) GAGES:

FIRST NUMBER FOR ELEMENT THUS ▭.
OTHER ELEMENTS NUMBERED CLOCKWISE.

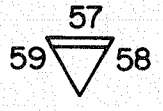

PRINCIPAL STRESSES:

DIRECTION OF PRINCIPAL STRESS GIVEN COUNTER-CLOCKWISE REFERRED TO FIRST ELEMENT.

ALL STRESSES GIVEN IN ksi

FIG. 6.5 GAGE LOCATIONS FOR 45° WYE-JUNCTION MODEL

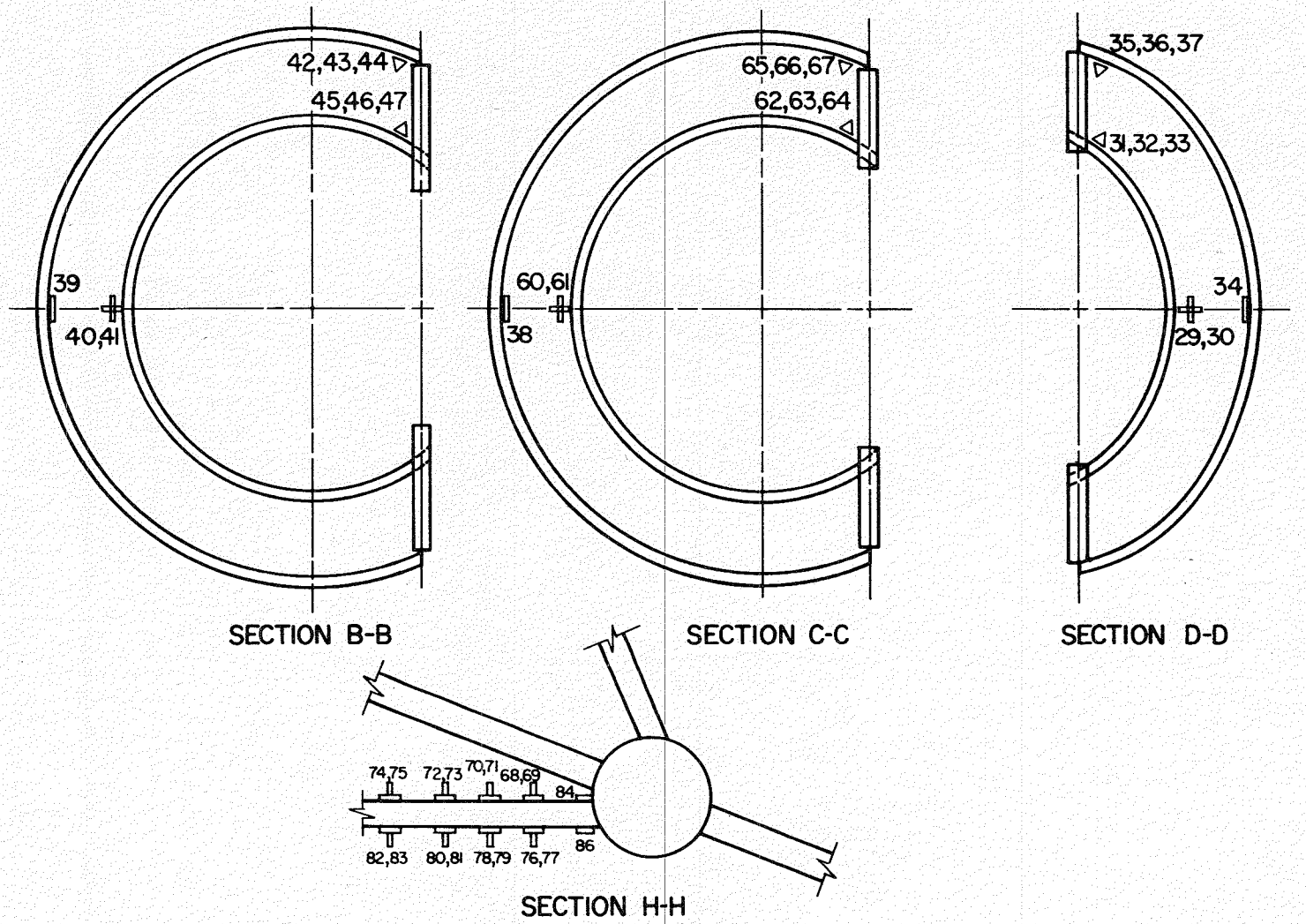

FIG. 6.6 GAGE LOCATIONS FOR 45° WYE-JUNCTION MODEL

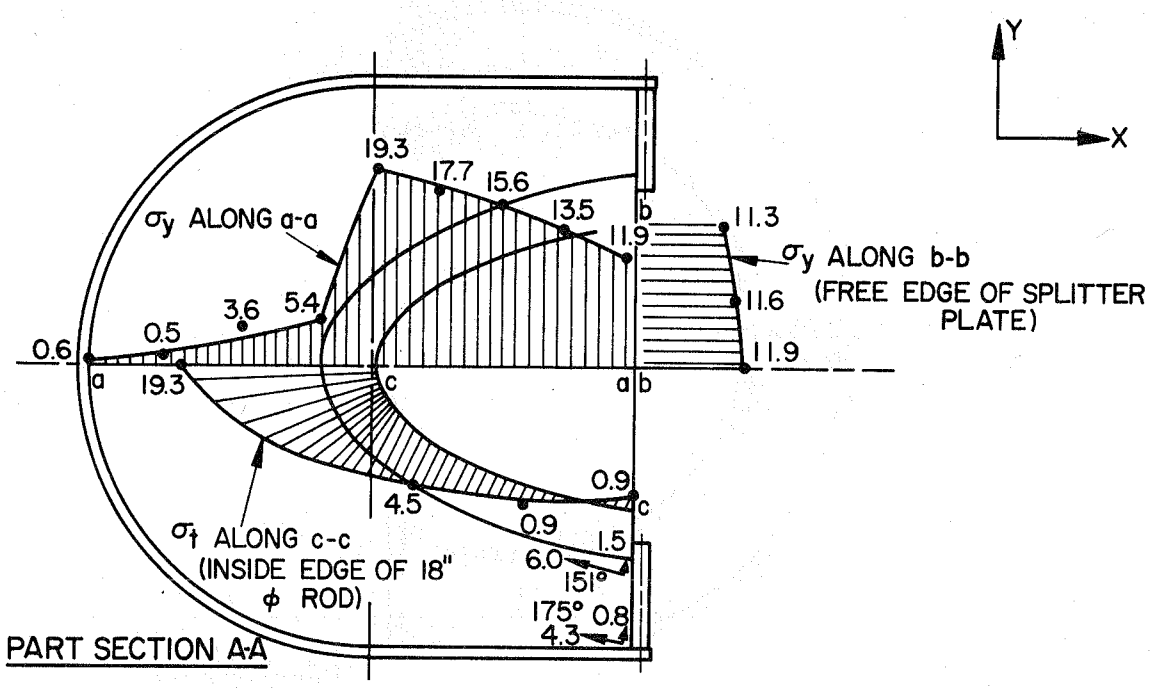

FIG. 6.7 PROTOTYPE STRESSES (KSI) AT 1050 PSI PRESSURE FOR 45° WYE-JUNCTION MODEL WITH FULL SPLITTER PLATE

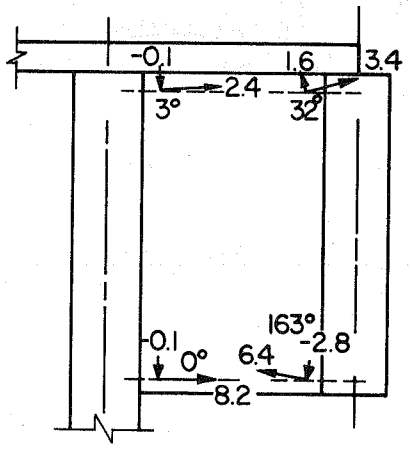

FIG. 6.8 PROTOTYPE STRESSES (KSI) AT 1050 PSI PRESSURE FOR 45° WYE-JUNCTION MODEL WITH FULL SPLITTER PLATE

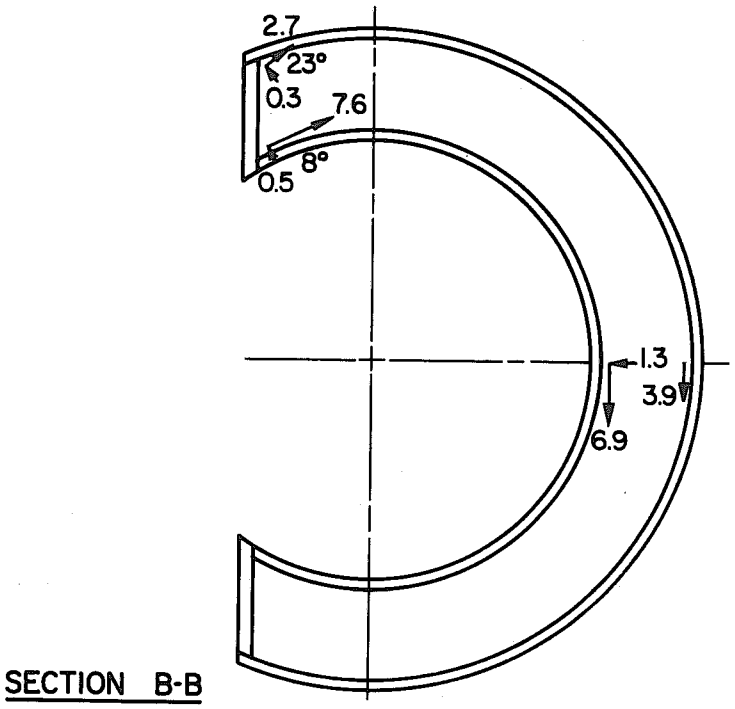

FIG. 6.9 PROTOTYPE STRESSES (KSI) AT 1050 PSI PRESSURE FOR 45° WYE-JUNCTION MODEL WITH FULL SPLITTER PLATE

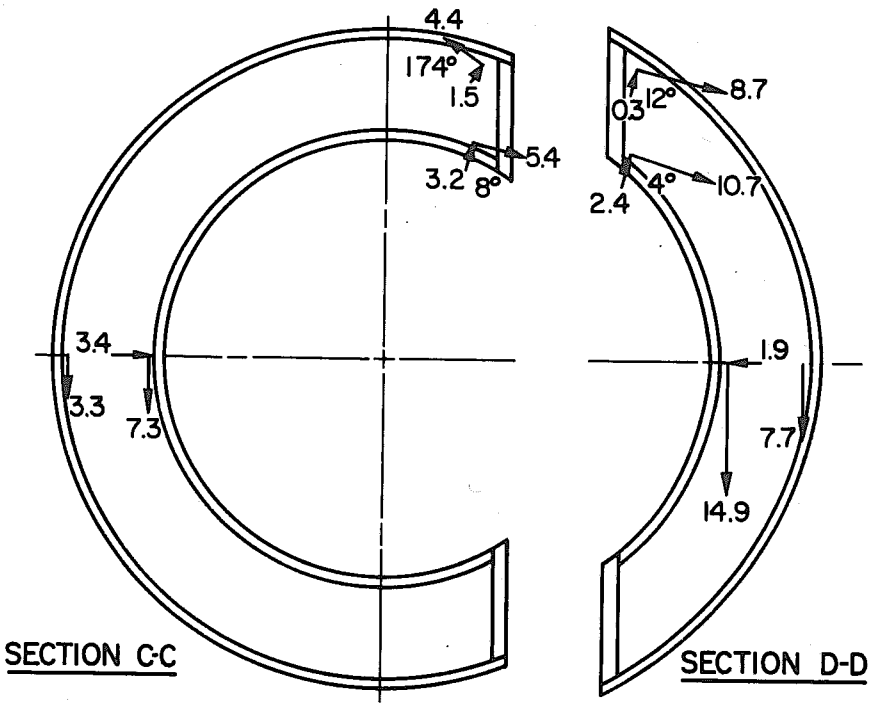

FIG. 6.10 PROTOTYPE STRESSES (KSI) AT 1050 PSI PRESSURE FOR 45° WYE-JUNCTION MODEL WITH FULL SPLITTER PLATE

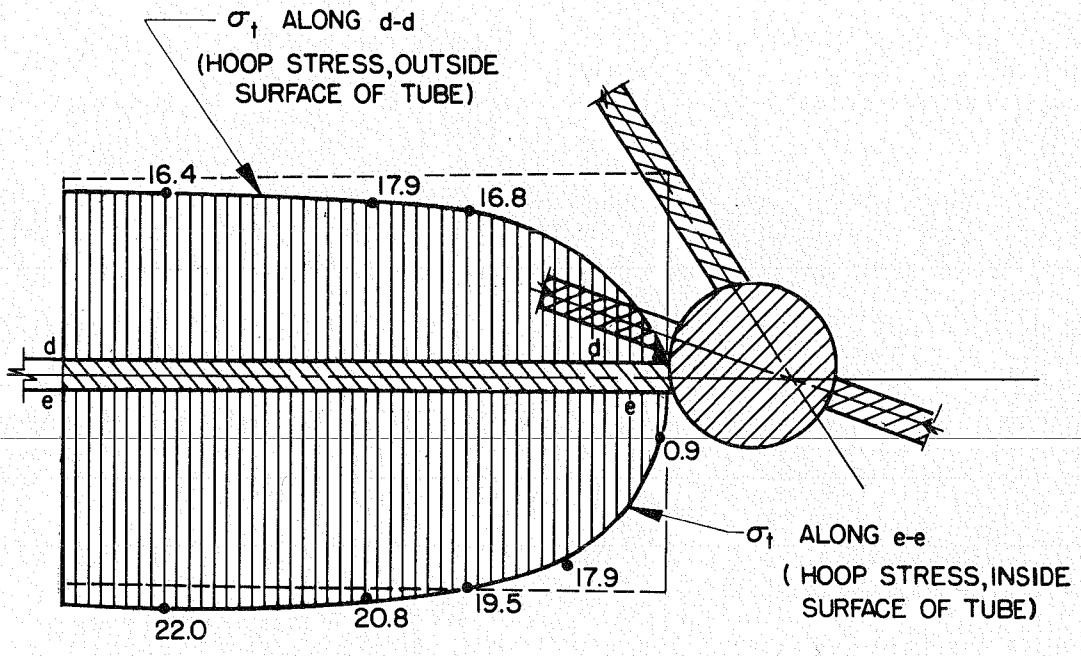

FIG. 6.11 PROTOTYPE STRESSES (KSI) AT 1050 PSI PRESSURE FOR 45° WYE-JUNCTION MODEL WITH FULL SPLITTER PLATE

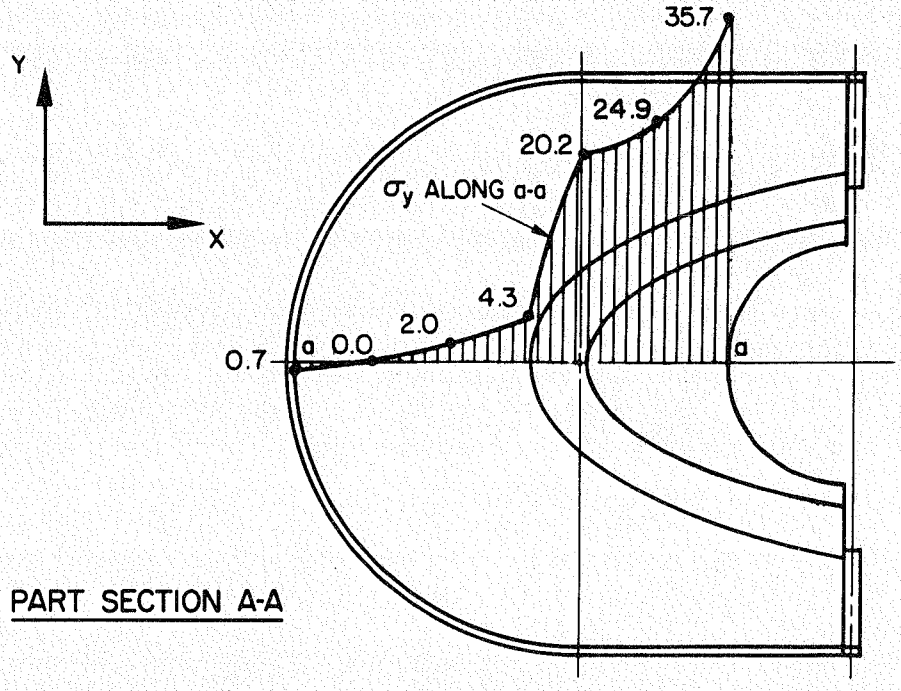

FIG. 6.12 PROTOTYPE STRESSES (KSI) AT 1050 PSI PRESSURE FOR 45° WYE - JUNCTION MODEL WITH PARTIAL SPLITTER PLATE

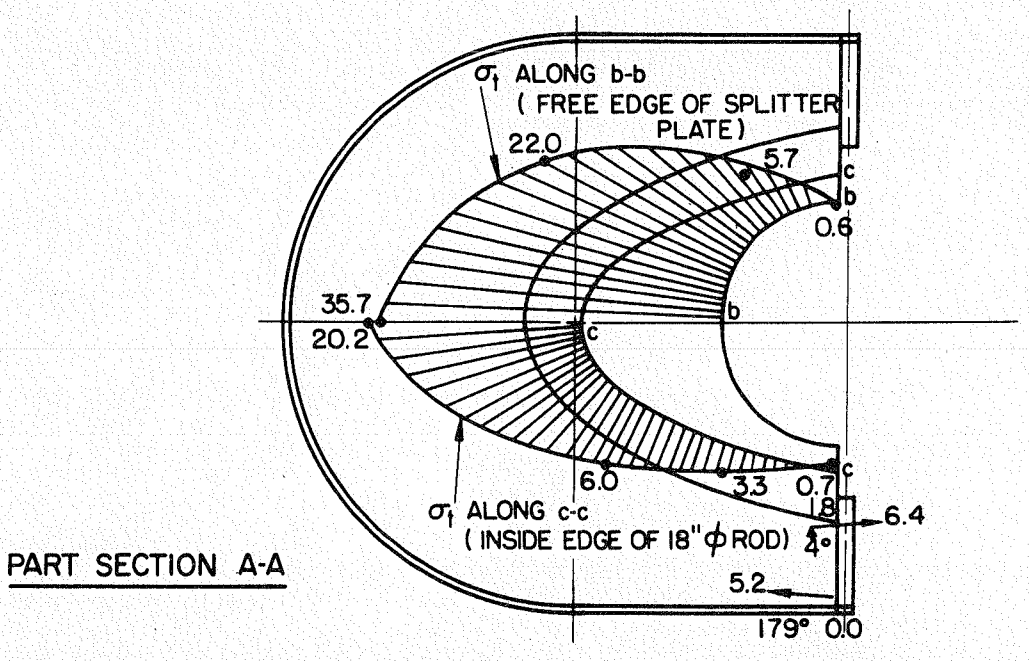

FIG. 6.13 PROTOTYPE STRESSES (KSI) AT 1050 PSI PRESSURE FOR 45° WYE - JUNCTION MODEL WITH PARTIAL SPLITTER PLATE

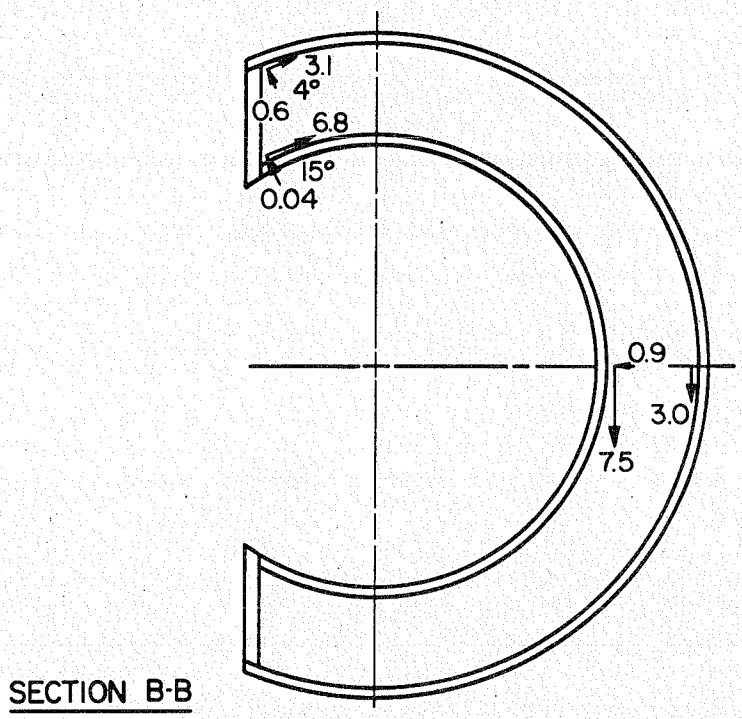

FIG. 6.14 PROTOTYPE STRESSES (KSI) AT 1050 PSI PRESSURE FOR 45° WYE-JUNCTION MODEL WITH PARTIAL SPLITTER PLATE

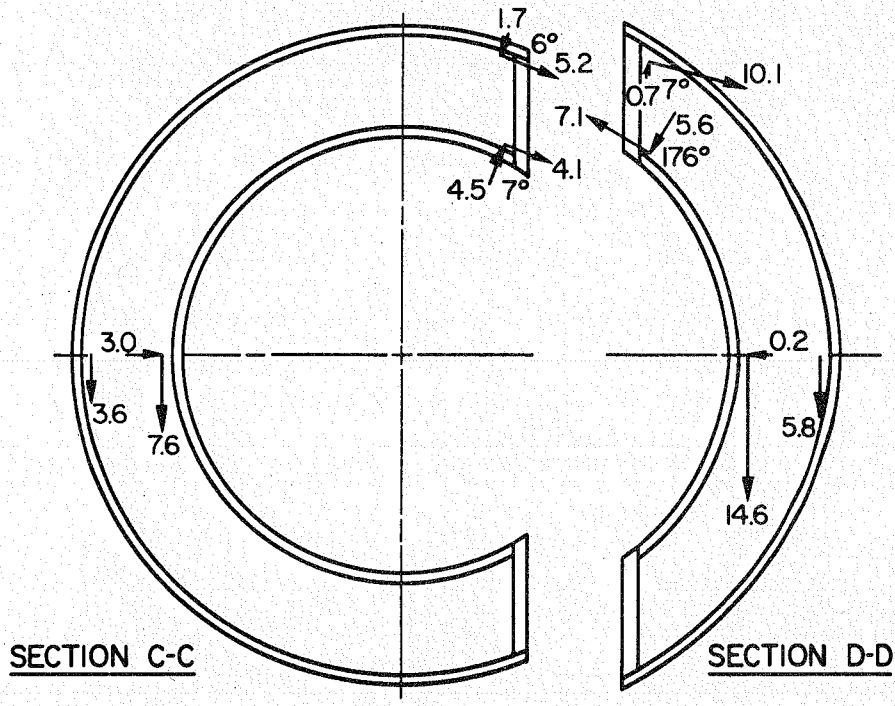

FIG. 6.15 PROTOTYPE STRESSES (KSI) AT 1050 PSI PRESSURE FOR 45° WYE-JUNCTION MODEL WITH PARTIAL SPLITTER PLATE

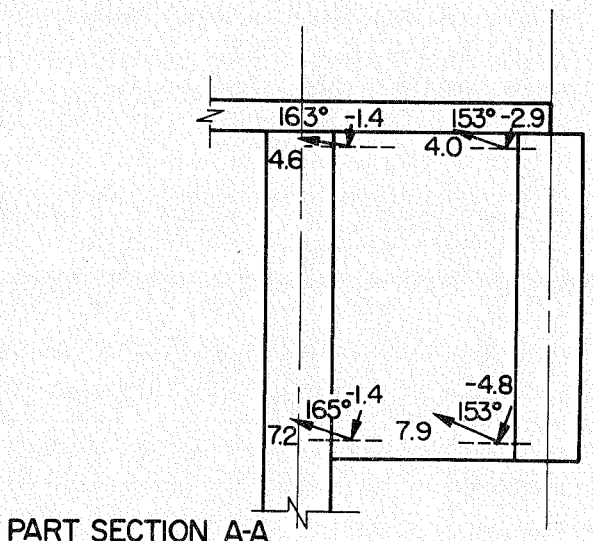

PART SECTION A-A

FIG. 6.16 PROTOTYPE STRESSES (KSI) AT 1050 PSI PRESSURE FOR 45° WYE-JUNCTION MODEL WITH PARTIAL SPLITTER PLATE

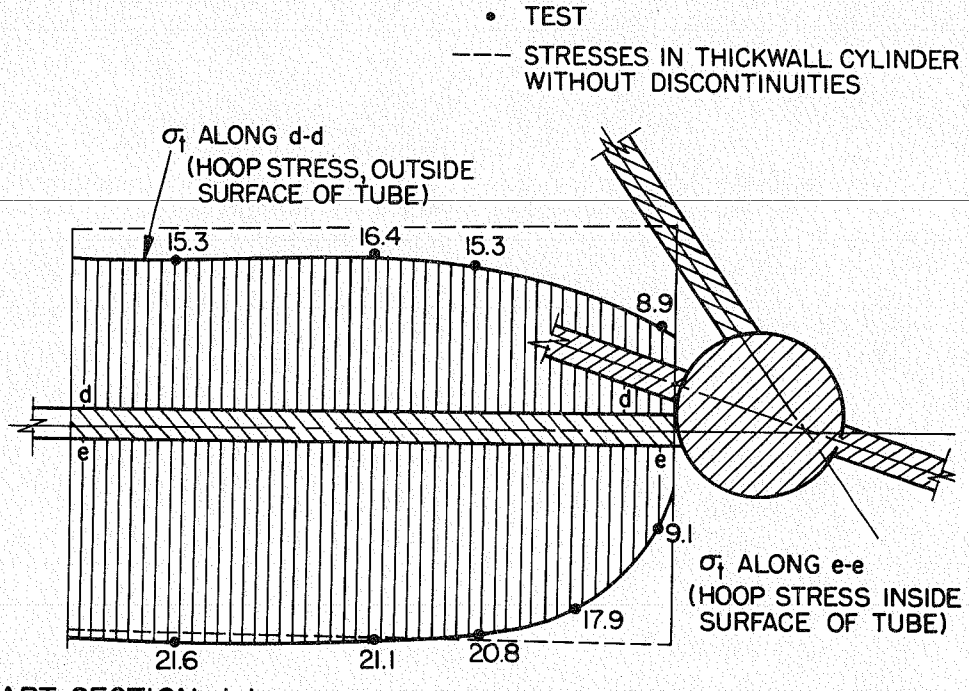

PART SECTION J-J

FIG. 6.17 PROTOTYPE STRESSES (KSI) AT 1050 PSI PRESSURE FOR 45° WYE-JUNCTION MODEL WITH PARTIAL SPLITTER PLATE

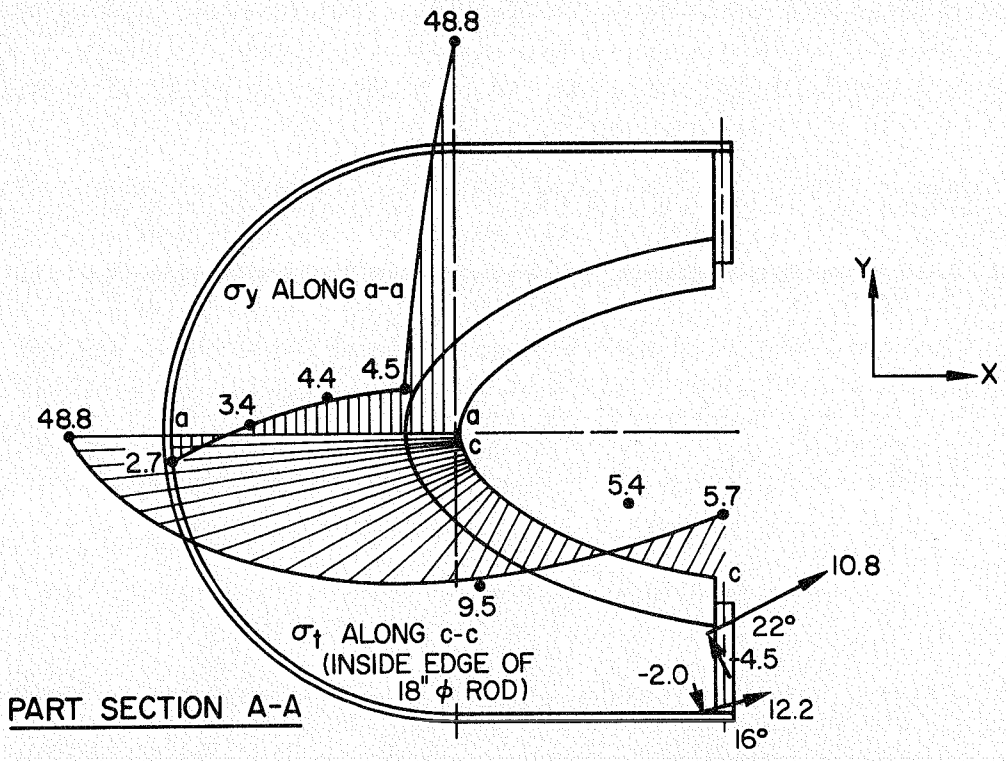

FIG. 6.18 PROTOTYPE STRESSES (KSI) AT 1050 PSI PRESSURE FOR 45° WYE-JUNCTION MODEL WITHOUT SPLITTER PLATE

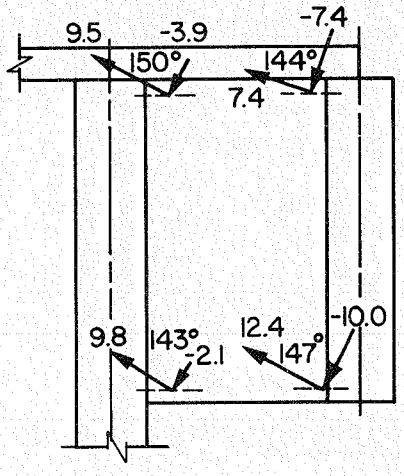

FIG. 6.19 PROTOTYPE STRESSES (KSI) AT 1050 PSI PRESSURE FOR 45° WYE-JUNCTION MODEL WITHOUT SPLITTER PLATE

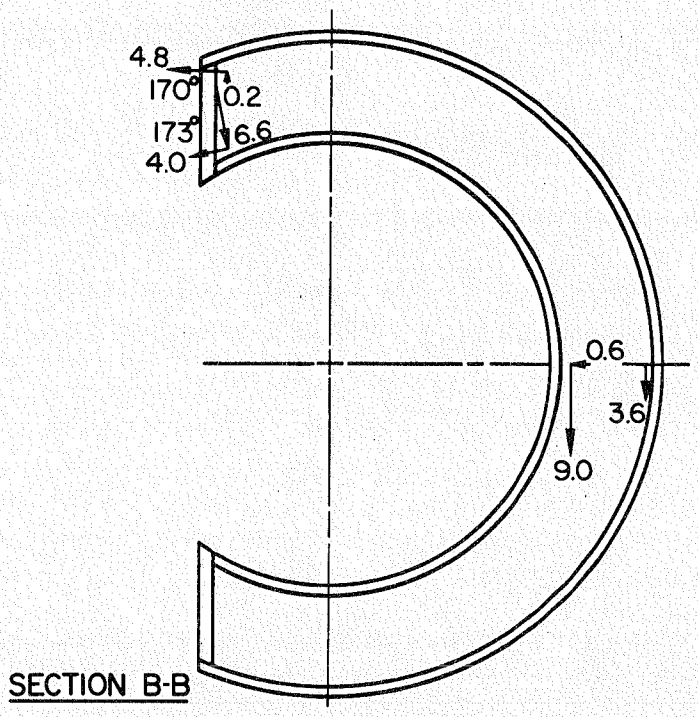

FIG. 6.20 PROTOTYPE STRESSES (KSI) AT 1050 PSI PRESSURE FOR 45° WYE-JUNCTION MODEL WITHOUT SPLITTER PLATE

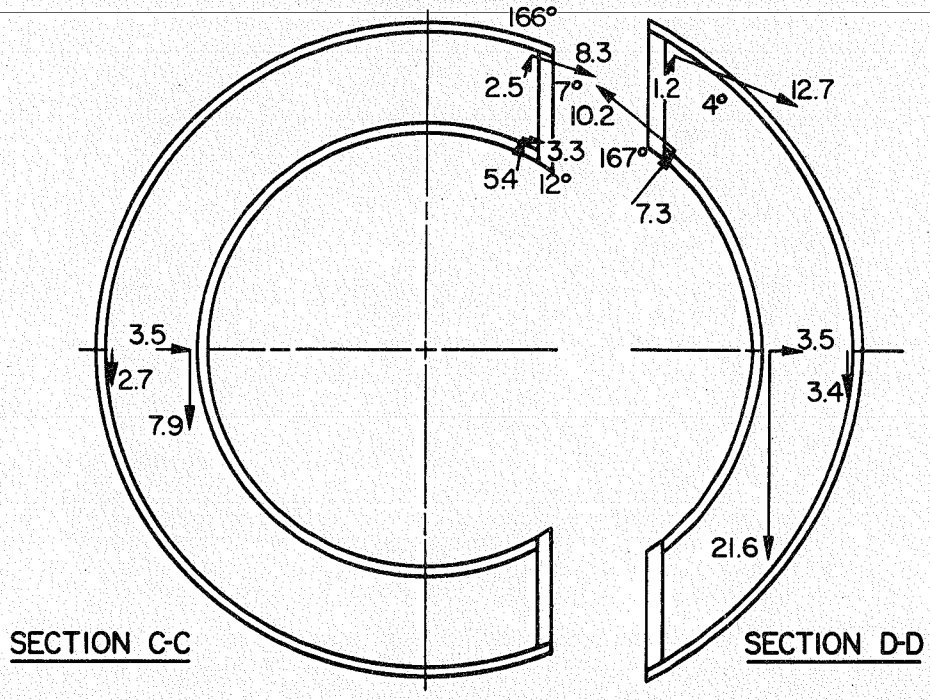

FIG. 6.21 PROTOTYPE STRESSES (KSI) AT 1050 PSI PRESSURE FOR 45° WYE-JUNCTION MODEL WITHOUT SPLITTER PLATE

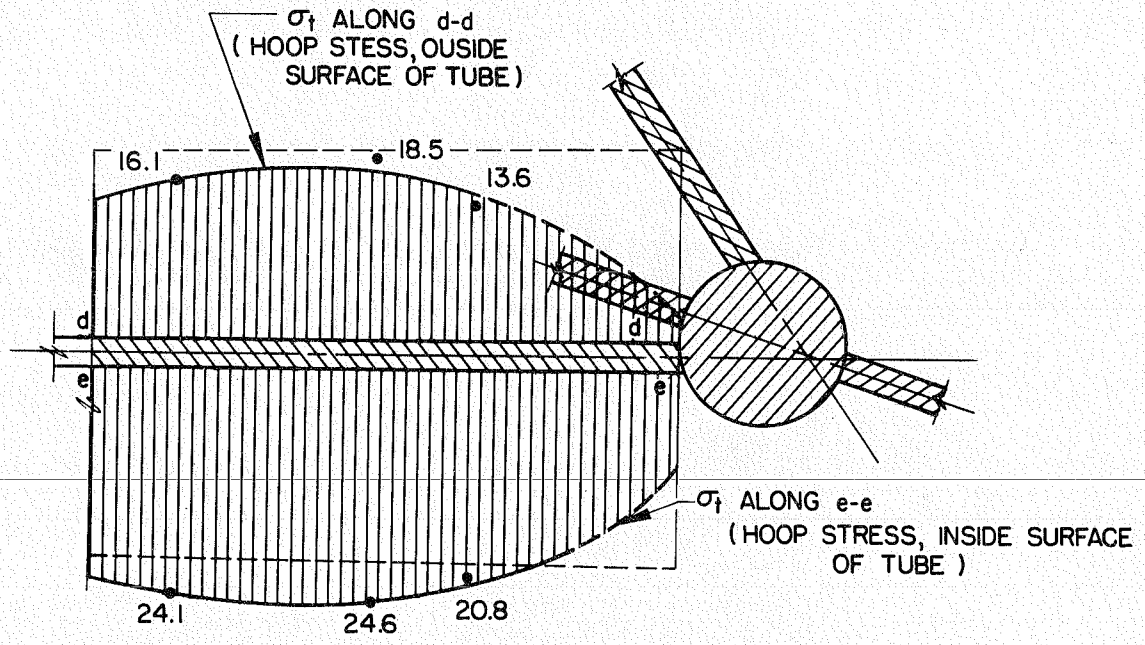

FIG. 6.22 PROTOTYPE STRESSES (KSI) AT 1050 PSI PRESSURE FOR 45° WYE - JUNCTION MODEL WITHOUT SPLITTER PLATE

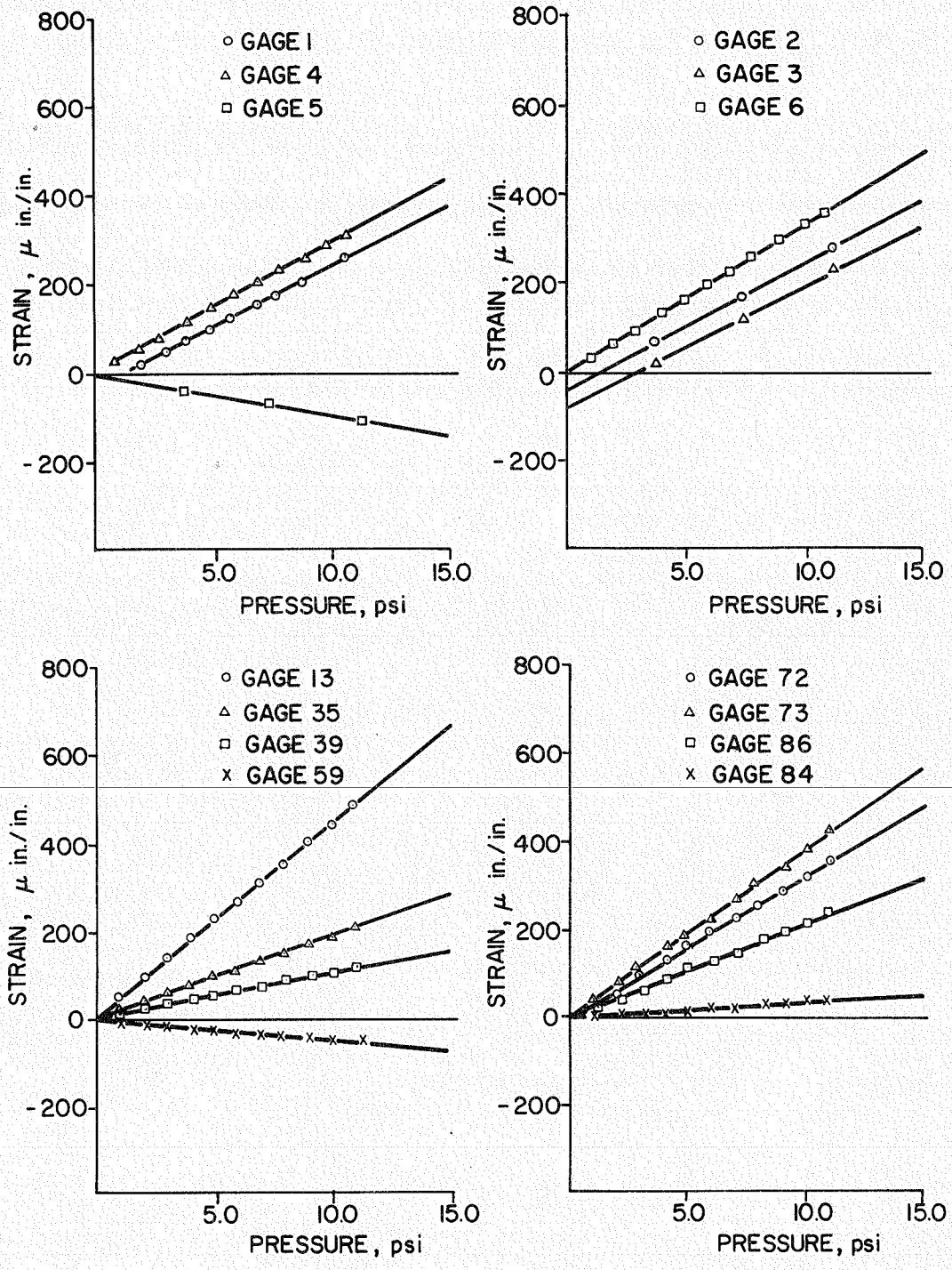

FIG. 6.23 STRAIN - PRESSURE GRAPHS AT REPRESENTATIVE GAGE LOCATIONS FOR 45° WYE - JUNCTION MODEL WITH FULL SPLITTER - PLATE

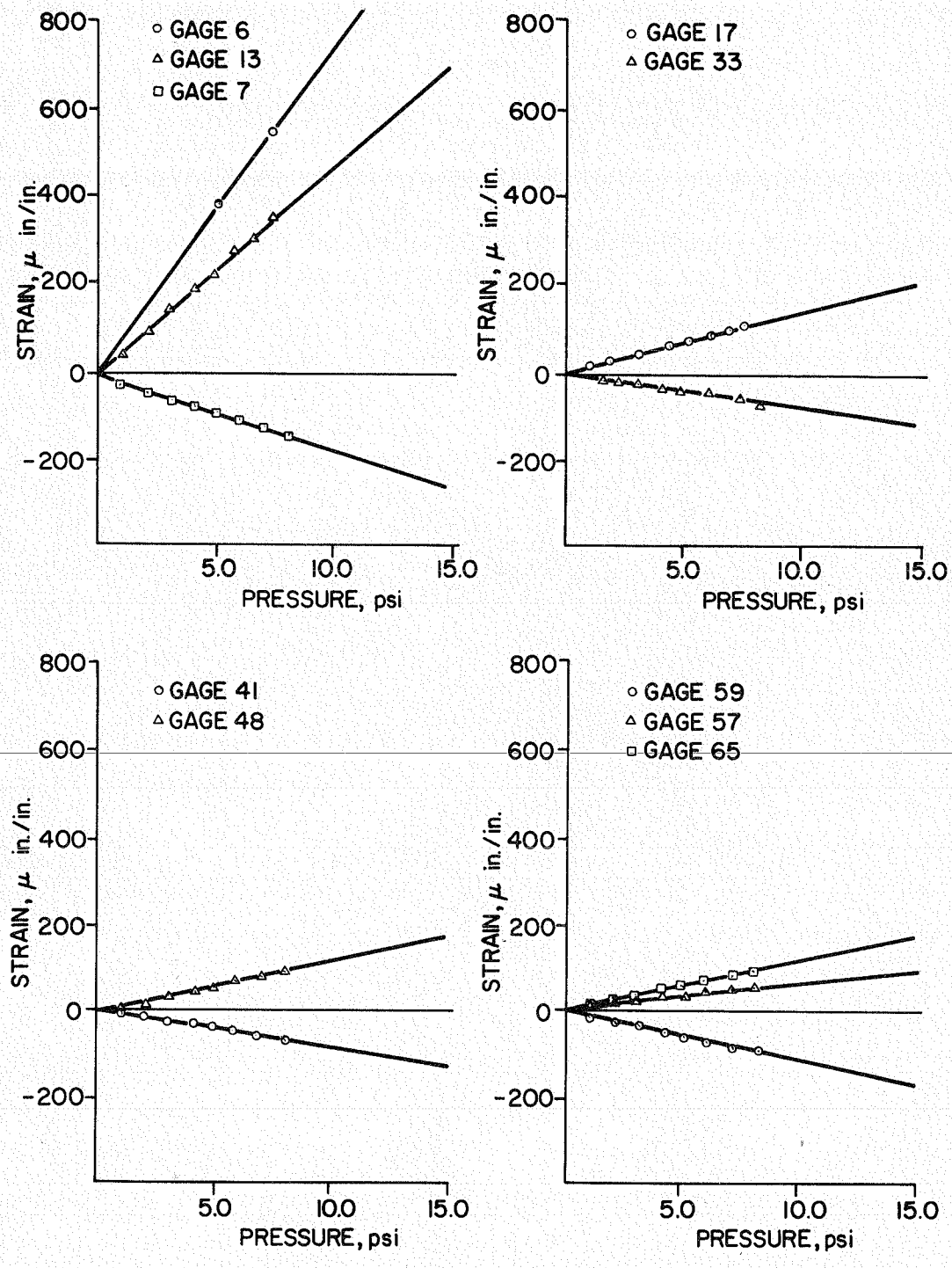

FIG. 6.24 STRAIN-PRESSURE GRAPHS AT REPRESENTATIVE GAGE LOCATIONS FOR 45° WYE-JUNCTION MODEL WITH PARTIAL SPLITTER-PLATE

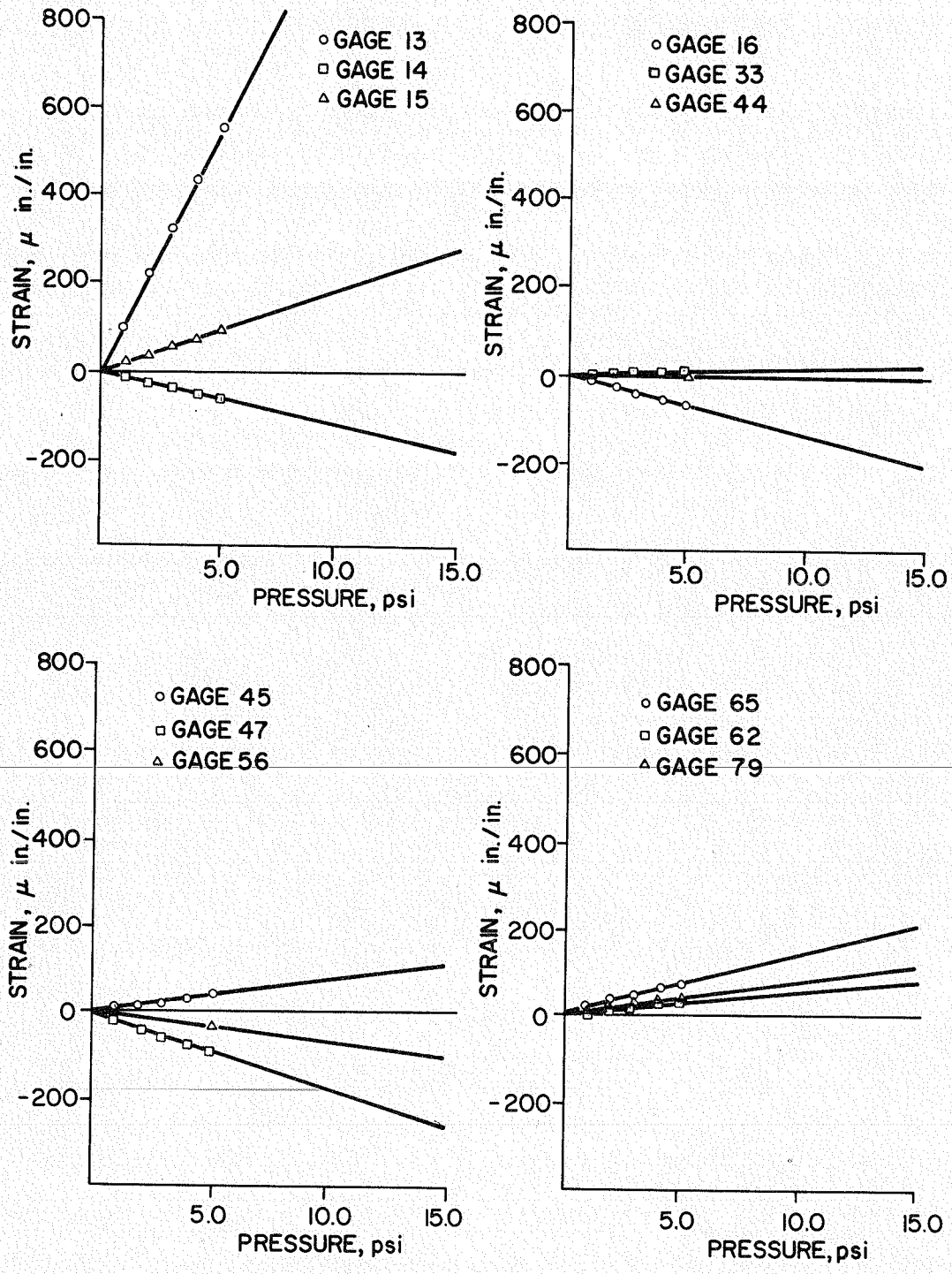

FIG. 6.25 STRAIN-PRESSURE GRAPHS AT REPRESENTATIVE GAGE LOCATIONS FOR 45° WYE-JUNCTION MODEL WITHOUT SPLITTER-PLATE

VII TEST SERIES II - 60° WYE-JUNCTION

7.1 Design of the Structure

Test Series II consisted of the structural study of the 60° wye-junction model, which was the final design of the junction adopted for the Tehachapi Pumping Plant manifolds. The design is that specified by the Department of Water Resources, State of California, and is shown in Figs. 4.1 through 4.3. The wall thickness of the tube in this case is 4.00 in., and that of the splitter-plate 5.50 in. The design pressure of the prototype was increased to 1150 psi which corresponds to 16.44 psi pressure in the model.

The number of external stiffeners was reduced from 4 to 3 and the web flange thicknesses were suitably altered. The size and thickness of the external stiffener in the plane of the splitter-plate was also reduced. The overall design of the structure was in part based on the results of Test Series I. Two design variations were studied: full splitter-plate design, and partial splitter-plate design.

The full splitter-plate design is shown in Fig. 7.1 and Plate 4.6. The configuration of the splitter-plate is similar to that of the 45° wye-junction.

The partial splitter-plate design is shown in Fig. 7.2 and Plate 7.1. As indicated in the diagram, the splitter-plate has a semi-circular cut-out with a prototype radius of 5 ft. 6 in. This was the design finally adopted.

7.2 Test Procedure

(a) As shortage of time made it impossible to do a complete analysis of the full splitter-plate design, stresses were measured only along the axis of symmetry of the full splitter-plate. The results of

Test Series I indicated that this would be the critical component, and this data was judged to be adequate as a check on the accuracy of the computer solution. After this data was taken, the splitter-plate was cut back to its final design configuration. Strain data was taken at pressures of 4.1, 6.1, and 8.22 psi. This corresponds to 1/4, 3/8, and 1/2 of the design pressure respectively. To study repeatability, three sets of readings were taken for each pressure value.

(b) Partial splitter-plate design.

The required cut-out was made on the splitter-plate using the procedure described in Sec. 6.2 (b). Since this design was the final one to be adopted, a detailed study of the behavior of the structure was necessary. An analytical solution using the finite element procedure described in Chapter VIII was first carried out. The most critical stresses as computed by this procedure were in the shell tapers near the point where all three stiffeners intersect. Strain rosettes were located as close to this as practicable as indicated in Fig. 7.14. In addition to the other critical locations, stresses at these points were therefore studied. Strain data was taken at a total of 58 gage locations using 103 gage elements as shown in Figs. 7.3 through 7.5. Observations were taken at pressures of 4.1, 8.2, and 12.33 psi. Detailed linearity tests using 1.0 psi pressure increments were carried out for 42 gage elements.

Strain-pressure graphs at representative gage points are given in Figs. 7.15 and 7.16.

7.3 Linearity

A study of strain-pressure graphs for all gage locations indicates that the structure behaves essentially linearly in both full and partial splitter-plate designs. Also, all graphs pass through zero, indicating that the splitter-plate is essentially straight after the fabrication of the model. The absence of initial curvature of the splitter-plate can be attributed to the thicker plate, the simpler structural configuration of this design, and the improved fabrication due to experience gained on the previous model. It can, therefore, be reasonably expected that the prototype structure will also behave linearly and that the eccentricity effects in the splitter-plate will be minimal.

7.4 Reduction of the Strain Data

The slope of the strain-pressure graph was used in all cases for extrapolating to the strain values at design pressure. The reduced stress data corresponding to the gage locations in Figs. 7.3 through 7.5 is given in Table 7.1 The stress distribution in the prototype along various cross-sections is plotted in Figs. 7.6 through 7.14.

7.5 Discussion

A study of the splitting stresses along the plane of symmetry of the splitter-plate for the full splitter-plate design (Fig. 7.6) indicates a rapid drop of stresses from 14.6 psi at the junction with the rod to 1.5 psi at the free edge. As in the 45° design, the structure can therefore be cut back without a significant increase in the maximum stress level.

The stress distributions of Section AA of the structure for the partial splitter-plate design are shown in Figs. 7.7. The stresses in the splitter-plate along its plane of symmetry are fairly constant, increasing from 16.0 ksi at the junction with the rod to 18.8 ksi at the free edge. This indicates a fairly ideal design from the structural standpoint. It can be seen that the stresses in the external stiffener in the plane of the splitter-plate are still low, decreasing from 8.5 ksi at the rod to 1.4 ksi at the flange. Also, it is evident from Figs. 7.7 through 7.9 that the external stiffener is still taking a very small force when compared with that of the rod, and it is possible that the stiffener could be further reduced in size or eliminated completely along the axis of symmetry.

The stress distributions along the webs and flanges of sections BB and CC (Fig. 7.10) indicate that the flange stresses are fairly small when compared with the stresses in the rest of the structure and are reasonably constant.

Figs. 7.11 through 7.13 give tube wall stresses at various locations in the vicinity of the junction of the plane of symmetry of the structure. The stress distribution curves show that the main pipe behaves essentially as a thick wall cylinder except in the immediate vicinity of the junction. In all cases local effects die out within 2 ft. 6 in. of the junction in the prototype, and even within this region, the reduction in the stresses is small.

Stress values given in Fig. 7.14 indicate high bending stresses in the main taper near the point where the external stiffeners intersect.

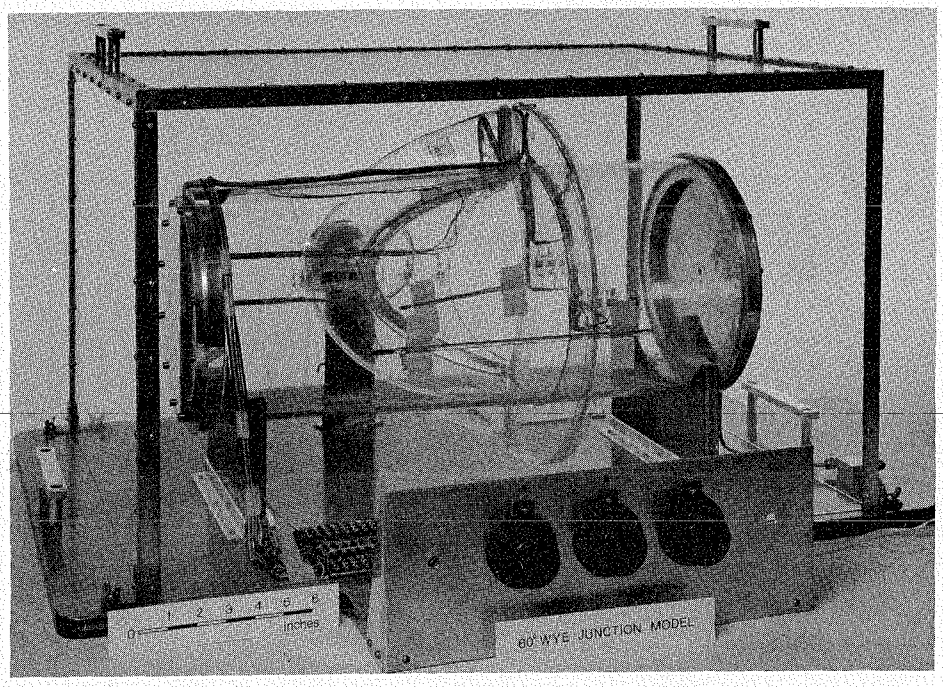

PLATE 7.1 60° WYE-JUNCTION WITH PARTIAL SPLITTER-PLATE UNDER TEST

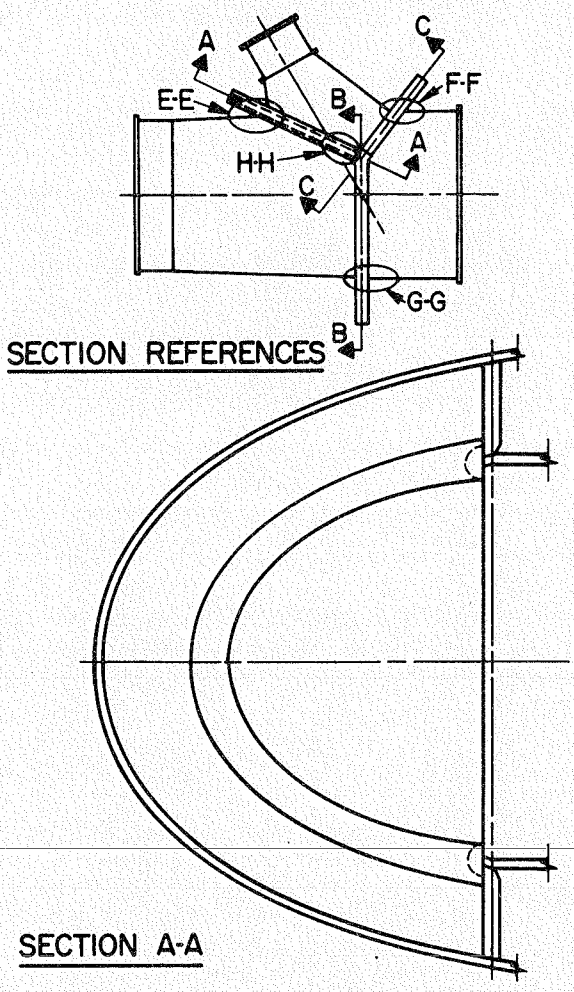

FIG. 7.1 60° WYE-JUNCTION MODEL WITH FULL SPLITTER PLATE

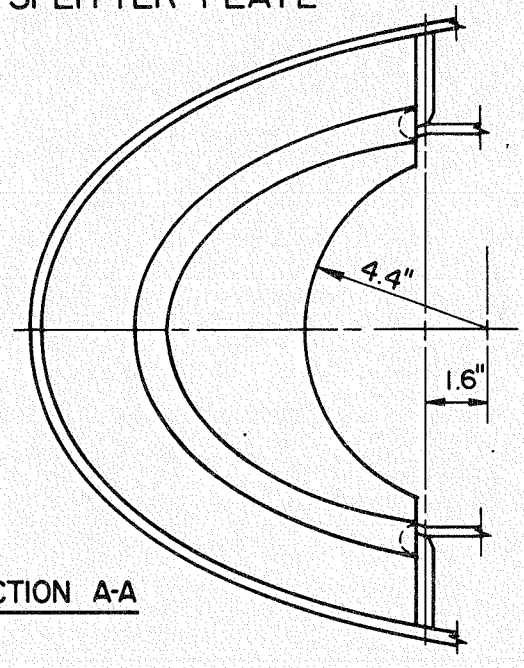

FIG. 7.2 60° WYE-JUNCTION MODEL WITH PARTIAL SPLITTER PLATE

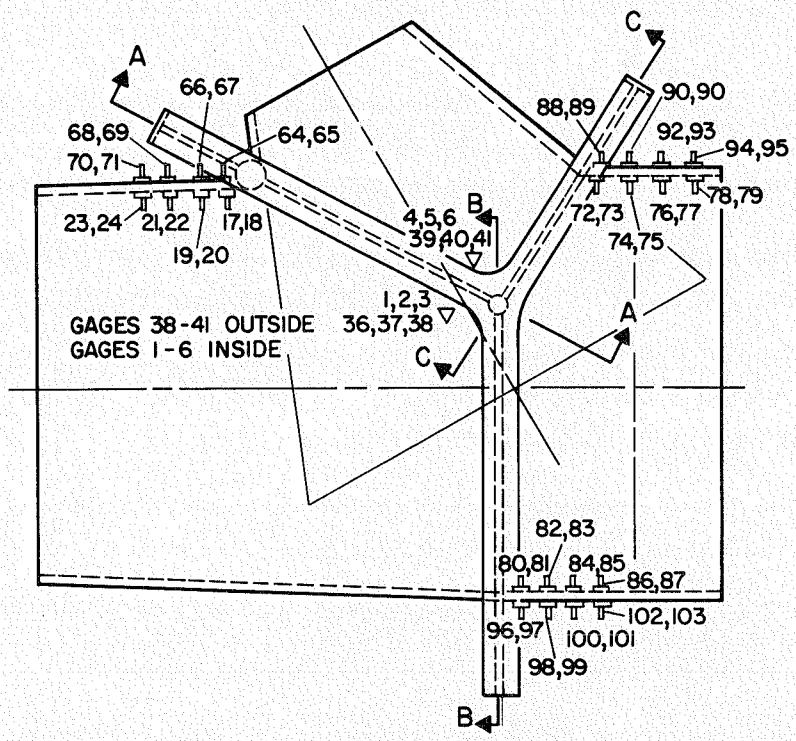

FIG. 7.3 GAGE LOCATIONS AND SECTION REFERENCES FOR 60° WYE-JUNCTION MODEL

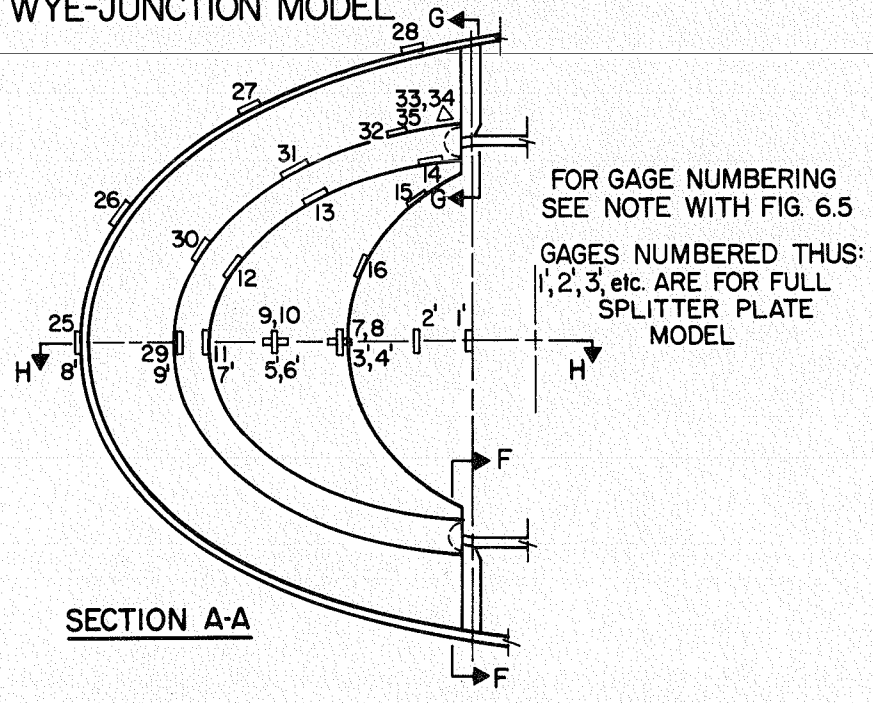

FIG. 7.4 GAGE LOCATIONS FOR 60° WYE-JUNCTION MODEL

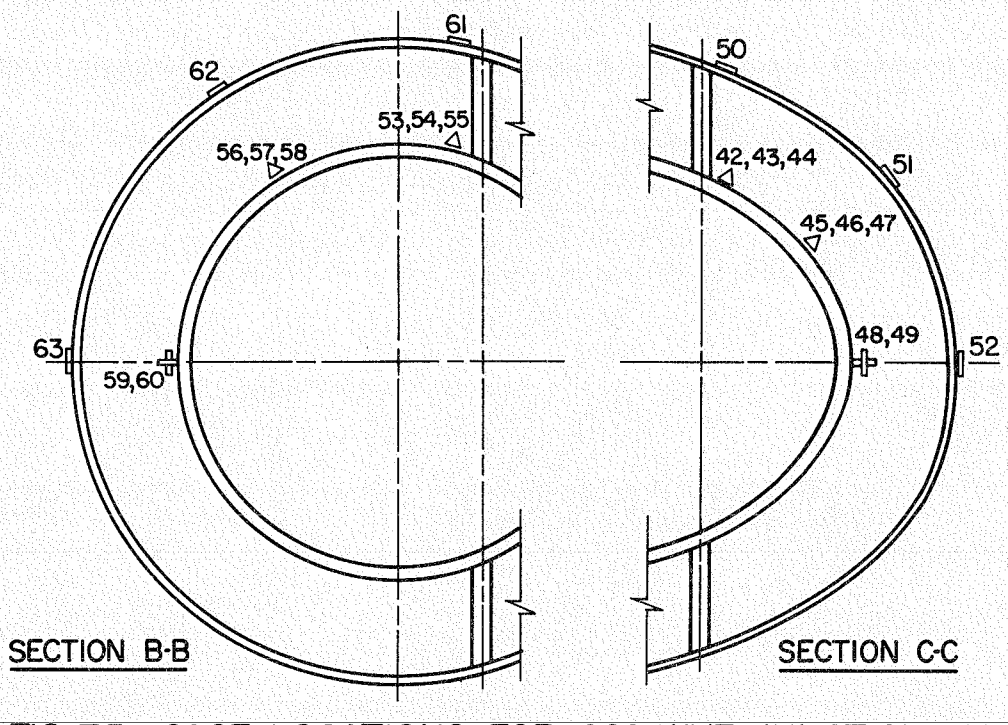

FIG. 7.5 GAGE LOCATIONS FOR 60° WYE-JUNCTION MODEL

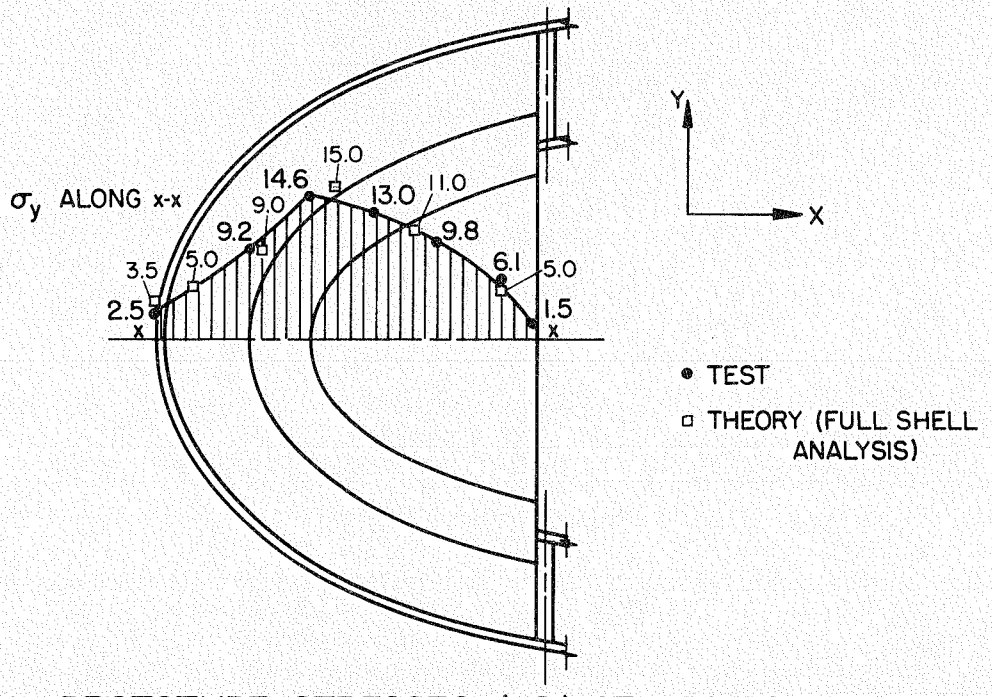

FIG. 7.6 PROTOTYPE STRESSES (KSI) AT 1150 PSI PRESSURE FOR 60° WYE-JUNCTION WITH FULL SPLITTER PLATE

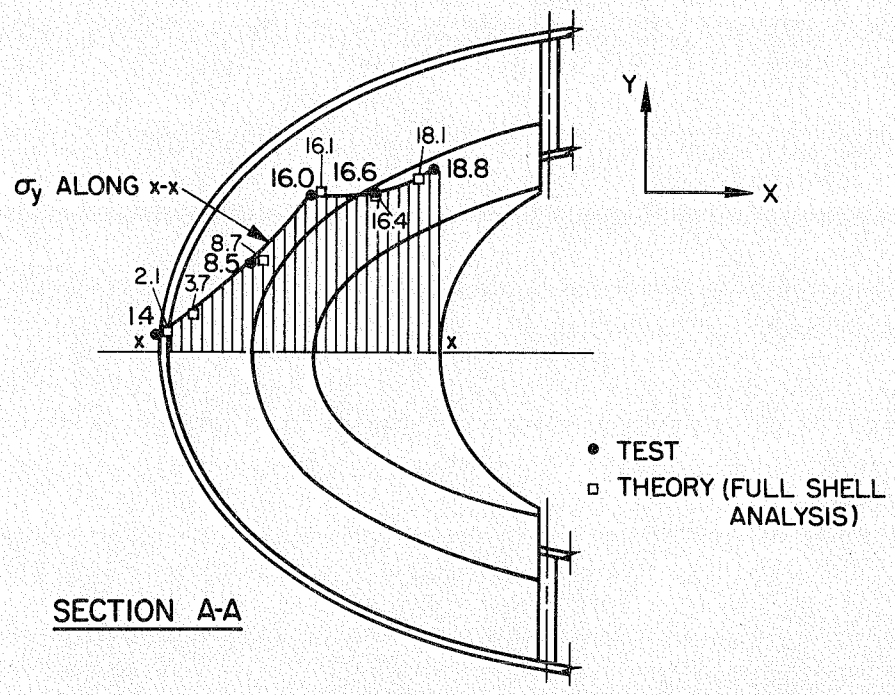

FIG. 7.7 PROTOTYPE STRESSES (KSI) AT 1150 PSI PRESSURE FOR 60° WYE-JUNCTION MODEL WITH PARTIAL SPLITTER PLATE

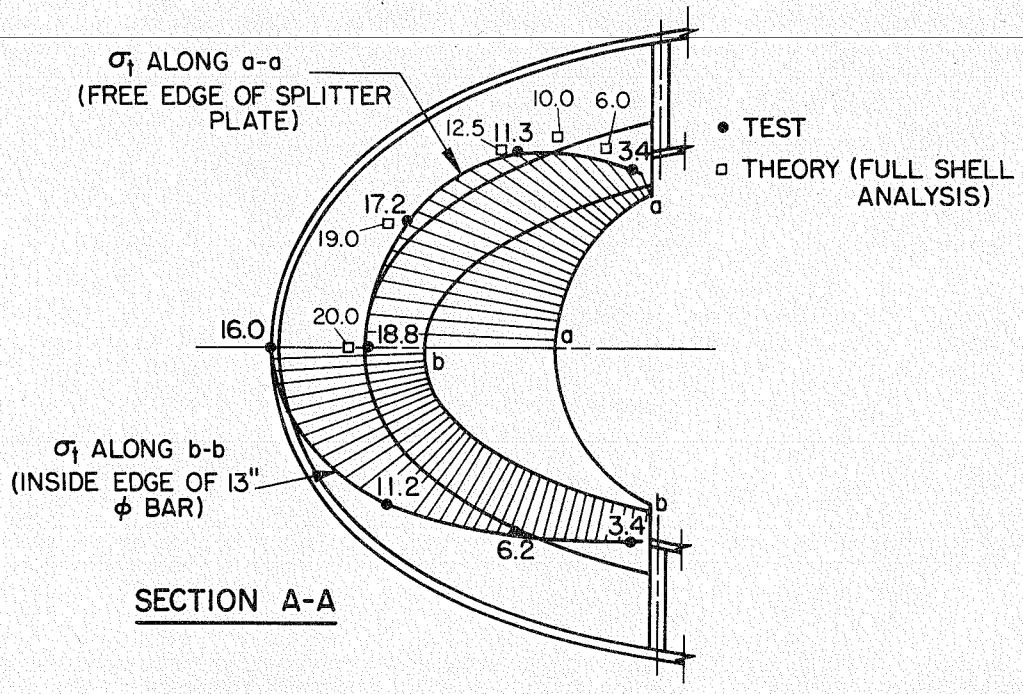

FIG. 7.8 PROTOTYPE STRESSES (KSI) AT 1150 PSI PRESSURE FOR 60° WYE-JUNCTION MODEL WITH PARTIAL SPLITTER PLATE

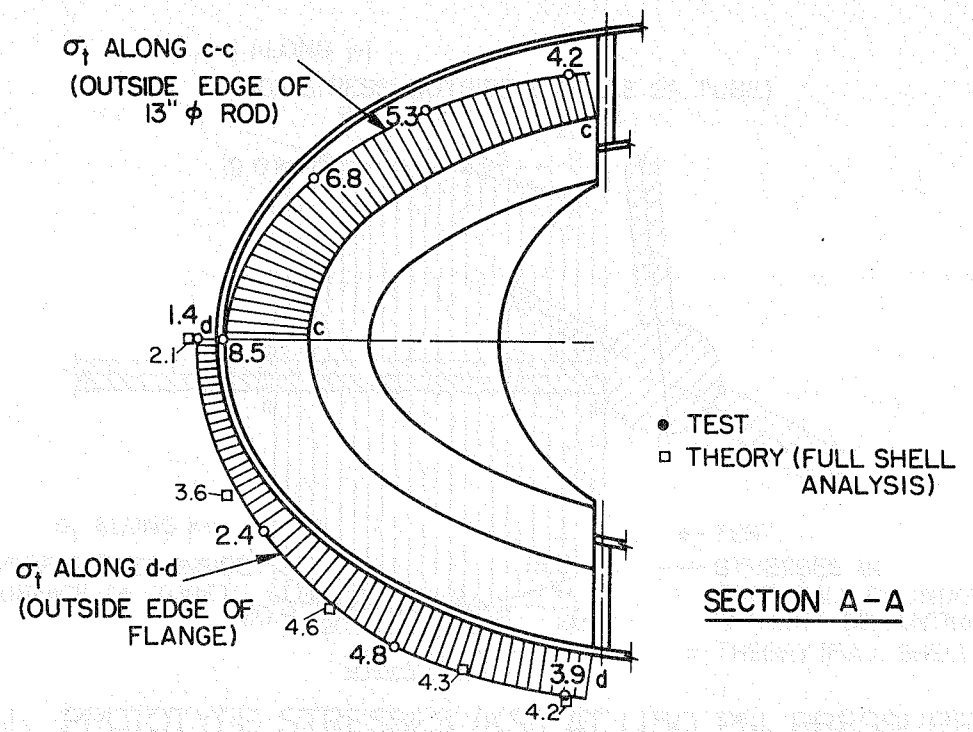

FIG. 7.9 PROTOTYPE STRESSES (KSI) AT 1150 PSI PRESSURE FOR 60° WYE-JUNCTION MODEL WITH PARTIAL SPLITTER PLATE

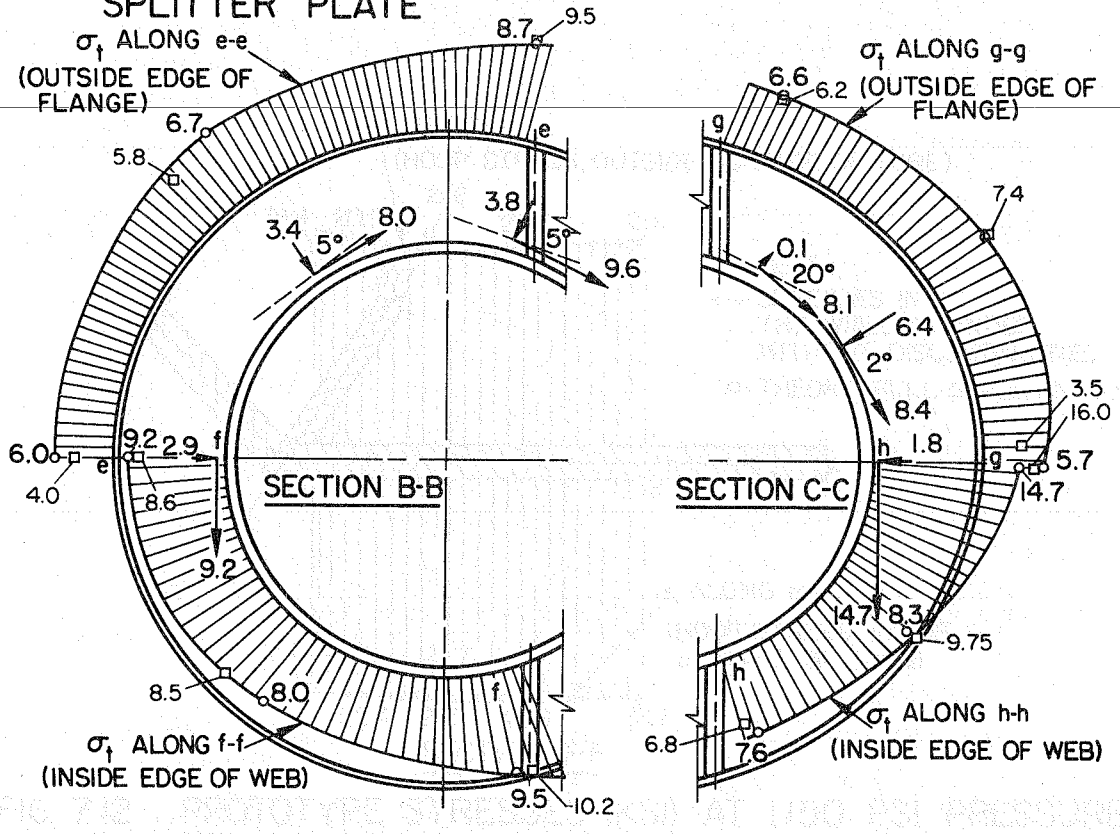

FIG. 7.10 PROTOTYPE STRESSES (KSI) AT 1150 PSI PRESSURE FOR 60° WYE-JUNCTION MODEL WITH PARTIAL SPLITTER PLATE

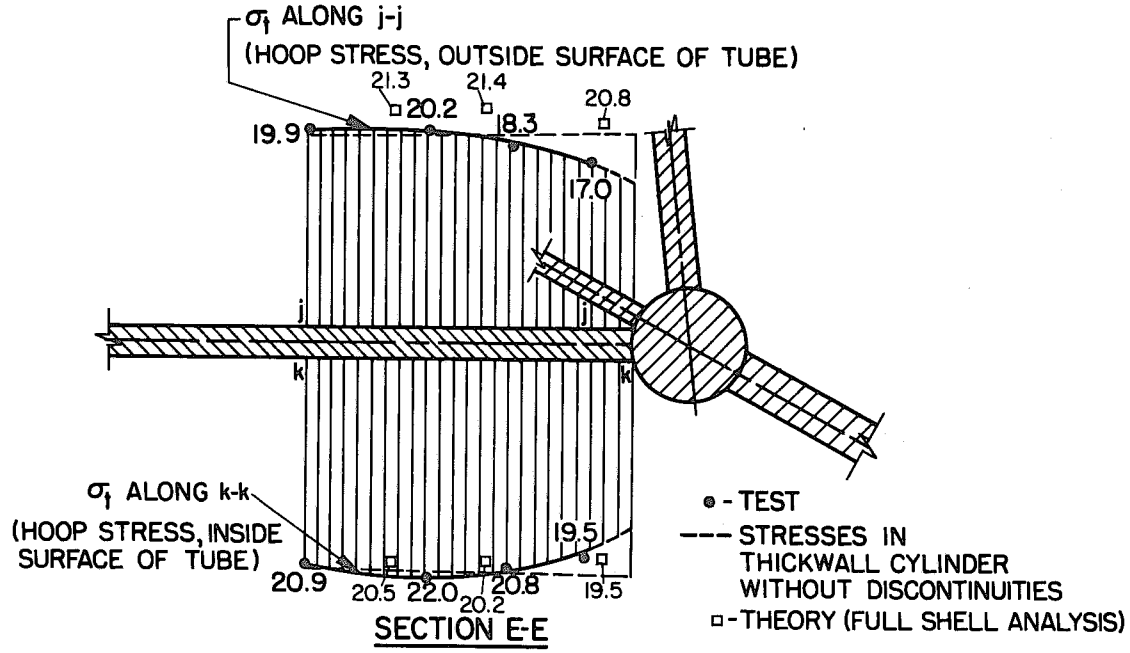

FIG. 7.11 PROTOTYPE STRESSES (KSI) AT 1150 PSI PRESSURE FOR 60° WYE-JUNCTION MODEL WITH PARTIAL SPLITTER PLATE

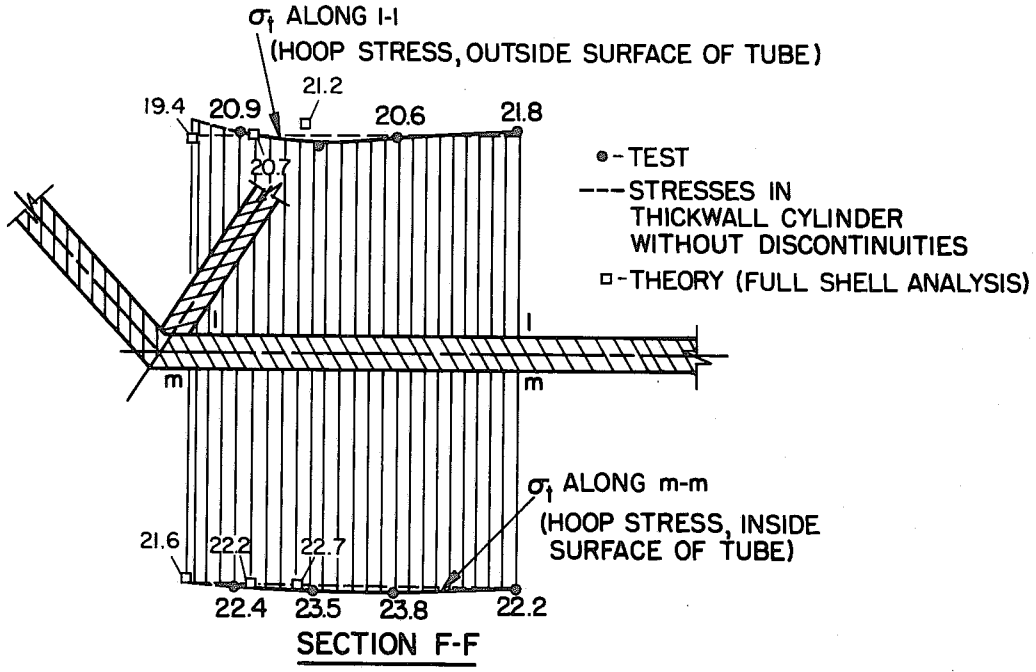

FIG. 7.12 PROTOTYPE STRESSES (KSI) AT 1150 PSI PRESSURE FOR 60° WYE-JUNCTION MODEL WITH PARTIAL SPLITTER PLATE

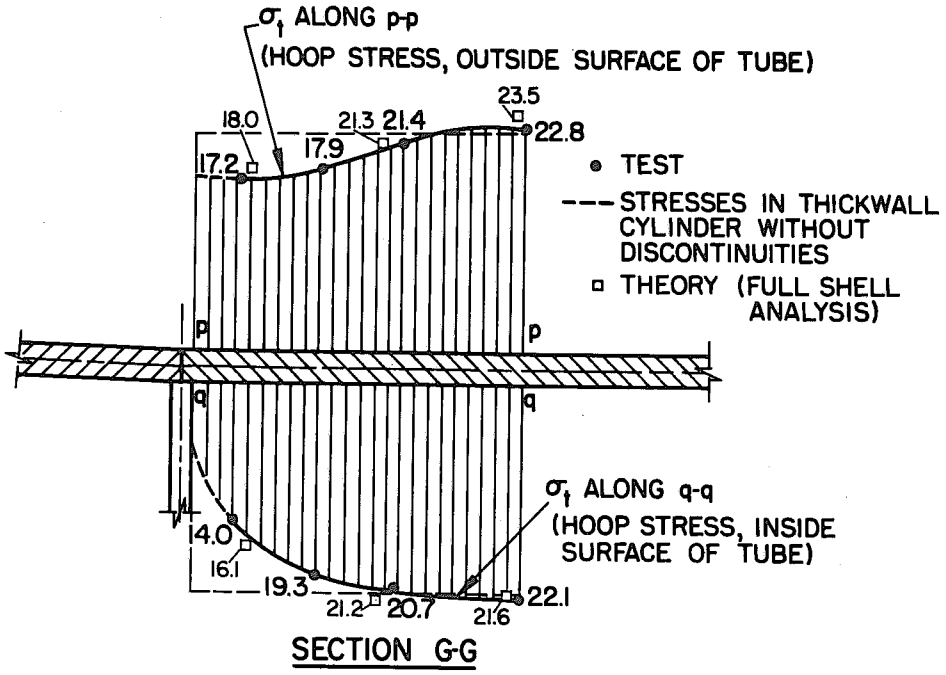

SECTION G-G

FIG. 7.13 PROTOTYPE STRESSES (KSI) AT 1150 PSI PRESSURE FOR 60° WYE-JUNCTION MODEL WITH PARTIAL SPLITTER PLATE

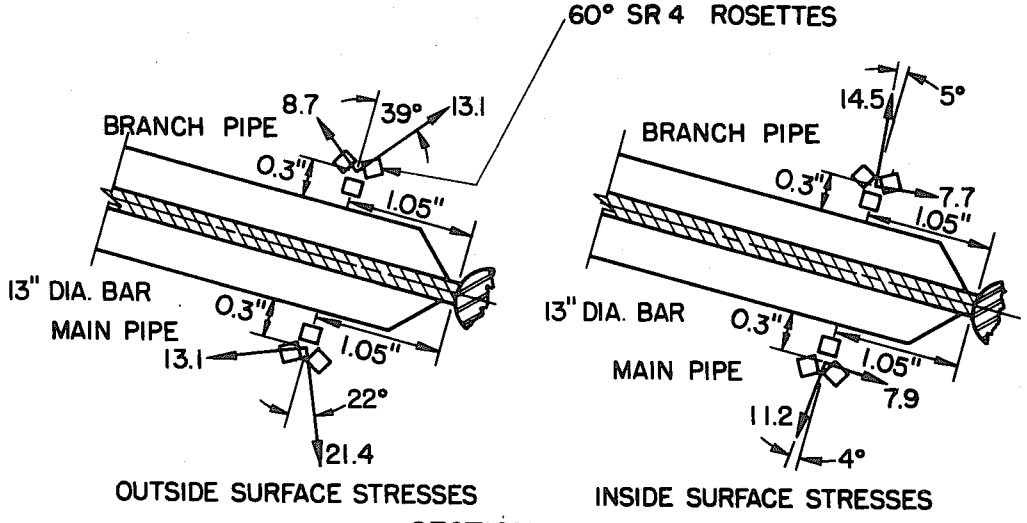

SECTION H-H

FIG. 7.14 PROTOTYPE STRESSES (KSI) AT 1150 PSI PRESSURE FOR 60° WYE-JUNCTION MODEL WITH PARTIAL SPLITTER PLATE

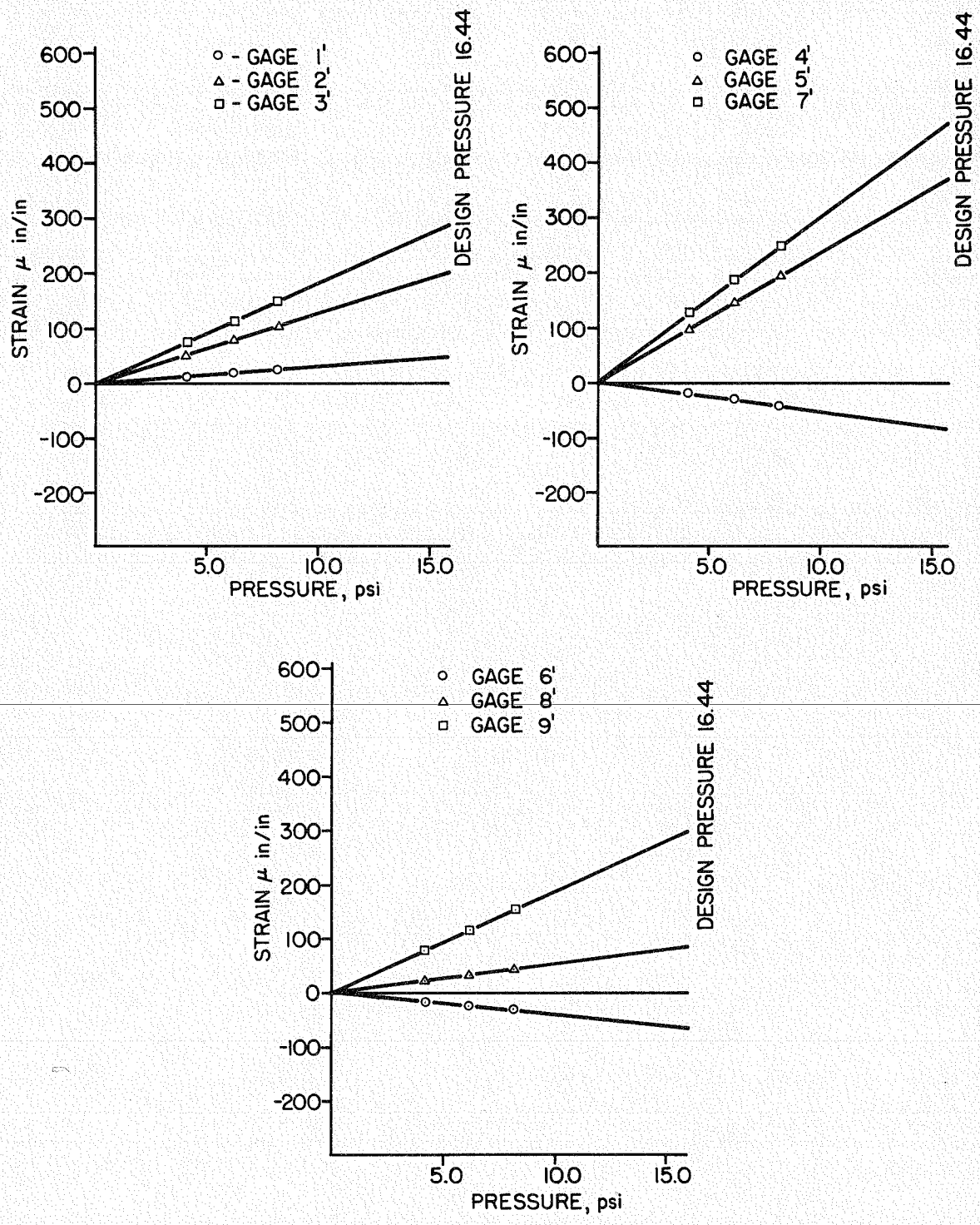

FIG. 7.15 STRAIN-PRESSURE GRAPHS FOR 60° WYE-JUNCTION MODEL WITH FULL SPLITTER-PLATE

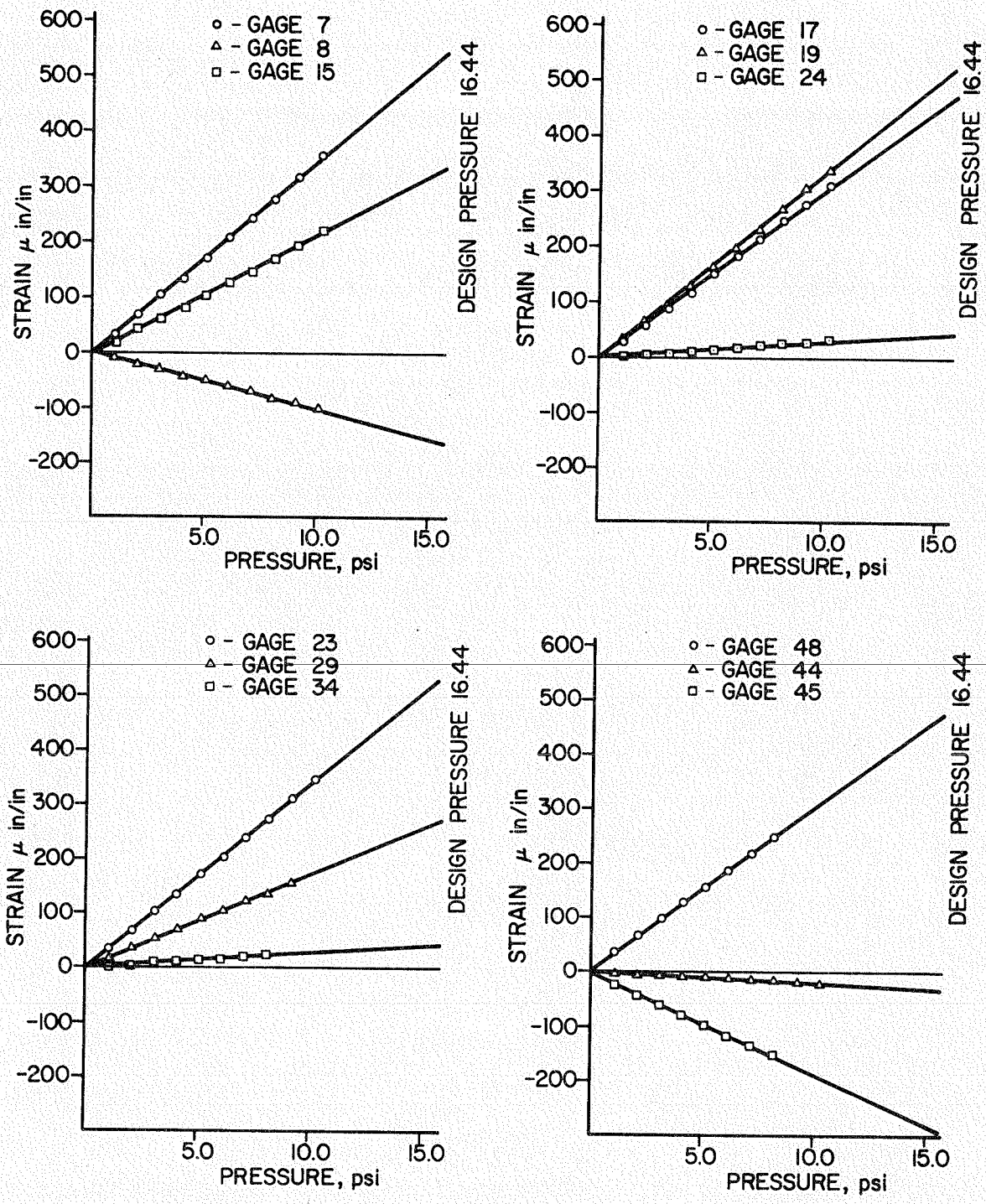

FIG. 7.16 STRAIN-PRESSURE GRAPHS AT REPRESENTATIVE GAGE LOCATIONS FOR 60° WYE-JUNCTION MODEL WITH PARTIAL SPLITTER-PLATE

VIII FINITE ELEMENT ANALYSIS

8.1 Introduction

The basic purpose of the model study as reported herein was to establish the finite-element method as an accurate tool for the stress-analysis of the reinforcement system for penstock wye-junctions. The preliminary design effort for the Tehachapi Pumping Plant Wye-Branches yielded reinforcing systems whose geometries were such that the stress distribution could not be accurately determined by curved beam theory. Discussion with Professor R. W. Clough of the University of California, Berkeley, coupled with a review of the available literature (1,2,4), indicated that proper application of the finite-element method could provide accurate stress distributions regardless of the geometries encountered

Shown in Fig. 8.1 is a typical wye-junction subjected to an internal pressure. The basic need for reinforcement arises from the unbalanced vertical forces P_V shown in Section AA. These forces are the algebraic sum of the vertical components of the natural hoop forces existing in each penstock branch. Therefore, their magnitude is a direct function of the diameters and pressures involved and their existence is an inevitable result of the joining of two penstock branches at some angle, θ.

The usual scheme for resisting the P_V forces is a structural system of curved beams connected to the pipe shell along lines 1-2, 3-2, and 4-2 of Fig. 8.1. Shown in Fig. 8.2 is the elevation of one such reinforcing beam which could be used along the line 1-2 of Fig. 8.1. For a limited range of pressure, stiffening beams may be designed such that the lengths a and b of Fig. 8.2 are small with respect to the length

of the neutral axis. For reinforcing beams of this proportion it is reasonable to idealize the reinforcing structure as an assemblage of one-dimensional elements, each with its own bending and axial stiffness as depicted by Fig. 8.4. Various analytical techniques can then be utilized to obtain the stress distributions; the most commonly used technique is the virtual work method.[3]

However, as the internal pressure requirement on a given set of penstock diameters increases, so must the dimensions a and b of Fig. 8.2. Furthermore, it is both structurally and hydraulically[5,6] advantageous to reinforce wye-branches internally along line 1-2 of Fig. 8.1 as shown in Fig. 8.3. A stiffening element of the properties shown in Fig. 8.3 cannot be analyzed by normal curved beam theory for the following reasons:

(a) The stress distribution is greatly affected by the fact that the loads and reactions are not applied at the neutral axis.

(b) The concept of a neutral axis as related to a plane of bending loses meaning as the element becomes deeper.

Accurate determination of stress distributions for structures of this type can best be determined by numerical procedures which consider the reinforcing elements as plate-systems rather than beam-systems. The finite element method is a recently developed numerical procedure capable of taking directly into account all of the above mentioned factors in an accurate, efficient and completely general manner.

8.2 Finite Element Method

The numerical procedures associated with the finite-element method can be derived from the Theorem of Minimum Potential Energy. Within the framework of this theorem one may formulate a finite-element

analysis for the simple bar structure shown in Fig. 8.5. The initial and most critical step in this formulation is the development of an expression for the rate of change of the potential energy of a given element. This rate of change or derivative must be expressed as a function of the given element's two nodal point displacements. Systematic addition of the "element potential energy derivatives" results in the total system's potential energy derivative. Equating this total derivative to zero then gives rise to a set algebraic simultaneous equations which when solved yield the final equilibrium displacement field of the structure.

The above description was made with reference to a structure consisting of one-dimensional elements (length) with a one-dimensional displacement field and as such is of little practical significance. However, spatial extension of either the elements themselves or the displacement field presents no new problems conceptually. For example, one may formulate a finite-element analysis for one-dimensional elements with both axial and bending stiffnesses within a three-dimensional space. The system unknowns then become x, y, and z displacements and rotations at each nodal point [2], i.e. there are six unknowns per node versus one per node as in Fig. 8.5. This type of element provides an analytical tool for three-dimensional frameworks, and the mathematical model for a reinforcement structure is as depicted in Fig. 8.4.

However, with reference to the analysis of wye-junction reinforcement, the most significant development has been that of finite-element analyses of structures consisting of two-dimensional (flat plate) elements within a three-dimensional space. With the use of such element representations there exists two distinct analytical procedures.

The first scheme consists of considering the reinforcing plates as a structure separate or uncoupled from the pipe shell. This procedure is referred to as the "Uncoupled Plate Analysis". The second scheme involves taking a more complete analytical view of the structure. It is accomplished by the inclusion of the pipe shell into the mathematical model of the finite element method. This procedure is referred to as the "Full Shell Analysis".

8.3 Uncoupled Plate Analysis

This analytical procedure considers the reinforcing plates as a three-member system divorced from the shell as shown in Fig. 8.6. The basic element used in this analysis is a two-dimensional membrane of triangular shape which is said to exist within a three-dimensional space. The membrane stiffness of each triangle is computed on the basis that the strain condition within the triangle is constant, and the system unknowns become the global x, y an z displacements at each corner of each triangle.[2] An appropriate number of triangles of this type are assembled so as to construct the mathematical model depicted in Fig. 8.6 wherein each rectangle represents two such triangles.

The general procedural details of the computerized Uncoupled Plate Analysis are as follows:

(a) An input generator program is used which requires only the definition of overall pipe and plate dimensions and a basic layout for the finite element mesh. With this data the computer develops the global coordinates and indices necessary to describe this structure mathematically. This information is generated in the form required by the parent finite-element computer program.[2]

(b) The loading to be applied to the uncoupled plate system is computed in the geometric program. Several basic assumptions are used to establish the unbalanced forces transferred from the pipe shell to its reinforcement. The assumptions used are as outlined by Rudd,[3] and the resultant loading will be referred to herein as the "Bureau Loading".

(c) Restraints are applied to the uncoupled plate system to approximate the stiffness or flange effect which the pipe shell provides when the structure is welded.

(d) The data generated as outlined above is then processed by the parent finite-element program. The resulting output data includes the displacements and stress condition for each element.

Thus, the Uncoupled Plate Analysis procedure used in this manner represents an extension of the traditional virtual work and curved beam methods. With it the computer solves for stresses in the indeterminate three-dimensional plate system in a manner which allows great refinement in the design of these junction reinforcements within the limitation of the uncoupled plate concept

8.4 Full Shell Analysis

The analysis procedure considers the entire structure as a unit as shown in Fig. 8.7. In this computerized solution it is not necessary to make assumptions as to the interaction between the pipe shell and its reinforcing plates. The total behavior of the structural system is mathematically modeled by the finite elements in both the shell and its reinforceing plates.

The basic element of this analysis possesses bending as well as membrane stiffness. The membrane action of the element in this analysis has a basis similar to that of the Uncoupled Plate Analysis. The bending action is accounted for by adding to the system unknowns a moment along each side of the basic element.[4] The rectangles comprising the assemblage of Fig. 8.7 each consist of four such "flat-plate" triangular elements[8]

Although this is the most accurate analysis procedure to date, there are two drawbacks to its exclusive use. The first is that the preparation of input data is very tedious. In general it does not lend itself to automatic data generation because of the inherent complex nature of the finite-element mesh. As a second drawback, the storage area required in the computer becomes very large. For the mesh represented by Fig. 8.7 there are 2400^{+} equations with 200 potential non-zero coefficients per equation. The most efficient equation solver known for this general type of problem then requires $80{,}000^{+}$ direct access storage locations for this array alone.

Nevertheless a Full Shell Analysis of the largest junction of the manifold system was made with the same general procedural details as those described in Sec. 8.3 for the Uncoupled Plate Analysis. Exceptions to this procedure are as follows:

(a) An input generator to compute the coordinate points only was written for the mesh shown in Fig. 8.7. Deviations from this particular layout would require program modification.

(b) The only loading required is an internal normal pressure on the pipe shell elements.[8]

(c) Restraints modeling the symmetry and longitudinal conditions are all that are required.[8]

(d) The very large amount of storage required was acquired on the IBM 360-65 computer through the use of two non-standard techniques. Single precision arithmetic of approximately eight significant figures was used for the equation solution. Also, the usual multiprogramming mode of operation for this computer was not used, i.e. the finite-element analysis was the only job being processed by the computer from the start to the finish of the job.

Of all the analytical techniques discussed above, the Full Shell Analysis procedure provides the most accurate stress values for the structures being considered. Furthermore, it allows realistic evaluation of the effects of various longitudinal restraint (bulkheaded, encased and unencased) and temperature conditions.

8.5 Summary of Studies

In order to establish the relative merit of the two proposed and existing analysis techniques, the following studies were made in conjunction with the 60° wye-junction model study reported herein:

1. STRUCTURE - Prototype junction with partial splitter.
   ANALYSIS - Full Shell Analysis
   LOADING - Pressure with longitudinal loading (simulation of bulkhead effect)

2. STRUCTURE - Prototype junction with full splitter
   ANALYSIS - Full Shell Analysis
   LOADING - Pressure with longitudinal loads

3 STRUCTURE - Prototype junction with partial splitter
   ANALYSIS - Full Shell Analysis
   LOADING - Pressure without longitudinal loads

4. STRUCTURE - Prototype junction with partial splitter
   ANALYSIS - Full Shell Analysis
   LOADING - Bureau loading

5. STRUCTURE - Prototype junction with partial splitter
   ANALYSIS - Uncoupled Plate Analysis
   LOADING - Bureau loading

6. STRUCTURE - Prototype junction with partial splitter and thin shell (t = 0.1 in.)
   ANALYSIS - Full Shell Analysis
   LOADING - Pressure without longitudinal loads

In addition to these studies, Uncoupled Plate Analyses were made of existing manifold structures for which strain gage data had been obtained from full scale prototype pressure tests. Finally, a full shell analysis was made of a smaller junction of the Tehachapi project which was instrumented in a full scale testing program.[7]

8.6 Results of Full Shell Analysis

The results of study No. 1 are given in Figs. 7.7 through 7.13 as they relate to the strain gage data obtained from the model study.

For purposes of discussion these results may be divided into two general areas; those relating to the stiffener plate system, and those relating to the shell system. Inspection of the results on the reinforcing system indicates that the full shell analysis provides an accurate overall mathematical model of the structure in that good correlation between computed and measured stresses exists in all portions of the system. Therefore, the loading and the resulting interaction of the various structural systems have been properly accounted for. On the other hand, the results relating to the shell stresses are indicative of

the basic weakness of the particular finite element program used in providing accurate values of localized bending stresses. For the particular results presented, there are three factors contributing to the errors in computed bending stresses:

(a) The structure has been modeled as a series of flat plate elements, thereby causing flat-plate type moments along the line of curvature. The magnitude of this perturbation is directly related to the size of the central angle subtended by the chord of the element and the basic R/t ratio of the structure.

(b) The localized bending stresses have been determined independently of the membrane solution. Since the entire shell structure is in tension, the inclusion of the membrane stresses in the bending moment solution would reduce all bending deformations and the resulting bending stresses.

(c) The results indicate that not all boundary conditions applied to the mathematical model as shown in Fig. 8.7 accurately represent the actual conditions in the structure. But an overall view of the results shows that good approximations have been effected, and that all ill effects are essentially local in nature.

From the above it is obvious that whereas membrane stresses are accurately represented in the Full Shell Analysis, some judgement must be used when interpreting data relating directly to shell bending stresses.

The theoretical data shown in Figs. 7.12 and 7.13 is actually that obtained at a section two elements round the circumference of the tube from the plane of symmetry. This was done in order to get sufficiently far from the boundary in the mathematical model (the plane of symmetry) for the local bending effects to have died out. When this

is done, the correlation with the measured data at the axis of symmetry is good. However, in the case of Fig. 7.11 this type of interpretation is not possible as the geometry of the structure changes quickly round the circumference. In the case of Fig. 7.14, which gives principal stresses both inside and outside the shell at two particular points on the main taper and branch taper in the vicinity of the 13 in. diameter rod, the theoretical results are affected by all three of the above factors, and no refinement by interpretation is possible. Hence with both Figs. 7.11 and 7.14 the actual raw theoretical data is presented with the measured data, and the correlation is poor.

The results of the second study emphasize the generality of the Full Shell Analysis. The most significant stress distribution, the full splitter stresses at the line of symmetry, is given in Figure 7.6. In this instance the traditional curved beam stress pattern in the splitter-plate has been reversed and the stress distribution for this geometry can more appropriately be characterized as a flat plate with tensile loading. The results of this study indicate that the Full Shell Analysis can produce accurate results for membrane stresses regardless of the geometries encountered.

Further confidence in the results of the model and the Full Shell Analysis was gained in the full scale testing program carried out on junction E-9 (Fig. 1.1 and Plate 1.1). The basic design concepts of this smaller junction were similar to those of the junction studied by model, the only difference being the size. The largest shell diameter of the full scale test junction was 8'-0" and the basic shell thickness was 2.5". These dimensions compare with the diameter of 12'-6" and the shell thickness of 4.0" for the prototype dimensions associated with the

model study. The strain gage program of the full scale test was similar in scope to that presented herein and was carried out by Southwest Research Institute of San Antonio, Texas. SwRI was contracted for this work by the fabricators for the prototype manifold assembly, Kaiser Steel Corporation, Fabricating Division, Fontana, California. The complete results of this study are given in Ref. 7 and the measured and computed stress distributions across the main reinforcement plate are included in Fig. 8.8.

Once the overall accuracy of the Full Shell Analysis had been established, it was further used in Studies Nos. 3, 4 and 6 to ascertain the relative influence of certain factors on the overall state of stress in the junction. These factors were respectively the effect of longitudinal loading (the bulkhead effect); the validity of idealizing the loading as used in the "Bureau Loading"; and the effect of shell thickness. These effects are discussed briefly in Sec. 8.7.

8.7 Results of Uncoupled Plate Analysis

The remainder of the studies relate to a study of the Uncoupled Plate Analysis in an effort to determine the limits within which it produces accurate results, and to understand the sources of error where the resulting accuracy is poor. Motivation for the use of this analytical procedure lies in its relative ease of application. Furthermore, at the time the basic design was to be accomplished, the Full Shell Analysis had not been fully developed.

The results of these studies show that the Uncoupled Plate Analysis must be applied with caution. Both good and bad results have been achieved, indicating that judgment must be used in its application.

Initial confidence in the Uncoupled Plate Analysis was gained in the study of existing manifold structures. The results of one such study, the Glendo Dam Bifurcation,[3] are given in Figures 8.9 and 8.10. In this case test data come from both a prototype test, and also a test on a plexiglas model study. Theoretical results come from the application of the Bureau Loading to the stiffener system treated as an assembly of curved beams, and also from the application of the Bureau Loading to the stiffener system plus part of the shell analyzed by the finite element method. This comparison shows that the Uncoupled Plate Analysis, when applied either by simple curved beam theory or by the more refined finite element method, will yield reasonable results for thin shell structures with beam-type reinforcement.

Good correspondence between the results of the Uncoupled Plate Analysis with Bureau Loading and the Full Shell Analysis with pressure is not possible for all ranges of geometry. In fact, the results of studies Nos. 3 and 5 as given in Figure 8.11 indicate that the two analytical techniques give stress values which differ by a factor of 2 for the geometry of the model study.

Two potential sources of error exist in the Uncoupled Plate Analysis, namely, those due to load idealization and structure idealization. The first is the error caused by replacing the actual surface pressure loading by an equivalent loading (see Fig. 8.2) applied directly to the uncoupled plate system. The second is the error caused by assuming that the only contribution of the tube walls to the structural action of the complete system is to provide flanges to the inside of the stiffening plates (Fig. 8.4). This assumption completely neglects the shell action of the tube walls. Studies Nos. 3, 4 and 6 represent an

attempt to determine the relative contribution of these two factors to the poor results of Study No. 5. These results, together with those of Study No. 1, are summarized in Figs. 8.11 and 8.12 with reference to the resulting stresses in the main stiffener plate on the axis of symmetry.

A comparison of the results from Studies Nos. 3 and 4 (Fig. 8.12) shows that the Bureau loading itself is not unreasonable. The two basic assumptions of the Bureau loading are that as the shell loads the reinforcing plates: (1) the effect of longitudinal shell forces are negligible and (2) the transfer of circumferential forces is independent of the relative shell stiffness. A check on the first of these assumptions was accomplished in Study No. 3 by removal of the longitudinal loads of Study No. 1. Figure 8.12 shows the comparative results of Studies 1 and 3 and indicates the sensitivity of the main splitter stresses to the longitudinal loads to be in the order of 3 ksi for the prototype structure under consideration. The second assumption of the Bureau loading was checked in Study 4 through the direct application of the Bureau loading in lieu of the pressure loading of Study 3 to the Full Shell Analysis. The results of this study, also given in Figure 8.12, shows that an additional error of approximately 2 ksi is introduced by this second assumption. Hence, the total difference between the pressure loading with longitudinal effects included and the Bureau loading is in the neighborhood of 5 ksi for the prototype structure as determined by the Full Shell Analysis. Therefore, the use of the Bureau loading accounts for approximately one-fourth of the difference between the results of the Full Shell Analysis with pressure and longitudinal loading (Study 1) and the Uncoupled Plate Analysis with Bureau loading (Study 5).

The above result suggests that the remainder of the error in Study 5 lies with the assumed role of the shell in the structural action of the combined system. The Uncoupled Plate Analysis was formulated on the basis that the role of the shell could be reasonably approximated through the inclusion of an "effective length" of shell in the finite-element grid. This "effective length" of shell was considered as a flange or line element with an appropriate axial and bending stiffness along the line of shell intersection. However, the poor result of Study 5 coupled with the good result of Glendo Dam Bifurcation Study (Fig. 8.10) indicates that the assumptions of the Uncoupled Plate Analysis are applicable only to thin shell, that is, low pressure manifold systems.

The connection between the Uncoupled Plate Analysis and thin shell structures was further verified by Study 6. In this study the prototype structure used in Study No. 1 was reduced to a thin shell structure by redefining the thicknesses of the shell elements as 0.1-inch in the Full Shell Analysis without altering the dimensions of the stiffeners. The effect of this substitution is to make the shell a membrane structure, with little or no bending stiffness, that transfers all of the unbalanced loading to the reinforcing plates. The main splitter stresses resulting from this study are given in Figure 8.11, and they show a remarkable correspondence to those of Study 5 considering the drastic reduction in shell thickness. In comparing the results of Studies 5 and 6 it will be noted that the shell thickness used in Study 5 is 4 in., whereas that used in Study 6 is 0.1 in. However, the comparison of these results is justified on the basis of the small influence that a change in shell thickness has on the Uncoupled Plate Analysis.

8.8 Recommendations

As the result of the work accomplished on this project several recommendations can be made in the field of manifold design. The number of man hours devoted to the design of any manifold system must necessarily be related to the cost of the prototype structure. Therefore, recommended design procedures will be made in accordance with the pressure requirement and scope of the project.

For low pressure manifolds the Uncoupled Plate Analysis is an accurate and efficient tool for the sizing of reinforcement plates or beams. The usual result of a low head requirement is a thin shell structure of low relative cost. Both of these factors point to the use of the Uncoupled Plate Analysis.

On the other hand, high pressure manifold systems will involve shell thickness too great for the valid use of the Uncoupled Plate Analysis. Fortunately, however, the economics of such systems will generally justify the time required to prepare the data for the Full Shell Analysis. The most difficult aspects of this job are the definition of an appropriate finite element mesh and the determination of the necessary shell coordinates. The coordinates on the reinforcing plates may be determined with the generator program for the Uncoupled Plate Analysis. Therefore, once the mesh and coordinates have been determined, one may proceed to analyze various reinforcement schemes without undue difficulty.

The Uncoupled Plate Analysis is relatively fast and inexpensive, but as it has a limited field of application it requires judgment in its use. The Full Shell Analysis is universal in application, but in its present state requires a large amount of work for data preparation and

hence is expensive. The advice given above is based on this difference, and only relates to the present state of the art. With the development of technology in the field of computer design in providing larger and faster systems and in the field of finite element analysis in developing conical shell elements in lieu of flat plate elements, the situation will undoubtedly change with time in favor of the Full Shell type of analysis which treats the structure as a complete integrated system.

REFERENCES

1. Zienkiewicz, O. C. and Cheung, Y. K., "The Finite Element Method in Structural and Continuum Mechanics," McGraw-Hill, 1967

2. Carr, A. J., "The Analysis of Three Dimensional Structures Using a High Speed Digital Computer," SESM Report No. 217, University of California, Berkeley, 1966.

3. Rudd, R. O., "Stress Analysis of Wye Branches," Engineering Monograph No. 32, U.S.B.R., 1964.

4. Herrmann, L. R., "Finite Element Bending Analysis for Plates," Journal of the Engineering Mechanics Division, ASCE, Vol. 93, No. EM5, Proc. Paper 5497, October 1967, Pages 13-26.

5. Amorocho, J., DeVries, J. J., and Curry, W., "Hydraulic Studies of the Tehachapi Pumping Plant Intake Channel and Manifold," Conference paper presented at Western Water and Power Symposium, Los Angeles, California, April 8 and 9, 1968.

6. Christ, A., "Research on Head Losses in Esher Wyss Type Distribution Pipes," Esher Wyss News, Vol. 39:2, 1966.

7. Keisling, E. W., "Final Report Test on Wye Branch of Discharge Manifold," Unpublished Report to Kaiser Steel Corp. (Fabrication Division, So. Calif.) from Southwest Research Institute (San Antonio, Texas), 11-68.

8. Herrmann, L. R., "User's Manual for General Isotropic Shell Program," Unpublished report to Aerojet-General Corp. (Computing Sciences, Div., Sacto., California), April 1967.

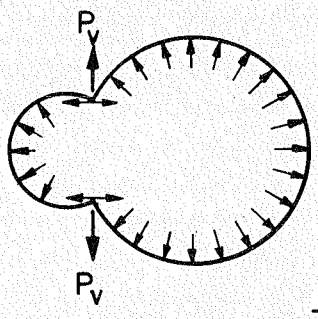

SECTION A-A

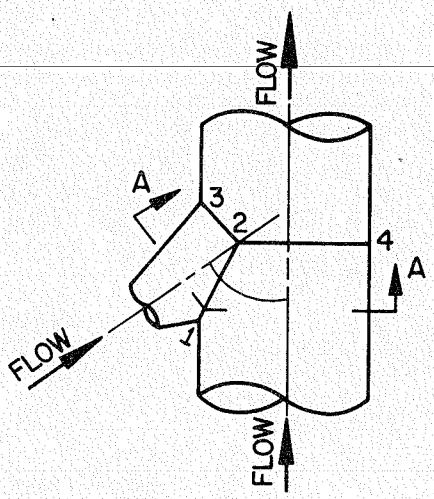

PLAN

FIG. 8.1 TYPICAL WYE-JUNCTION

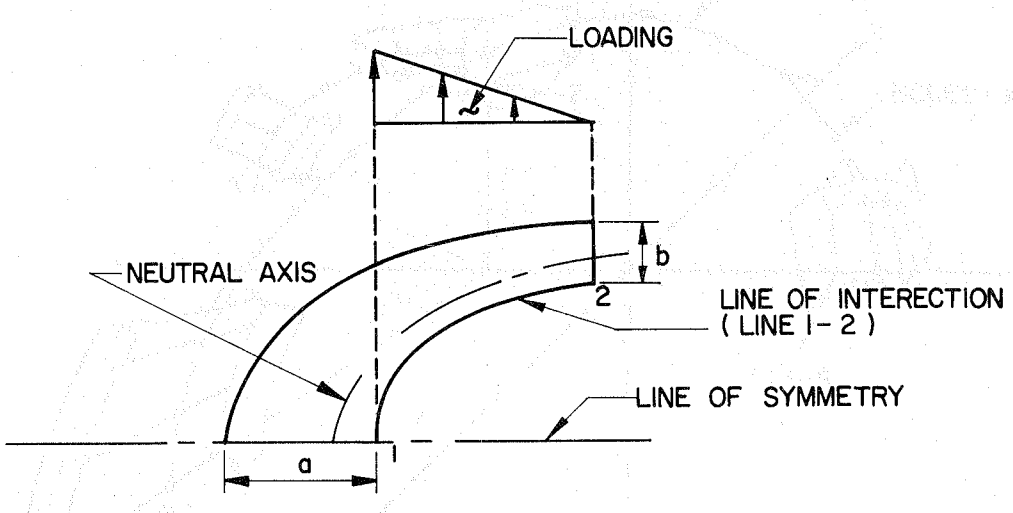

FIG. 8.2 TYPICAL REINFORCING BEAM

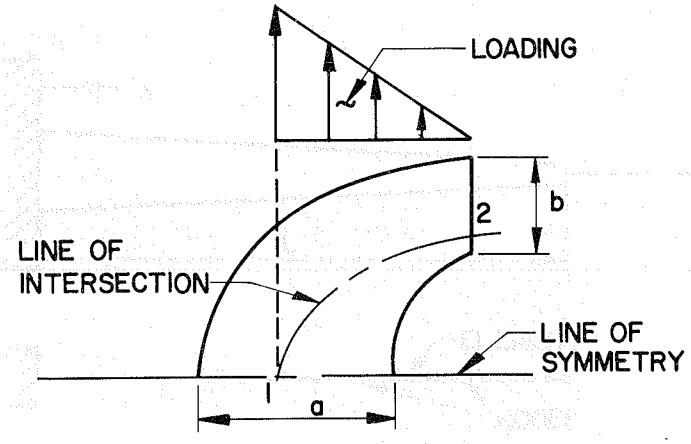

FIG. 8.3 TYPICAL REINFORCING PLATE

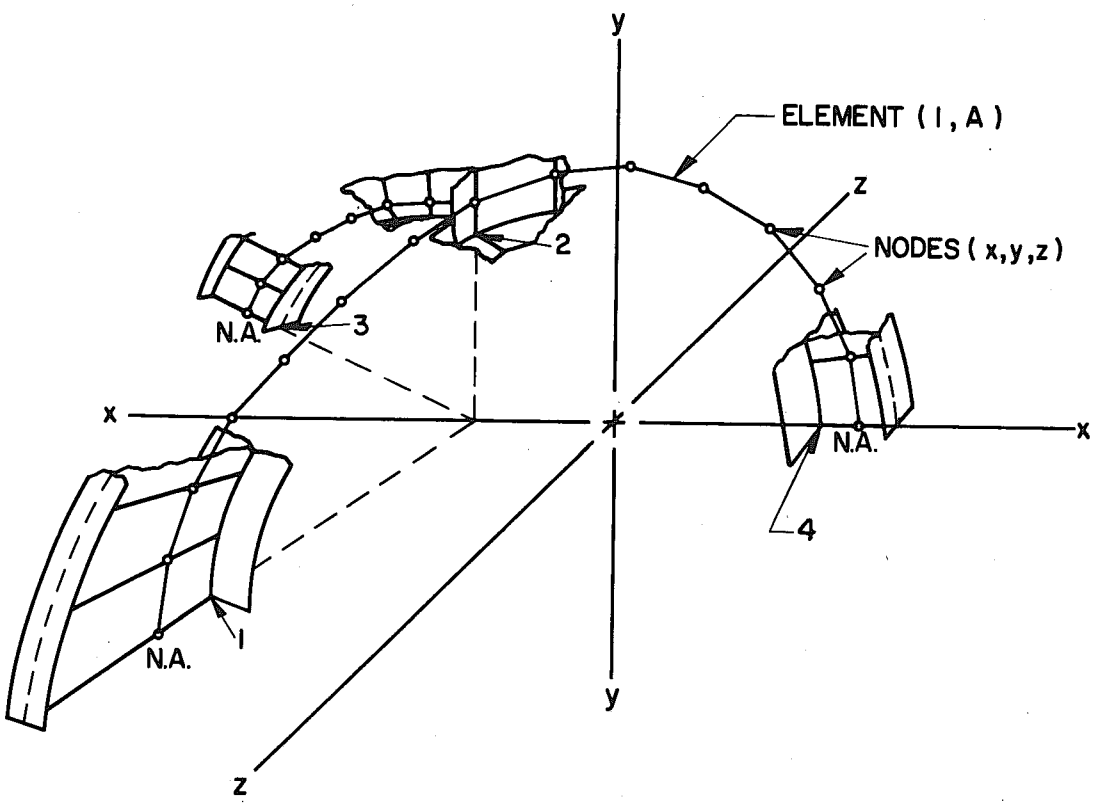

FIG. 8.4 MATHEMATICAL MODEL – BEAM STRUCTURE

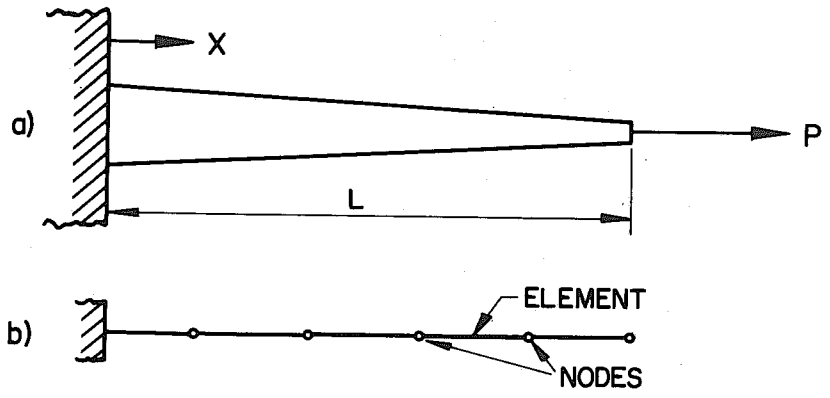

FIG. 8.5 MATHEMATICAL MODEL – SIMPLE BAR STRUCTURE

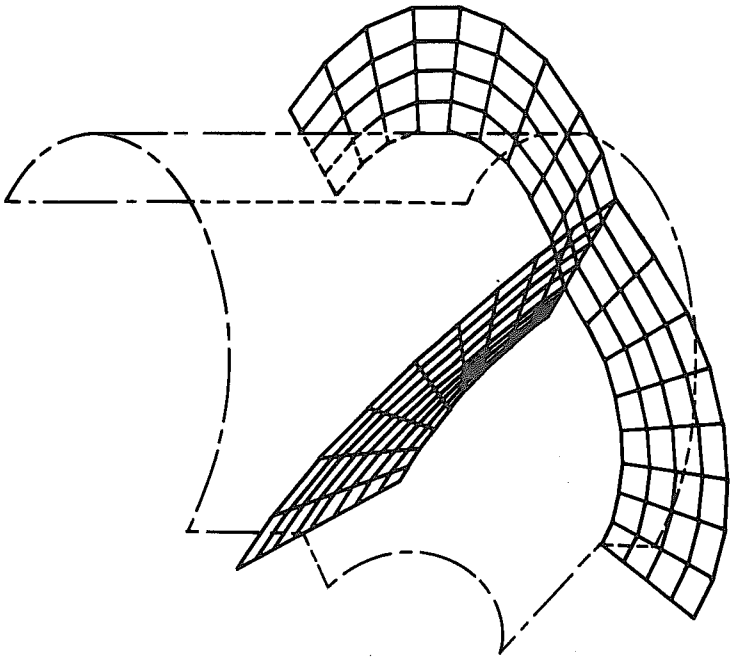

FIG. 8.6 MATHEMATICAL MODEL – UNCOUPLED PLATE ANALYSIS

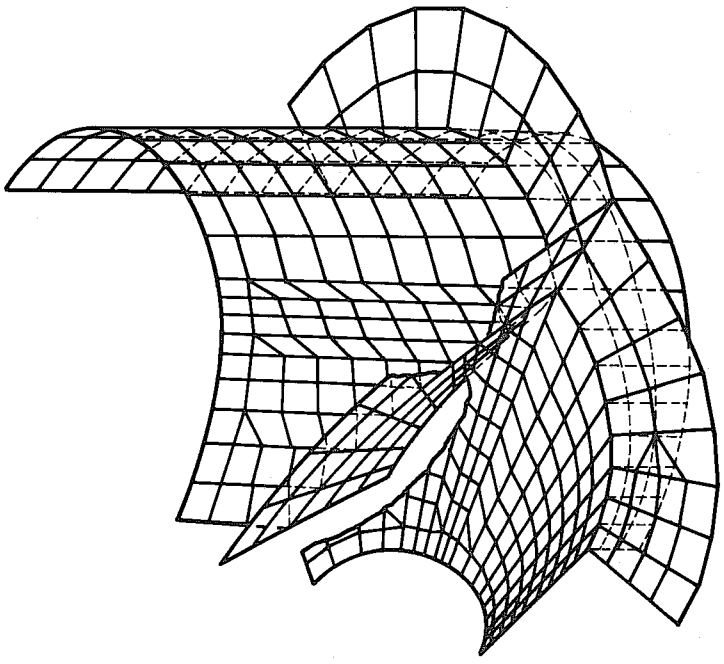

FIG. 8.7 MATHEMATICAL MODEL - FULL SHELL ANALYSIS

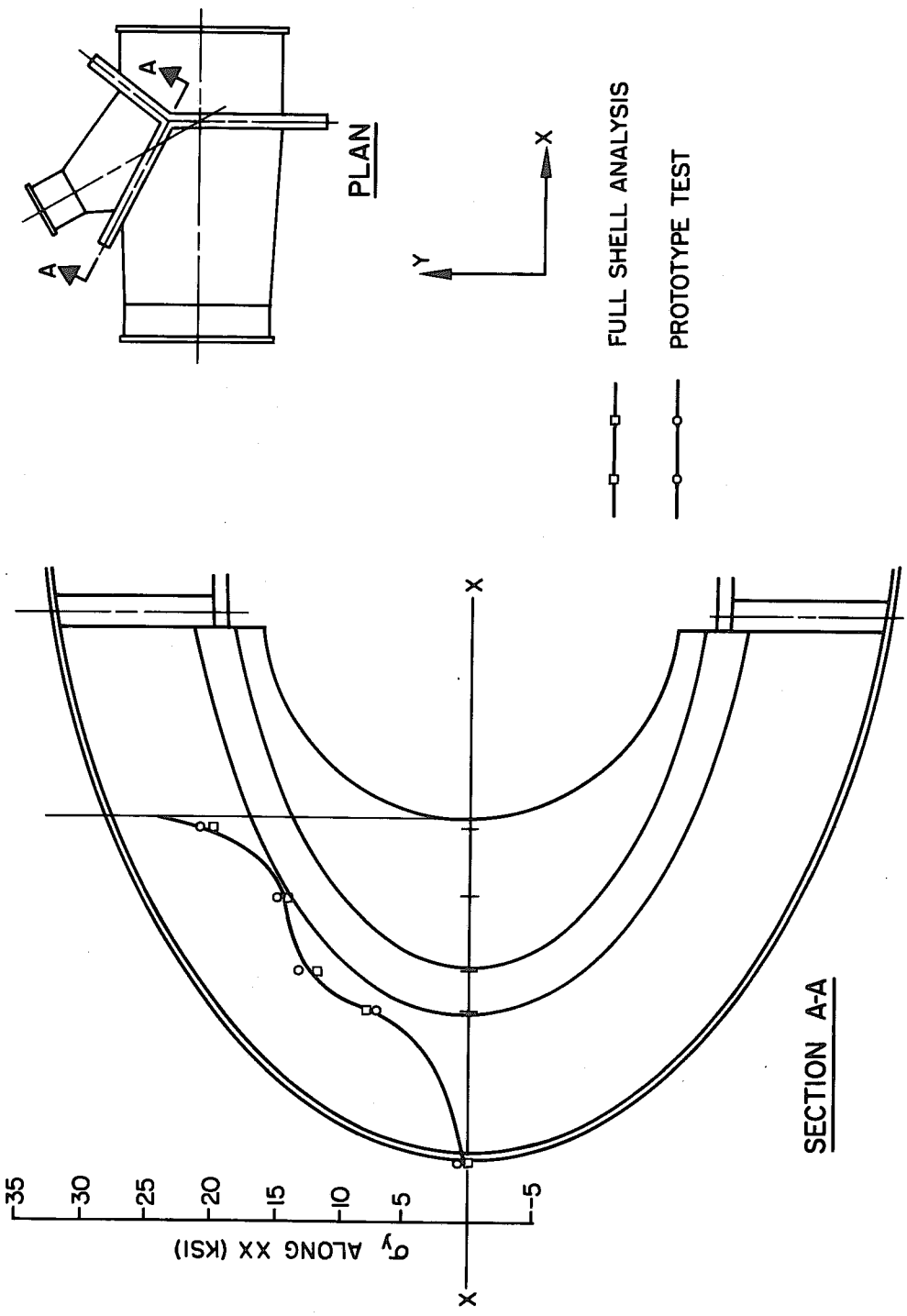

FIG. 8.8 PROTOTYPE TEST OF E-9 JUNCTION STRESSES AT 1150 PSI HYDROSTATIC PRESSURE

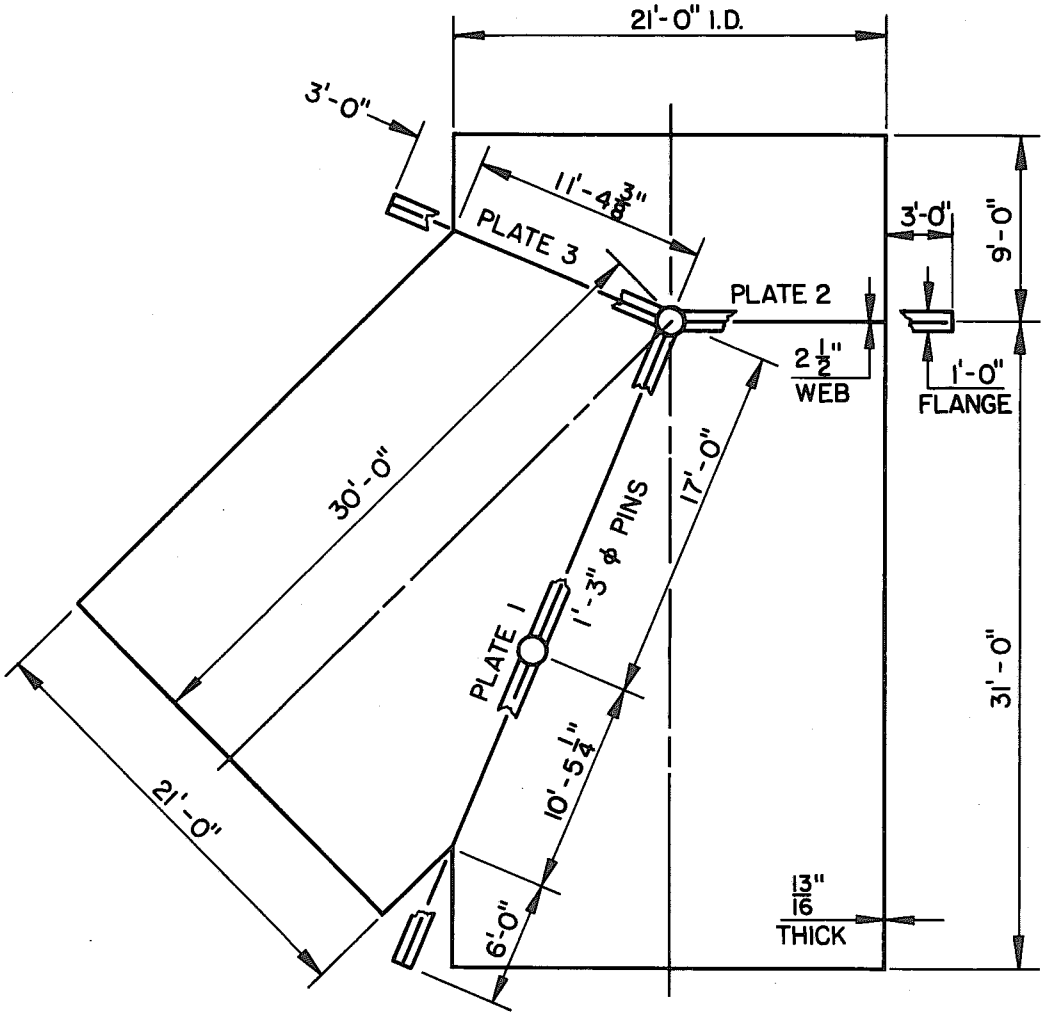

FIG. 8.9 GLENDO DAM BIFURCATION - BASIC STRUCTURE

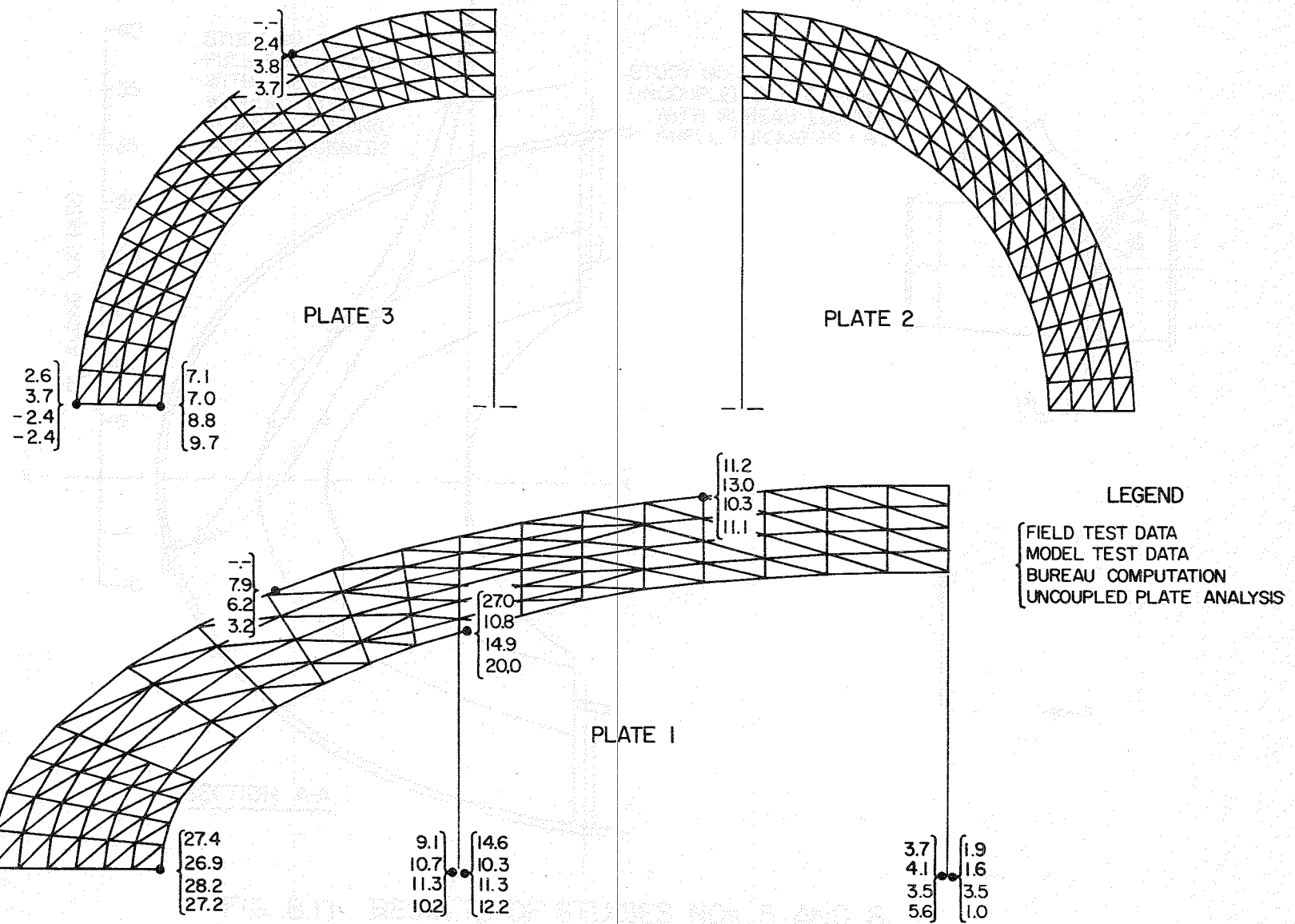

FIG. 8.10 GLENDO DAM BIFURCATION – STRESSES

APPENDIX

Strain Gage Readings and Predicted Prototype Values From Model Tests

45-DEG Y-JUNCTION - FULL SPLITTER PLATE - PROTOTYPE
STRESSES AT 1050 PSI PRESSURE

Material Properties: Young's modulus = 30000 ksi; Poisson's ratio = 0.375. Observations were taken at a gage factor of 2.00, the Young's modulus was therefore modified to take into account the change in gage factor.

Gage Factors: Single = 2.02 Delta = 1.98 Pair = 1.95

GAGE NUMBER	GAGE TYPE	OBSERVED MICROSTRAINS 1	2	3	PRINCIPAL STRESSES (KSI) MAX	MIN	ANGLE (DEG)
1	SINGLE	400.0			11.900		
2	SINGLE	390.0			11.602		
3	SINGLE	380.0			11.305		
4	PAIR	430.0	-140.0		13.530	.762	
6	PAIR	480.0	-120.0		15.590	2.150	
11	PAIR	530.0	-100.0		17.651	3.539	
13	SINGLE	650.0			19.337		
14	SINGLE	150.0			4.462		
15	SINGLE	30.0			.892		
16	SINGLE	-30.0			-.892		
17	DELTA	130.0	125.0	-25.0	5.958	1.476	-29.19
20	DELTA	130.0	25.0	0.0	4.260	.750	-5.22
23	PAIR	100.0	0.0		3.584	1.344	
25	PAIR	30.0	-40.0		.538	-1.030	
27	SINGLE	20.0			.595		
28	SINGLE	180.0			5.355		
29	PAIR	460.0	-120.0		14.874	1.882	
31	DELTA	380.0	-100.0	-25.0	10.691	-2.450	4.18
34	SINGLE	260.0			7.735		
35	DELTA	270.0	-80.0	70.0	8.670	-.266	12.64
38	SINGLE	110.0			3.272		
39	SINGLE	130.0			3.867		
40	PAIR	240.0	-125.0		6.992	-1.254	
42	DELTA	70.0	-40.0	45.0	2.679	-.255	23.74

TABLE 6.1

GAGE NUMBER	GAGE TYPE	OBSERVED MICROSTRAINS 1	2	3	PRINCIPAL STRESSES (KSI) MAX	MIN	ANGLE (DEG)
45	DELTA	250.0	-60.0	30.0	7.613	-.503	8.19
48	DELTA	210.0	-150.0	50.0	6.367	-2.812	16.84
51	DELTA	270.0	-10.0	-10.0	8.153	-.073	0.00
54	DELTA	80.0	0.0	-10.0	2.386	-.124	-2.91
57	DELTA	70.0	75.0	10.0	3.425	1.584	-31.98
60	PAIR	280.0	-200.0		7.347	-3.405	
62	DELTA	210.0	-120.0	-20.0	5.437	-3.175	8.59
65	DELTA	160.0	-10.0	-60.0	4.389	-1.480	-6.26
70	PAIR	430.0	100.0		16.755	9.363	
72	PAIR	470.0	80.0		17.920	9.184	
74	PAIR	455.0	10.0		16.442	6.474	
76	PAIR	450.0	130.0		17.875	10.707	
78	PAIR	530.0	40.0		19.533	8.557	
80	PAIR	570.0	30.0		20.832	8.736	
82	PAIR	570.0	120.0		22.042	11.962	
84	SINGLE	70.0			2.082		
86	SINGLE	30.0			.892		

TABLE 6.1 (cont.)

45-DEG Y-JUNCTION - PARTIAL SPLITTER PLATE - PROTOTYPE
STRESSES AT 1050 PSI PRESSURE

Material Properties: Young's modulus = 30000 ksi; Poisson's ratio = 0.375. Observations were taken at a gage factor of 2.00, the Young's modulus was therefore modified to take into account the change in gage factor.

Gage Factors: Single = 2.02 Delta = 1.98 Pair = 1.95

GAGE NUMBER	GAGE TYPE	OBSERVED MICROSTRAINS 1	2	3	PRINCIPAL STRESSES (KSI) MAX	MIN	ANGLE (DEG)
6	PAIR	1090.0	-250.0		35.706	5.690	
8	SINGLE	740.0			22.015		
9	SINGLE	190.0			5.652		
10	SINGLE	-20.0			-.595		
11	PAIR	725.0	-80.0		24.909	6.877	
13	SINGLE	680.0			20.230		
14	SINGLE	200.0			5.950		
15	SINGLE	110.0			3.272		
16	SINGLE	-25.0			-.744		
17	DELTA	230.0	-70.0	-20.0	6.352	-1.827	4.47
20	DELTA	170.0	0.0	-10.0	5.160	.012	-1.42
23	PAIR	45.0	30.0		2.016	1.680	
25	PAIR	0.0	0.0		0.000	0.000	
27	SINGLE	-25.0			-.744		
28	SINGLE	145.0			4.314		
29	PAIR	470.0	-170.0		14.560	.224	
31	DELTA	300.0	-95.0	-160.0	7.062	-5.607	-3.75
34	SINGLE	195.0			5.801		
35	DELTA	335.0	-75.0	30.0	10.106	-.733	7.14
38	SINGLE	120.0			3.570		
39	SINGLE	100.0			2.975		
40	PAIR	255.0	-120.0		7.526	-.874	
42	DELTA	110.0	-25.0	-5.0	3.147	-.561	3.94
45	DELTA	205.0	-65.0	70.0	6.829	-.042	15.00

TABLE 6.2

GAGE NUMBER	GAGE TYPE	OBSERVED MICROSTRAINS 1	2	3	PRINCIPAL STRESSES (KSI) MAX	MIN	ANGLE (DEG)
48	DELTA	200.0	-255.0	150.0	7.884	-4.814	27.12
51	DELTA	230.0	-110.0	60.0	7.235	-1.417	15.00
54	DELTA	145.0	-90.0	45.0	4.617	-1.385	17.46
57	DELTA	105.0	-145.0	75.0	4.039	-2.908	26.85
60	PAIR	285.0	-195.0		7.594	-3.158	
62	DELTA	185.0	-140.0	-60.0	4.066	-4.551	6.83
65	DELTA	190.0	-70.0	-10.0	5.242	-1.686	6.37
70	PAIR	390.0	95.0		15.254	8.646	
72	PAIR	430.0	75.0		16.419	8.467	
74	PAIR	425.0	5.0		15.299	5.891	
76	PAIR	435.0	175.0		17.942	12.118	
78	PAIR	565.0	40.0		20.787	9.027	
80	PAIR	570.0	50.0		21.101	9.453	
82	PAIR	560.0	115.0		21.616	11.648	
84	SINGLE	300.0			8.925		
86	SINGLE	305.0			9.074		

TABLE 6.2 (cont.)

45-DEG Y-JUNCTION - NO SPLITTER PLATE - PROTOTYPE
STRESSES AT 1050 PSI PRESSURE

Material Properties: Young's modulus = 30000 ksi; Poisson's ratio = 0.375. Observations were taken at a gage factor of 2.00, the Young's modulus was therefore modified to take into account the change in gage factor.

Gage Factors: Single = 2.02 Delta = 1.98 Pair = 1.95

GAGE NUMBER	GAGE TYPE	OBSERVED MICROSTRAINS 1	2	4	PRINCIPAL STRESSES (KSI) MAX	MIN	ANGLE (DEG)
13	SINGLE	1640.0			48.790		
14	SINGLE	320.0			9.520		
15	SINGLE	-180.0			-5.355		
16	SINGLE	-190.0			-5.652		
17	DELTA	315.0	-270.0	150.0	10.826	-4.524	22.06
20	DELTA	375.0	-180.0	120.0	12.159	-1.978	16.34
23	PAIR	45.0	105.0		4.368	3.024	
25	PAIR	-30.0	105.0		3.360	.336	
27	SINGLE	-90.0			-2.677		
28	SINGLE	150.0			4.462		
29	PAIR	660.0	-150.0		21.638	3.494	
31	DELTA	390.0	0.0	-300.0	10.258	-7.349	-12.85
34	SINGLE	180.0			5.355		
35	DELTA	430.0	-75.0	0.0	12.671	-1.197	3.95
38	SINGLE	90.0			2.677		
39	SINGLE	120.0			3.570		
40	PAIR	285.0	-90.0		9.005	.605	
42	DELTA	150.0	35.0	-30.0	4.824	.185	-10.44
45	DELTA	205.0	-90.0	-195.0	3.984	-6.570	-7.33
48	DELTA	225.0	-480.0	330.0	12.420	-9.996	33.42
51	DELTA	150.0	-180.0	270.0	9.808	-2.051	37.46
54	DELTA	210.0	-245.0	210.0	9.512	-3.856	30.00
57	DELTA	105.0	-330.0	225.0	7.431	-7.431	35.93
60	PAIR	300.0	-210.0		7.930	-3.494	

TABLE 6,3

GAGE NUMBER	GAGE TYPE	OBSERVED MICROSTRAINS 1	2	3	PRINCIPAL STRESSES (KSI) MAX	MIN	ANGLE (DEG)
62	DELTA	160.0	-180.0	-45.0	3.306	-5.407	11.61
65	DELTA	230.0	105.0	0.0	8.344	2.484	-13.56
70	PAIR	300.0	210.0		13.574	11.558	
72	PAIR	450.0	180.0		18.547	12.499	
74	PAIR	420.0	75.0		16.061	8.333	
78	PAIR	540.0	105.0		20.765	11.021	
80	PAIR	630.0	150.0		24.595	13.843	
82	PAIR	600.0	195.0		24.125	15.053	

TABLE 6.3 (cont.)

60-DEG Y-JUNCTION PARTIAL SPUTTER PLATE - PROTOTYPE
STRESSES AT 1150 PSI PRESSURE

Material Properties: Young's modulus = 30000 ksi; Poisson's ratio = 0.375. Observations were taken at a gage factor of 2.00, the Young's modulus was therefore modified to take into account the change in gage factor.

Gage Factors: Single = 2.02 Delta = 1.98 Pair = 1.95

GAGE NUMBER	GAGE TYPE	OBSERVED MICROSTRAINS 1	2	3	PRINCIPAL STRESSES (KSI) MAX	MIN	ANGLE (DEG)
1	DELTA	272.0	150.0	169.0	11.221	7.880	4.16
4	DELTA	381.0	174.0	131.0	14.487	7.685	-4.63
7	PAIR	588.0	-168.0		18.816	1.882	
9	PAIR	486.0	-58.0		16.639	4.453	
11	SINGLE	538.0			16.005		
12	SINGLE	375.0			11.156		
13	SINGLE	209.0			6.218		
14	SINGLE	115.0			3.421		
15	SINGLE	380.0			11.305		
16	SINGLE	580.0			17.255		
17	PAIR	520.0	40.0		19.174	8.422	
19	PAIR	566.0	35.0		20.756	8.861	
21	PAIR	596.0	50.0		22.033	9.802	
23	PAIR	562.0	60.0		20.948	9.704	
25	SINGLE	48.0			1.428		
26	SINGLE	80.0			2.380		
27	SINGLE	162.0			4.819		
28	SINGLE	130.0			3.867		
29	SINGLE	286.0			8.508		
30	SINGLE	230.0			6.842		
31	SINGLE	179.0			5.325		
32	SINGLE	142.0			4.224		
33	DELTA	-20.0	102.0	52.0	3.726	.605	-77.97
36	DELTA	492.0	174.0	400.0	21.390	13.063	21.84

TABLE 7.1

GAGE NUMBER	GAGE TYPE	OBSERVED MICROSTRAINS 1	2	3	PRINCIPAL STRESSES (KSI) MAX	MIN	ANGLE (DEG)
39	DELTA	245.0	298.0	131.0	13.063	8.720	-39.05
42	DELTA	-41.0	36.0	260.0	8.100	.142	67.13
45	DELTA	-314.0	172.0	206.0	8.436	-6.368	88.32
48	PAIR	499.0	-238.0		14.685	-1.823	
50	SINGLE	210.0			6.247		
51	SINGLE	246.0			7.318		
52	SINGLE	192.0			5.712		
53	DELTA	-240.0	168.0	250.0	9.555	-3.802	85.51
56	DELTA	-208.0	140.0	210.0	7.991	-3.402	85.50
59	PAIR	335.0	-208.0		9.211	-2.952	
61	SINGLE	291.0			8.657		
62	SINGLE	225.0			6.694		
63	SINGLE	202.0			6.009		
64	PAIR	425.0	134.0		17.033	10.515	
66	PAIR	473.0	99.0		18.283	9.905	
68	PAIR	530.0	90.0		20.205	10.349	
70	PAIR	531.0	66.0		19.918	9.502	
72	PAIR	620.0	16.0		22.436	8.906	
74	PAIR	641.0	40.0		23.511	10.049	
76	PAIR	640.0	67.0		23.838	11.003	
78	PAIR	612.0	23.0		22.243	9.050	
80	PAIR	415.0	171.0		17.172	11.706	
82	PAIR	490.0	27.0		17.924	7.553	
84	PAIR	591.0	19.0		21.437	8.624	
86	PAIR	617.0	51.0		22.799	10.120	
88	PAIR	554.0	75.0		20.863	10.134	
90	PAIR	528.0	60.0		19.730	9.247	
92	PAIR	557.0	45.0		20.568	9.099	
96	PAIR	568.0	110.0		21.836	11.576	
96	PAIR	370.0	56.0		14.013	6.980	
98	PAIR	482.0	150.0		19.291	11.854	
100	PAIR	530.0	129.0		20.729	11.747	
102	PAIR	586.0	82.0		22.104	10.815	

TABLE 7.1 (cont.)